UNIVERSITY OF OKLAHOMA

GRADUATE COLLEGE

MECHANISMS OF SERINE ACETYLTRANSFERASE AND *O*-ACETYLSERINE SULFHYDRYLASE

A DISSERTATION
SUBMITTED TO THE GRADUATE FACULTY
in partial fulfillment of the requirements for the
Degree of
DOCTOR OF PHILOSOPHY

By
RONG GUAN
Norman, Oklahoma
2009

MECHANISMS OF SERINE ACETYLTRANSFERASE AND *O*-ACETYLSERINE SULFHYDRYLASE

A DISSERTATION APPROVED FOR THE
DEPARTMENT OF CHEMISTRY AND BIOCHEMISTRY

BY

Dr. Paul F. Cook, Chair

Dr. Ann H. West

Dr. George B. Richter-Addo

Dr. Helen I. Zgurskaya

Dr. Michael J. McInerney

To my dear wife, Yun Liu,

and my parents

Acknowledgement

Five years ago, I was twenty six. I came to USA for my PH.D. degree, my science career and most important, to realize myself as a decent and useful person. Five years later, now, I finished my thesis. I feel I am a better person no matter in science or in daily life. I understand myself on a new level and am prepared for the new start after my Ph.D. studies. Life treats me well because I have wonderful people around me, helping me. I would like to express all my gratitude and appreciation to them.

Dr. Paul F. Cook is the first person I am willing to thank. He is one of the best major advisors in this world, if not the best. Being a world-class enzymologist, he knows nearly everything about enzyme kinetics, and can easily answer all kinds of tough questions I had during my Ph.D. studies. He tried to develop his students to be knowledgeable and nice people, who can independently think and investigate, who can fulfill themselves and contribute to the world. I am so proud to be one of his academic kids and working with Dr. Cook will be one of the most cherishable memories in my life.

I am also grateful to all members of my graduate committee, including **Dr. Ann H. West, Dr. George B. Richter-Addo, Dr. Helen I. Zgurskaya, Dr. Michael J. McInerney, and Dr. Bruce A. Roe**, who substituted for Dr. Cook in my general exam. I highly appreciate all the help, encouragement and valuable suggestions I received from them. They are all wonderful scientists and wonderful advisors.

I would like to thank all my past and present colleagues in Dr. Cook's Lab **(Dr.**

William E. Karsten and his wife Dr. Lillian Chooback, Jean Keil, Dr. Wael M. Rabeh, Dr. Lei Li, Mamar Baizid, Dr. Hengyu Xu, Dr. Jinghua Qian, Dr. Deniz F. Aktas, Ashwani K. Vashishtha, Devi K. Ekanayake, Dr. Ying Lin, Qiong Xue, Dr. Francesca Speroni, Hui Tian, Kostyantyn Bobyk, Chaonan Hsu, Vidya Kumar, Enea Salsi) and my closest neighbors from Dr. West's lab **(Dr. Babak Andi, Dr. Hui Tan, Dr. Daniel Copeland, Alla Kaserer, Dr. Xiaodong Zhao, Lu Zhou)** for their kind support and help.

I really enjoy the working experiences with my experimental collaborators and appreciate their advice and support. They are **Dr. Klaus D. Schnackerz** from Universität Würzburg, **Dr. Susan A. Nimmo** from University of Oklahoma, **Dr. Bin Huang and Dr. Steven L. Roderick** from Albert Einstein College of Medicine, **Dr. Andrea Mozzarelli** from University of Parma, and **Dr. Jialing Lin** from University of Oklahoma Health Sciences Center. I am especially impressed by Dr. Schnackerz, who dedicates himself to scientific research even after his retirement. He did the experiments by himself in his seventies, which is a good example of a true researcher.

Lastly, I want to dedicate this dissertation to **my dear wife, Yun Liu**, for her endless love and trust. I am blessed to have her standing beside me during these five years. Together, we experienced good times, bad times and we always held each others hands. This is happiness I pursued all these years. This dissertation is also dedicated to **my parents** for their support and encouragement for so many years.

Table of Contents

Acknowledgement ······ **IV**

Table of Contents ······ **VI**

List of Tables ······ **X**

List of Figures ······ **XI**

List of Schemes ······ **XIII**

List of Abbreviations ······ **XIV**

Abstract ······ **XVI**

Chapter 1 Introduction ······ **1**

C.1.1 Biosynthesis of Cysteine ······ 1

C1.1.1 Sulfate Reduction in Enteric Bacteria ······ 1

C1.1.2 Cysteine Biosynthesis in Enteric Bacteria ······ 5

C1.1.3 Cysteine Synthase ······ 8

C1.2 Serine Acetyltransferase ······ 11

C1.2.1 Structure of SAT ······ 11

C1.2.2 Kinetic Mechanism of SAT ······ 18

C1.2.3 Rate-limiting Steps ······ 19

C1.2.4 Chemical Mechanism of SAT ······ 20

C1.3 *O*-Acetylserine Sulfhydrylase ······ 22

C1.3.1 Structure of OASS ······ 23

C1.3.1.1 Structure of OASS-A ······ 23

C1.3.1.2 Structure of OASS-B ······ 25

C1.3.2 Kinetic Mechanism of OASS ······ 28

C1.3.3 Chemical Mechanism of OASS ······ 29

C1.3.3.1 Chemical Mechanism of OASS-A ······ 29

C1.3.3.2 Chemical Mechanism of OASS-B ······ 33

C1.4 Research Carried Out in this Dissertation ······ 35

Chapter 2 Roles of H154, H189, and D139 in the Active Site of Serine Acetyltransferase from *Haemophilus influenzae* ··· **38**

C2.1 Introduction ··· 38

C2.2 Material and Methods ··· 41

C2.2.1 Chemicals ··· 41

C2.2.2 Plasmid Construction and Site-directed Mutagenesis ··· 41

C2.2.3 Enzyme ··· 42

C2.2.4 Enzyme Assays ··· 43

C2.2.5 pH Studies ··· 44

C2.2.6 Solvent Deuterium Kinetic Isotope Effects ··· 44

C2.2.7 Data Processing ··· 44

C2.3 Results ··· 46

C2.3.1 Kinetic Parameters of the Mutant Enzymes ··· 46

C2.3.2 pH Dependence of Kinetic Parameters ··· 47

C2.3.3 Solvent Deuterium Kinetic Isotope Effects ··· 51

C2.4 Discussion ··· 52

C2.4.1 H154N Mutant Enzyme ··· 52

C2.4.2 H189N Mutant Enzyme ··· 54

C2.4.3 H154N/H189N Mutant Enzyme ··· 55

C2.4.4 D139N Mutant Enzyme ··· 56

C2.4.5 Proposed Roles of H154, H189, and D139 in *Hi*SAT ··· 59

Chapter 3 ^{31}P NMR Studies of *O*-Acetylserine Sulfhydrylase-B from *Salmonella typhimurium* ··· **61**

C3.1 Introduction ··· 61

C3.2 Materials and Methods ··· 63

C3.2.1 Chemicals ··· 63

C3.2.2 Enzyme ··· 63

C3.2.3 ^{31}P NMR Spectroscopy ··· 64

C3.2.4 Enzyme Assays ··· 65

C3.2.5 Resolution of PLP from OASS-B ··· 65

C3.2.6 Reconstitution of PLP with Apo OASS-B ··· 66

C3.2.7 Ultraviolet-visible Spectral Studies ········ 66
C3.2.8 Steady-state Fluorescence Mesurement ········ 66
C3.3 Results ········ 67
C3.3.1 ^{31}P NMR Spectroscopy ········ 67
C3.3.2 Resolution of PLP from OASS-B ········ 69
C3.3.3 Reconstitution of PLP with Apo OASS-B ········ 71
C3.4 Discussion ········ 72
C3.4.1 Pyridoxal 5′-Phosphate Binding Site of OASS ········ 72
C3.4.2 ^{31}P NMR Spectra ········ 73
C3.4.3 Characterization of Apo and Reconstituted OASS-B ········ 77

Appendix I Fluorescence Spectroscopy of *O*-Acetylserine Sulfhydrylase-B from *Salmonella typhimurium* ········ 79
AI.1 Introduction ········ 79
AI.2 Materials and Methods ········ 81
AI.2.1 Chemicals ········ 81
AI.2.2 Site-directed Mutagenesis ········ 81
AI.2.3 Enzyme Preparation ········ 82
AI.2.4 Enzyme Assays ········ 83
AI.2.5 Initial Velocity Studies ········ 83
AI.2.6 Rapid-scanning Stopped-flow Studies ········ 83
AI.2.7 UV-visible Spectral Studies ········ 84
AI.2.8 Fluoresence Lifetime Studies ········ 84
AI.3 Results and Discussion ········ 85
AI.3.1 Kinetic Data ········ 85
AI.3.2 UV-visible Spectra ········ 86
AI.3.3 Fluorescence Lifetime Studies ········ 88

Appendix II Subcloning and Expression of *O*-Acetylserine Sulfhydrylase-A from *Salmonella typhimurium* ········ 91

Appendix III p$K_{i(cysteine)}$ Profile of Serine Acetyltransferase from *Haemophilus influenzae* ········ **93**

AIII.1 Introduction ········ 93

AIII.2 Materials and Methods ········ 93

AIII.2.1 Chemicals ········ 94

AIII.2.2 Enzyme Preparation ········ 94

AIII.2.3 Enzyme Assays and p$K_{i(cysteine)}$ Profile ········ 94

AIII.3 Results and Discussion ········ 95

Appendix IV Other Research ········ **98**

References ········ **100**

List of Tables

Chapter 2 Roles of H154, H189, and D139 in the Active Site of

Serine Acetyltransferase from *Haemophilus influenzae* ······ 38

Table C2-1. Sequence of oligonucleotide primers ······ 42

Table C2-2. Kinetic parameters for *Hi*SAT wild type and mutant enzymes at pH 7.3 ······ 47

Table C2-3. Summary of pK_a values for wild type and mutant *Hi*SAT ······ 50

Table C2-4. Summary of *SKIE* values for wild type and mutant enzymes ······ 51

Chapter 3 ^{31}P NMR Studies of *O*-Acetylserine Sulfhydrylase-B

from *Salmonella typhimurium* ······ 61

Table C3-1. ^{31}P NMR-Chemical Shifts and Line Widths of OASS-B ······ 68

Appendix I Fluorescence Spectroscopy of *O*-Acetylserine Sulfhydrylase-B

from *Salmonella typhimurium* ······ 79

Table AI-1. Sequence of oligonucleotide primers ······ 82

Table AI-2. Initial velocity and stopped-flow data

of tryptophan mutants of *St*OASS-B ······ 85

Table AI-3. Extinction coefficient at 414 nm of tryptophan mutant enzymes ······ 87

Table AI-4. Fluorescence lifetime data of tryptophan mutant enzymes of *St*OASS-B ······ 89

Appendix II Subcloning and Expression of *O*-Acetylserine Sulfhydrylase-A

from *Salmonella typhimurium* ······ 91

Table AII-1. Sequence of oligonucleotide primers ······ 91

Appendix IV Other Research ······ 98

Table AIV-1. Sequence of oligonucleotide primers ······ 98

List of Figures

Chapter 1 Introduction ······ **1**

Figure C1-1. *Hi*SAT with cysteine bound ······ 12

Figure C1-2. A *Hi*SAT monomer ······ 13

Figure C1-3. Homodimeric structure of *St*OASS-B ······ 27

Chapter 2 Roles of H154, H189, and D139 in the Active Site of Serine Acetyltransferase from *Haemophilus influenzae* ······ **38**

Figure C2-1. Proposed chemical mechanism of *Hi*SAT ······ 39

Figure C2-2. Close-up of the active site of *Hi*SAT with cysteine bound ······ 40

Figure C2-3. pH dependence of V_1/E_t (A) and $V_1/K_{ser}E_t$ (B) for the H154N, H189N and H154N/H189N mutant enzymes ······ 48

Figure C2-4. pH(D) dependence of V_1/E_t (A), $V_1/K_{ser}E_t$ (B) and $V_1/K_{AcCoA}E_t$ (C) for the D139N mutant of *Hi*SAT ······ 49

Chapter 3 ^{31}P NMR Studies of *O*-Acetylserine Sulfhydrylase-B from *Salmonella typhimurium* ······ **61**

Figure C3-1. ^{31}P NMR spectrum for OASS-B without ligand bound ······ 67

Figure C3-2. UV-visible absorption spectra of OASS-B ······ 69

Figure C3-3. Steady-state fluorescence spectra of OASS-B ······ 70

Figure C3-4. Kinetics of reconstitution of apo OASS-B upon addition of PLP ······ 72

Figure C3-5. Superposition of the PLP cofactor in the phosphate binding site of OASS-A (green) and OASS-B (purple) and their respective hydrogen bonding networks ······ 74

Figure C3-6. Superposition of the internal Schiff base of OASS-A (green) and OASS-B (purple) ······ 76

Appendix I Fluorescence Spectroscopy of *O*-Acetylserine Sulfhydrylase-B from *Salmonella typhimurium* ······ 79

Figure AI-1. Overlay of *St*OASS-A and -B with their tryptophans of one subunit shown in sticks ······ 80

Figure AI-2. UV-visible absorption spectra of *St*OASS-B ······ 86

Appendix III p$K_{i(cysteine)}$ Profile of Serine Acetyltransferase from *Haemophilus influenzae* ······ 93

Figure AIII-1. pH dependence of p$K_{i(cysteine)}$ values of *Hi*SAT ······ 96

List of Schemes

Chapter 1 Introduction ········ **1**

Scheme C1-1. Sulfur interconversion among species ········ 2

Scheme C1-2. Sulfate reduction pathway in enteric bacteria ········ 3

Scheme C1-3. Two-step pathway for L-cysteine biosynthesis in enteric bacteria ········ 6

Scheme C1-4. The interactions of *Hi*SAT with its feedback inhibitor, L-cysteine ········ 15

Scheme C1-5. Minimal chemical mechanism of *St*OASS-A ········ 30

List of Abbreviations

AA	α-aminoacrylate external Schiff base intermediate
AcCoA	acetyl Coenzyme A
APS	adenosine 5′-phosphosulfate
BCA	β-chloro-L-alanine
BSA	bovine serum albumin
Ches	2-(*N*-cyclohexylamino)ethanesulfonic acid
CoA	coenzyme A
D_2O	deuterium oxide
DTNB	5, 5′-dithiobis(2-nitrobenzoate)
DTT	dithiothreitol
ESB	external Schiff base
ESI	electrospray ionization
Hepes	*N*-(2-hydroxyethyl)piperazine-*N′*-(2-ethanesulfonic acid)
***Hi*SAT**	serine acetyltransferase from *Haemophilus influenzae*
IPTG	isopropyl β-D-1-thiogalactopyranoside
ISB	internal Schiff base
LβH	left-handed parallel β-helix
Mes	2-(*N*-morpholino)ethanesulfonic acid
Ni-NTA	nickel-nitrilotriacetic acid
NMR	nuclear magnetic resonance
OAS	*O*-acetyl-L-serine
OASS	*O*-acetylserine sulfhydrylase
OASS-A	A-isozyme of *O*-acetylserine sulfhydrylase
OASS-B	B-isozyme of *O*-acetylserine sulfhydrylase
PAPS	3′-phosphoadenosine 5′-phosphosulfate

PCR	polymerase chain reaction
PLP	pyridoxal 5′-phosphate
RSSF	rapid-scanning stopped-flow
ser	L-serine
SKIE	solvent deuterium kinetic isotope effect
TNB	5-thio-2-nitrobenzoate
Tris	tris(hydroxymethyl)aminomethane

Abstract

The *de novo* biosynthesis of L-cysteine in enteric bacteria and higher plants is a two-step pathway. The first step is catalyzed by serine acetyltransferase (SAT), which converts acetyl CoA and L-serine to *O*-acetyl-L-serine and CoA via a sequential kinetic mechanism. A crystal structure of SAT with cysteine bound in the serine subsite of the active site shows that both H154 and H189 are within hydrogen-bonding distance to the cysteine thiol (Olsen, L. R., Huang, B., Vetting, M. W., and Roderick, S. L. (2004) Biochemistry *43*, 6013-6019.). In addition, H154 is in an apparent dyad linkage with D139. The structure suggests that H154 is the most likely catalytic general base, and that H189 and D139 may also play important roles during the catalytic reaction. Site-directed mutagenesis was performed to mutate each of these three residues to Asn, one at a time. The V_1/E_t value of all of the single mutant enzymes decreased, with the largest decrease (~1240-fold) exhibited by the H154N mutant enzyme. Mutation of both histidines, H154N/H189N, gave a V_1/E_t ~23700-fold lower than that of the wild type enzyme. An increase in K_{ser} was observed for the H189N, D139N and H154N/H189N mutant enzymes, while the H154N mutant enzyme gave an 8-fold decrease in K_{ser}. For all three single mutant enzymes, V_1/E_t and $V_1/K_{ser}E_t$ decrease at low pH and give a pK_a of about 7, while the V_1/E_t of the double mutant enzyme was pH independent. The solvent deuterium kinetic isotope effects on V_1 and V_1/K_{ser} decreased compared to wild type for the H154N mutant enzyme, and increased for the H189N mutant enzyme, but was about the same as

that of wild type for D139N and H154N/H189N. Data suggest that H154, H189, and D139 play different catalytic roles for SAT. H154 likely serves as a general base, accepting a proton from the β-hydroxyl of serine as the tetrahedral intermediate is formed upon nucleophilic attack on the thioester carbonyl of acetyl CoA. However, activity is not completely lost upon elimination of H154 and thus, H189 may be able to serve as a back-up general base at a lower efficiency compared to H154; it also aids in binding and orienting the serine substrate. Aspartate 139, in dyad linkage with H154, likely facilitates catalysis, by increasing the basicity of H154.

O-acetylserine sulfhydrylase (OASS) is a pyridoxal 5′-phosphate (PLP)-dependent enzyme that catalyzes the second and last step of the biosynthesis of L-cysteine, the conversion of *O*-acetylserine and bisulfide to L-cysteine and acetate via a ping-pong kinetic mechanism. Enteric bacteria have two isozymes of *O*-acetylserine sulfhydrylase, A and B, which have different substrate specificity. The A- and B-isozymes are found under aerobic and anaerobic growth conditions, respectively. The ^{31}P chemical shift of PLP is very sensitive to change in environment as intermediates along the reaction pathway are formed. The ^{31}P chemical shift of the internal and external Schiff bases of PLP in OASS-B are further downfield compared to those of OASS-A, suggesting a tighter binding of the cofactor in the B-isozyme. The chemical shift of the internal Schiff base (ISB) of OASS-B is 6.2 ppm, which is the highest chemical shift reported for the internal Schiff base of a PLP-dependent enzyme. In the A-isozyme, for comparison, the chemical shift is 5.2 ppm, previously the highest reported (Cook, P. F., Hara, S., Nalabolu, S., and Schnackerz, K. D. (1992) *Biochemistry 31*, 2298-2303.). Considering the similarity in the binding sites of the PLP cofactor for both isozymes, torsional strain of the C5-C5′ bond (O4′-C5′-C5-C4) of the Schiff base is proposed to contribute to the further downfield shift. The chemical shift of lanthionine external Schiff base (ESB) of OASS-B is 6.0 ppm, upfield from 6.2 ppm of unliganded OASS-B, while that of serine ESB is 6.3 ppm, which is further downfield. The movements of chemical shift may suggest that torsional strain of PLP is changing as the formation of the ESBs. The line width of ISB is very similar to those of ESBs for OASS-B, indicating that there are no multiple conformers in ESBs of B-isozyme, consistent with the results obtained from UV-visible spectra studies (Chattopadhyay, A., Meier, M., Ivaninskii, S., Burkhard, P., Speroni, F., Campanini, B., Bettati, S., Mozzarelli, A., Rabeh, W. M., Li, L., and Cook, P. F. (2007) *Biochemistry 46*, 8315-8330.).

A method was developed to prepare the apoenzyme of OASS-B, using hydroxylamine as the resolving reagent. Apoenzyme can be reconstituted to holoezyme by addition of PLP. Reconstitution is pseudo first-order and exhibits a final maximum recovery of 81.4%. The apoenzyme shows no visible absorbance, while the reconstituted enzyme has a UV-visible spectrum that is nearly identical to that of the holoenzyme. Steady-state fluorescence spectra (with excitation at 298 nm) gave emission of the apoenzyme that is 3.3-fold higher than the emission of either the native or reconstituted enzyme, suggesting that PLP is a potent quencher of tryptophan emission.

Chapter 1

Introduction

C1.1 Biosynthesis of Cysteine

Sulfur exists in its elemental state and a wide range of oxidation and reduction states. Interconversion between oxidized and reduced forms of sulfur occurs in various organisms and the pathways for these interconversions are different among species, scheme C1-1. Cysteine, an important sulfur-containing amino acid, is closely related to those pathways with respect to the route for its synthesis. In mammals, L-cysteine is synthesized from homocysteine, a derivative of methionine (*1*). Methionine is an essential amino acid for mammals, which makes cysteine an indirectly essential amino acid, while in bacteria， plants and fungi, L-cysteine can be obtained by *de novo* synthesis from inorganic sulfur (*2*-*6*).

The *de novo* synthesis of L-cysteine has an essentially identical pathway for all the sulfate-assimilating organisms (*7*). The sulfur source for this process is inorganic sulfate, which is taken up by cells and reduced to sulfide via the sulfate reduction pathway (*3*). Sulfide then reacts as a substrate for the final enzyme-catalyzed reaction to produce L-cysteine. The genes participating in all steps of the pathway (the cys regulon) have been described in detail for both *Escherichia coli* and *Salmonella enterica* (*3*).

C1.1.1 Sulfate Reduction Pathway in Enteric Bacteria

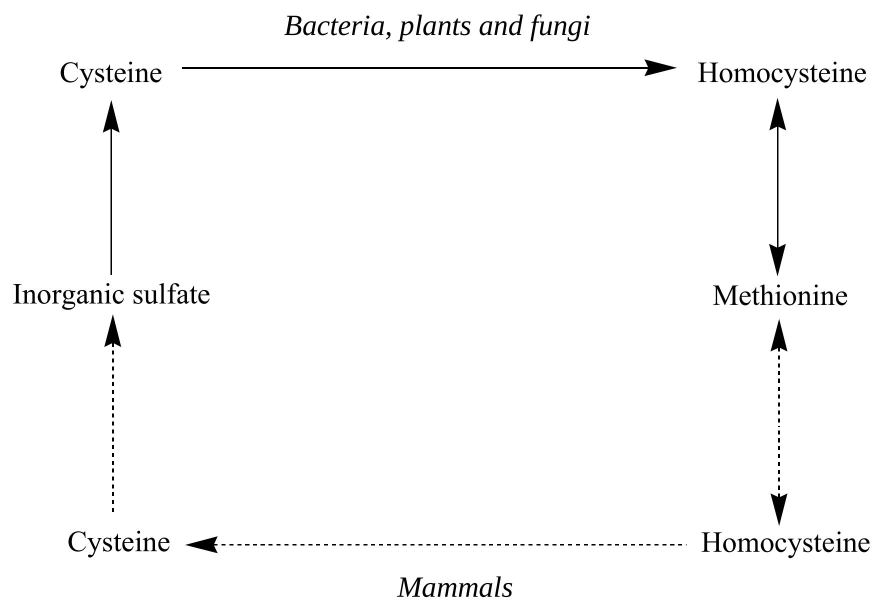

Scheme C1-1. Sulfur interconversion among species.

The sulfate reduction pathway for enteric bacteria begins with the uptake of sulfate and ends with the generation of sulfide. The sulfate uptake process is carried out by sulfate permease, which is an efficient enzyme for transport of both sulfate and thiosulfate into the cell (*8*). The contiguous genes, *cysP*, *cysT*, *cysW* and *cysA*, and the unlinked gene, *sbp* encode the components of sulfate permease from *E. coli* and *S. typhimurium*(*3*). The products of *cysT* and *cysW* genes span the membrane to form a channel for the transport of sulfate and related ions, the *cysA* gene encodes a hydrophilic membrane-associated ATP-binding protein, and in the periplasm, two separate binding proteins for sulfate and thiosulfate are encoded by the *sbp* gene and the *cysP* gene, respectively (*9-11*). Each of these two binding proteins has a leader sequence to aid in ion transport from the inner membrane into the cytoplasm (*12*).

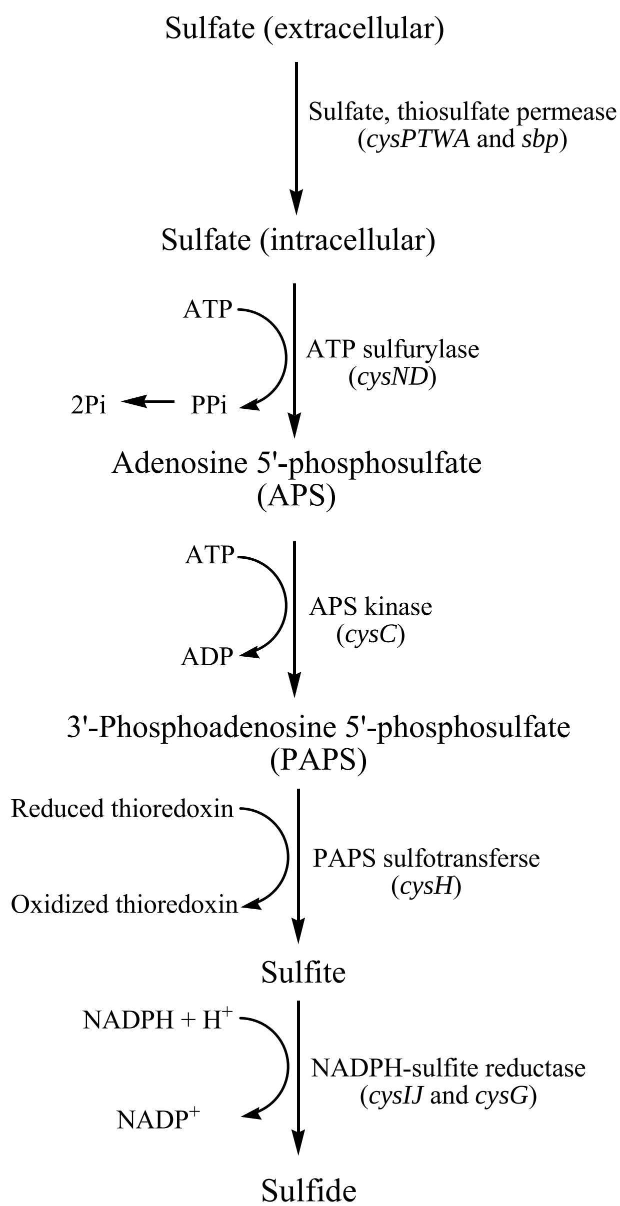

Scheme C1-2. Sulfate reduction pathway in enteric bacteria. The genes for corresponding enzymes are labeled beside the enzyme name.

Activation and reduction reactions for sulfate are carried out following its uptake, which is necessary for sulfate to be utilized for metabolic purposes, scheme C1-2. Once sulfate is in the cell, it is activated by ATP sulfurylase by forming a mixed anhydride with AMP (*13*). ATP sulfurylase is a heteroctamer of four catalytic subunits and four regulatory subunits(*14*). It uses MgATP and sulfate as substrates to produce adenosine 5′-phosphosulfate (APS) and PPi. The equilibrium constant for this conversion is approximately 10^{-8} in solution (*13*). Since the equilibrium constant is very low, which means the reaction is energetically unfavorable; the inorganic pyrophosphate produced is hydrolyzed by inorganic pyrophosphatase to help drive the reaction toward APS formation, and the hydrolysis of GTP by the Ras-like regulatory subunit is coupled to form an AMP-(ATP sulfurylase) complex, the intermediate that gives APS once attacked by sulfate (*15-18*). The APS is then phosphorylated by dimeric APS kinase to produce 3′-phosphoadenosine 5′-phosphosulfate (PAPS) via a second MgATP-dependent phosphorylation; a phosphoenzyme intermediate is thought to be important for this reaction (*19, 20*). Sulfite is then generated by PAPS sulfotransferase, which is a homodimeric enzyme (*21*). This enzyme catalyzes the transfer of the sulfonyl moiety of PAPS to one of the thiols of thioredoxin to form –S-SO_3 acceptor, which generates oxidized thioredoxin and sulfite (*22, 23*). The final step of the sulfate reduction pathway is catalyzed by sulfite reductase, which reduces the sulfite to sulfide via a six-electron reduction. The sulfite reductase reaction is complex; the enzyme has two different subunits, α, a flavoprotein with either FMN or FAD bound, and β, a hemoprotein with a Fe_4S_4 cluster and siroheme components (*24*). The overall stoichiometry of the enzyme complex is $\alpha_8\beta_4$, with four FMN and four FAD bound to the eight α subunits. Electron transfer for this reduction reaction is from NADPH $\rightarrow$ FAD $\rightarrow$ FMN $\rightarrow$ Fe_4S_4 $\rightarrow$ siroheme $\rightarrow$ sulfite (*25, 26*). The sulfide is thus generated and ready for the final biosynthesis of cysteine in enteric bacteria.

1.1.2 Cysteine Biosynthesis in Enteric Bacteria

The biosynthesis of L-cysteine in enteric bacteria proceeds via a two-step pathway, scheme C1-3. Serine acetyltransferase (SAT) catalyzes the first step. It acetylates the β-hydroxyl of L-serine using acetyl CoA as the acyl donor and produces *O*-acetyl-L-serine (OAS) and CoASH (*27*). In the second step, OAS and sulfide are converted by *O*-acetylserine sulfhydrylase (OASS) to L-cysteine and acetate (*28*). In addition to the two-step biosynthetic pathway, L-cysteine can also be obtained from more reduced forms of sulfur, such as thiosulfate .

The regulation of cysteine biosynthesis in enteric bacteria, *E. coli and S. typhimurium*, has been well documented. There are several means for regulating cysteine biosynthesis, which includes gene regulation, feedback inhibition by the end product, cysteine, and enzyme degradation (*3*). A regulon is formed by the genes in *S. typhimurium* that encode the enzymes for the cysteine biosynthetic pathway. The following genes are included in the cysteine regulon: *cysPTWA* and *sbp* (sulfate permease), *cysND* (ATP sulfurylase), *cysC* (APS kinase), *cysH* (PAPS sulfotransferase), *cysIJ* (sulfite reductase), *cysG* (siroheme synthesis), *cysK* (*O*-acetylserine sulfhydrylase-A), *cysM* (*O*-acetylserine sulfhydrylase-B), *cysE* (serine acetyltransferase), and *cysB* (regulatory protein). Overall, the genes are sorted into positively regulated operons, the negatively autoregulated *cysB* gene, and the nonregulated *cysE* and *cysG* genes.

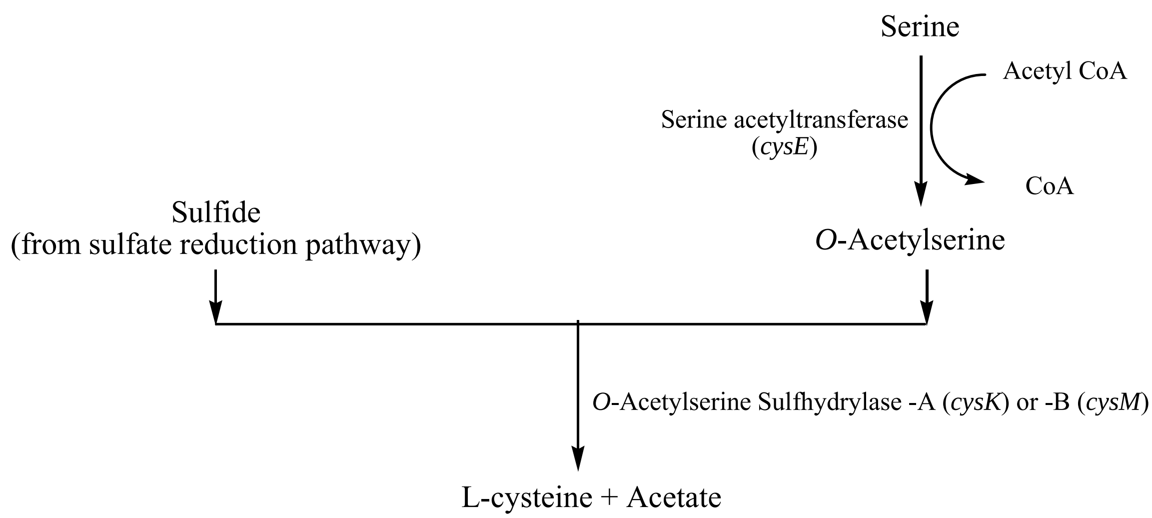

Scheme C1-3. Two-step pathway for L-cysteine biosynthesis in enteric bacteria

Three factors are required for high level expression of the cysteine regulon: sulfur limitation, the presence of OAS to give NAS as inducer and the *cysB* protein (*3*). The c*ysB* protein acts as a tetramer to facilitate transcription initiation by binding upstream from the positively regulated promoters and it also regulates its own synthesis by binding to the promoter of the *cysB* gene and inhibiting transcription (*3*). The *cysE* and *cysG* genes are not regulated by the *cysB* protein although *cysE* is required for OAS synthesis. Thus these two genes are not considered as parts of the cysteine regulon. Increased levels of sulfate, sulfide, cysteine or cystine decrease the activities of the enzymes in the pathway, while the maximum derepression was shown by djenkolic acid and reduced glutathione. *O*-Acetyl-serine is not only the precursor of cysteine; it can also form *N*-acetyl-serine by intramolecular rearrangement, which enhances transcription of the cysteine regulon by binding to the *cysB* protein, and this binding action is opposed by sulfide (*29*).

Serine acetyltransferase is inhibited by the end product, cysteine, which is the major physiologically significant form of kinetic regulation in the pathway. The K_i of cysteine for SAT is about 1 μM at 0.1 mM acetyl CoA, whether enzyme is free or in complex with OASS (*30*). Multiple SAT isoforms exit in plants in at least three cellular compartments, cytosol, chloroplast and mitochondria with differential sensitivity to the inhibition by L-cysteine (*31, 32*). Regulation of cysteine biosynthesis also differs depending on the subcellular compartment via feed back inhibition of SAT (*33*). A good example of these differences is demonstrated in *Arabidopsis thaliana*. The SAT isoforms in the chloroplast and mitochondria are insensitive to the feedback inhibition, while the cytosolic isform shows high sensitivity to inhibition (*34*). Research on SAT from *Haemophilus influenzae* (*Hi*SAT) indicates that L-cysteine is a competitive inhibitor against both substrates in the direction of L-serine acetylation (*35*) and the crystal structure of *Hi*SAT in complex with L-cysteine reveals the structural basis for the competitive inhibition (*36*). All of the above evidence proves that cysteine is a potent and diverse inhibitor that regulates its own biosynthesis.

On the other hand, OASS is partially inhibited by its substrate, sulfide, with a K_i of about 10 μM (*27, 29, 37, 38*). This substrate inhibition is proposed to control the runaway cysteine biosynthesis when the concentration of cysteine is low (*38*).

1.1.3 Cysteine Synthase

A multienzyme complex called cysteine synthase is formed *in vivo* by physical association of SAT and OASS (*30*). Only 5% of the total cellular OASS activity comes from the complex, while the remaining 95% of the OASS activity comes from uncomplexed OASS (*30*). The cysteine synthase complex dissociates to free SAT and OASS when the concentration of OAS is greater than 10^{-4} M, but in the absence of OAS, the resolved SAT and OASS can be reconstituted by combining the component enzymes (*30*). The cysteine synthase complex is composed of a single ~160,000 Da hexamer of SAT (*39*) and two 69,000 Da dimers of OASS-A (*40*). Unlike tryptophan synthase, cysteine synthase does not channel its intermediate product, OAS, between the active sites of the two component enzymes. In contrast, OAS is released into solution and must reassociate with OASS to produce L-cysteine (*41*).

The role of the cysteine synthase complex is still not fully understand and is under investigation. Some mutant and truncated forms of SAT have been studied to provide more insight into the function of the complex. An M256I SAT mutant enzyme from *E. coli* SAT shows lower susceptibility to cysteine inhibition but it can still associate with OASS to form the cysteine synthase complex (*42*). A truncated *E. coli* SAT, missing the last twenty amino acid residues from the C-terminus, will not form a complex with OASS-A, although it is still active and shows a sensitivity to cysteine inhibition similar to the M256I mutant enzyme (*42*). Further studies have shown that the 20 amino acids of the truncated SAT are at least partially responsible for the interaction with OASS-A to form the complex (*43*). An investigation carried out via the yeast two-hybrid system, suggests that the interaction of SAT from *A. thaliana* with OASS results from the C-terminus of SAT (*44*). For the mitochondrial isoform of SAT, however, the C-terminus has a bifunctional role, and is important for both the transferase activity and the interaction with OASS (*45*).

The C-terminal region of SAT is well conserved (*44*) in bacteria and plants, and an aspartic acid residue and a glutamic acid residue, located less than 10 residues from the C-terminus, are considered key amino acids for the interaction between SAT and OASS (*46*). Studies of the C-terminal deletion mutants of *E. coli* SAT indicate that the last ten amino acid residues of SAT are involved in complex formation, but not involved in regulation, while studies of residues 11-20, indicate this region is partially responsible for the sensitivity to L-cysteine's feed back inhibition (*46*). In addition, several amino acids around Met256 are also thought to be related to the feed back inhibition by participating in the conformational change involved in the inhibition (*43, 47*).

OASS-A is only 50% active in the cysteine synthase multienzyme complex compared to its free form (*3*). The presence of OASS-A, however, is in a large excess to SAT in higher plants (*48-50*) and bacteria (*27*), which ensures the formation of the cysteine synthase complex and the overall synthesis of L-cysteine (*46*). SAT from *A. thaliana* shows a high propensity to form high-molecular mass aggregates and tends to be unstable in solution, while the presence of OASS can prevent this aggregation (*34*). The maximum production of L-cysteine in this pathway is achieved with < 60-fold excess of OASS.

Recently, the crystal structure of OASS in complex with a C-terminal peptide required to form the cysteine synthase complex has been determined (*51*). This 10-residue peptide binds to the active site of OASS from *H. influenza* (*Hi*OASS) and its C-terminal carboxyl group occupies an anion binding pocket, which is also the binding pocket for the α-carboxylate group of *O*-acetyl-serine, the amino acid substrate for OASS (*51*). These results provide a reasonable explanation for the dissociation of cysteine synthase complex to its component enzymes caused by OAS as well as the partial inhibition of OASS activity when it is in complex. Evidence, using pyridoxal 5′-phosphate fluorescence as a probe, indicates that binding of SAT by its C-terminal decapeptide to the α-carboxyl subsite of *Hi*OASS triggers the conformational change from the open to closed conformation of OASS (*52*). To better understand the mechanisms involved in the cysteine synthase complex formation, gel chromatography and surface plasmon resonance technique were employed to study *Ec*SAT (SAT from *E. coli*) mutant enzymes. Several C-terminal residues of *Ec*SAT, Ile273, Glu268 and Asp271, appear to be essential for the complex formation (*53*).

Although studies of site-directed and truncation mutants of SAT have provided useful information on the formation of the cysteine synthase complex, the only significant advantage for complex formation appears to be an increase in stability of SAT; complex formation protects the SAT from cold inactivation and proteolysis (*54*). However, it is still unknown why there is an excess of OASS-A to SAT (*30, 55*). Another finding is that sulfide inhibits the dissociation of the complex by binding tightly to the interaction site (*38, 53*). So the increased stability of the complex to OAS in the presence of sulfide may be part of the regulation of the L-cysteine biosynthetic pathway (*56*) and is an interesting topic for further investigation.

1.2 Serine Acetyltransferase

Serine acetyltransferase catalyzes the first step in the two-step pathway for L-cysteine synthesis in bacteria and higher plants (*27, 57*). SAT is encoded by the *cysE* gene and not considered a component of the cysteine regulon. It can form a multienzyme complex, cysteine synthase, with OASS (*30*). SAT catalyzes the rate-limiting step in the two-step pathway and the amount of SAT is low relative to OASS (*30, 57*).

1.2.1 Structure of SAT

SAT belongs to the hexapeptide acyltransferase superfamily. This family is known to have imperfect tandem repeats of a hexapeptide sequence described as [LIV]-[GAED]-X_2-[STAV]-X (*58-60*). These repeat sequences encode the folding of an unusual left-handed parallel β–helix (LβH) domain (*61*), which is a large left-handed coil as if wound around the surface of an equilateral prism. Three to five β-stands, depending on the enzyme, form the β–sheets and three of these flat parallel β-sheets form the faces of the helical prism.

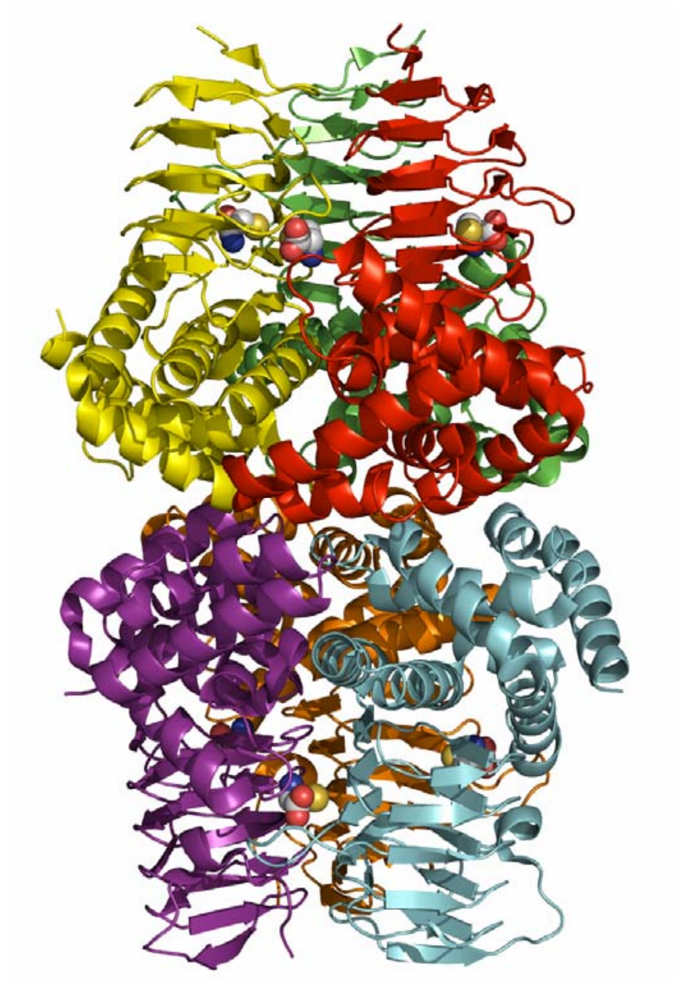

Figure C1-1. *Hi*SAT with cysteine bound. Two trimers, (green, yellow and red) and (purple, orange and cyan), form a dimer. The binding sites of cysteine are shown. This figure was created using Pymol from DeLano Scientific LLC. The structure used in this figure has access number of 1SSQ in the Protein Data Bank.

The X-ray crystallographic structure of SAT from *H. influenzae* has been determined by two independent groups. The crystal structure of *Hi*SAT apoenzyme and its binary complexes with cysteine and CoA were obtained by Roderick *et al.* at a resolution of 2.15

Å, 1.85 Å, and 2.00 Å, respectively (*36*). A structure of the apoenzyme of *Hi*SAT was also solved to 2.7 Å by Shapiro *et al.* (*62*).

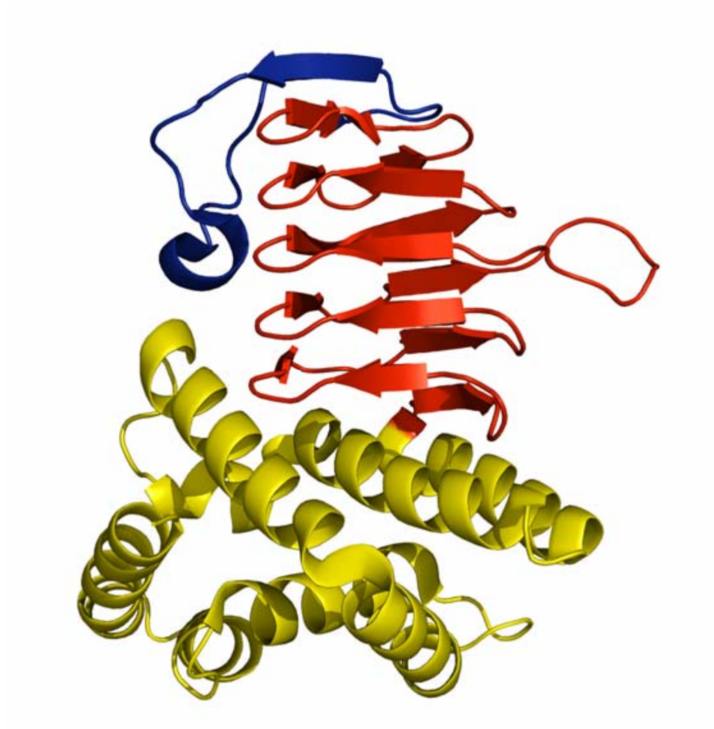

Figure C1-2. A *Hi*SAT monomer. The α–helical N-terminal domain is in yellow. The other two domains, left-handed parallel β-helix domain and C-terminal segment, are in red and blue, respectively. This figure was created using Pymol from DeLano Scientific LLC. The structure used in this figure has access number of 1SSQ in the Protein Data Bank.

Most enzymes containing the β–helix domain are reported to have a trimetric structure (*63-65*). However, *Hi*SAT displays a hexameric structure, arranged as a dimer of trimers, Fig. C1-1. There are three domains in each of the 267 residue subunits: a largely α–helical N-terminal domain, a left-handed parallel β-helix domain and a C-terminal segment, Fig. C1-2. In the third coil of the LβH domain, residues 179-189 extend out to form a loop located between two adjacent LβH domains, one from each of the two subunits. The C-terminus residues 258-276, are not visible in any of the *Hi*SAT structures, although the crystals were composed of protein with full length, indicated by the analysis of mass spectrometry (*36, 62*).

Interactions to form the trimer of *Hi*SAT are extensive, from the β-helices and α–helical N-terminal domains. The interactions between β-helices are mainly polar, while interactions between the α–helical N-terminal domains are mostly hydrophobic, and includes Met22, Leu23, Phe26 and Tyr100 of one subunit and Pro 52, Ile53, Pro55 and Try127 of the related subunit (*62*).

In the hexameric structure of *Hi*SAT, the two trimers are positioned head to head, with a staggered orientation such that one subunit of each trimer interacts with two subunits from the related trimer. This twofold symmetry interface is assembled by ionic, hydrophobic and hydrogen-bonding interactions. As a result of the formation of the twofold and three fold interfaces, a cavity is formed in the center of *Hi*SAT, with dimensions of 40 Å from top to bottom (parallel to the threefold axis), and 18 Å across (perpendicular to the threefold axis) (*62*).

All of the residues involved in the interactions at the trimer-trimer interface are from approximately 80 amino acids from the N-terminal extension, which is only formed in a subset of SATs. It is possible to separate the SATs into two categories: those that have the N-terminal extension and adopt a hexameric structure and those that do not and are most likely to be trimeric (*62*).

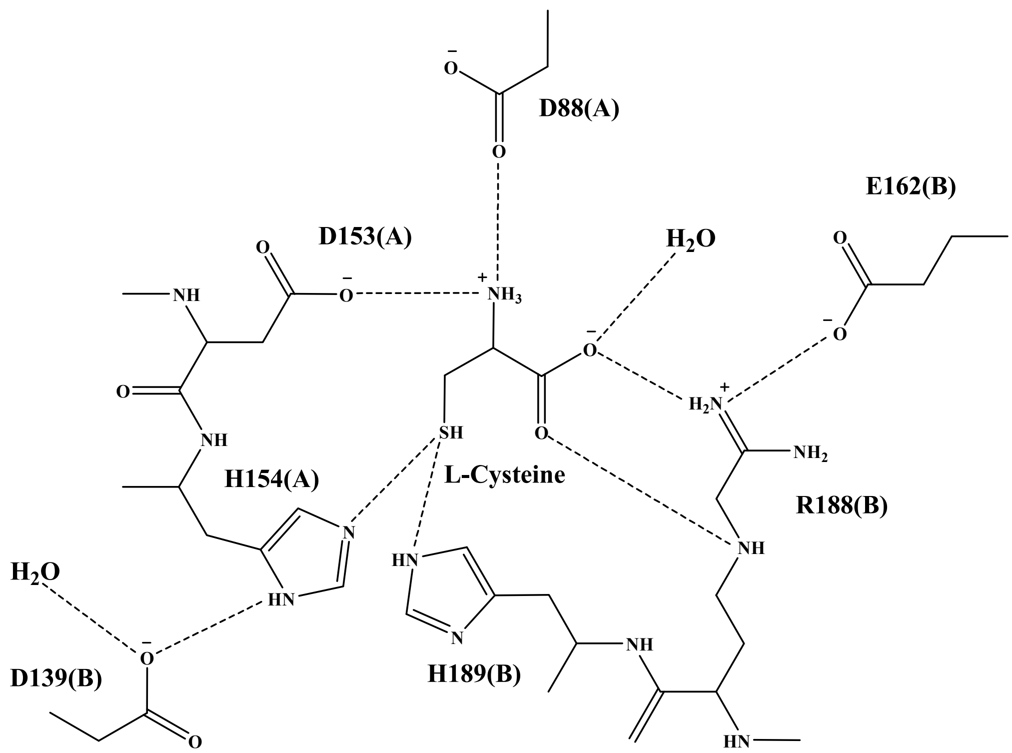

Scheme C1-4. The interactions of *Hi*SAT with its feedback inhibitor, L-cysteine. The A and B here indicate two adjacent subunits, respectively.

The binding pocket for the feedback inhibitor, cysteine, is formed by the extended LβH loop from one subunit (A) and two other loops from an adjacent subunit (B). One of these two loops is from N-terminal domain, joining helices α5 and α6, and the other one is an LβH loop inserted at the T2 turn of coil 2. Detailed interactions between *Hi*SAT and L-cysteine are shown in scheme C1-4. Two histidine residues, H154(A) and H189(B), are located on either side of the cysteine thiol and within hydrogen-bonding distance to it; the H154(A):D139(B) hydrogen-bonded pair forms a dyad. Three other residues, R188(B), D88(A) and D153(A) interact with cysteine as shown to neutralize charge on the α-amine and α-carboxylate. The side chain of R188(B) interacts with carboxyl group of cysteine; whereas D88(A) and D153(A) are responsible for the interactions with cysteine's amino group. R188(B) interact with E162(B), too. Alignment of the amino acid sequences of fifteen SATs (*62*) indicates that all of these residues, with the exception of D139(B), are completely conserved; D139(B) can be replaced by glutamate.

The CoA binding site in *Hi*SAT is in a crevice between β-helices of two adjacent subunits. Carbonyl groups of the pantothenyl arm of CoA form hydrogen bonds with A200(A) and A218(A). Its amide groups form hydrogen bonds with the peptide oxygen of the extended loop residues, G180(B) and T181(B). The position of the CoA thiol group is close to the H154(A) 3.6 Å. A superposition of the cysteine and CoA binding complex structures shows that the distance between thiol groups of cysteine and CoA are within 2.9 Å and both thiol groups are very close to the N_ε of H154(A). The proximity of the cysteine binding site to the CoA thiol group as well as the structural similarity between serine and cysteine suggests that the cysteine binding site is the active site for serine. This conclusion is supported by both the kinetic and microcalorimetric data obtained using serine analogs (*66*) and the structures of four other hexapeptide acetyltransferases (*63-65, 67*). The substrate binding sites of these four enzymes are located between two adjacent LβH domains and are close to the CoA thiol group, which is identical to the binding characteristics of the cysteine pocket of *Hi*SAT.

Superposition of the cysteine and CoA binding complexes indicates that with cysteine bound, the CoA site is no longer available, i.e., there is a competition for binding to the extended LβH loop by the C-terminal segment in the cysteine complex and the pantothenyl arm of CoA. Specifically, residues 254(A)-257(A) of the C-terminal segment occupy the same position as the pantothenyl arm of CoA, with the hydrophobic side chain of F256(A) occupying the adenine binding site of the cofactor. In the cysteine binding complex, the amide nitrogen of G180(B) forms a hydrogen bond with the cysteine thiol and the side chain of T181(B) forms a hydrogen bond with the peptide group of Q254(A) of the C-terminal segment. In the CoA complex, the interactions of G180(B) and T181(B) are different; two hydrogen bonds are formed between the peptide oxygen of these two residues and two pantothenyl amide groups of the cofactor. In addition, the solvent-accessible surface area of *Hi*SAT is reduced by 93% upon binding of the cysteine inhibitor, leaving no apparent diffusion path from the enzyme.

The structures of the *Hi*SAT:cysteine and *Hi*SAT:CoA binding complexes provide an explanation for the potent inhibition by cysteine. In addition to the direct competition between cysteine and serine, binding of cysteine also locks the C-terminal segment and the extended LβH loop by the interactions between them, which blocks access to both substrates of *Hi*SAT. Kinetic and calorimetric studies of *Ec*SAT (*27, 30, 66*) and *Hi*SAT (*35*) are consistent with this explanation. In these studies, the reduced affinity of serine and acetyl CoA are both observed upon binding of cysteine. Data from cysteine-desensitized mutant *Hi*SATs are also consistent with the above explanation. All of the mutant enzymes exhibit an activity loss, and the mutations are either at active site residues near the loops that close to generate the active site, or in the C-terminal loop, which is supposed to stabilize the closed conformation (*46, 47, 54, 68*).

A crystal structure of *Sc*SAT is also available (*69*) and is very similar to that of *Hi*SAT. Both enzymes are hexameric and share a 70% sequence identity with each other. Although several SAT structures have now been solved, no structure of a SAT with serine or acetyl CoA bound has been obtained. These would be invaluable, and would aid in studies of the mechanism of SAT.

1.2.2 Kinetic Mechanism of SAT

A steady-state random kinetic mechanism was proposed for *Ec*SAT on the basis of initial rate studies on both reaction directions (*70*). The results of equilibrium isotope exchange experiments as well as the pre-steady-state analysis ruled out a ping pong mechanism for *Ec*SAT. The random mechanism for *Ec*SAT is also in agreement with the results obtained from substrate analogue and microcalorimetric studies (*40, 66*). It is also consistent with the sequential mechanisms found for all of the other LβH acyltransferases (*40, 64, 67, 71*).

Recently, a sequential kinetic mechanism was also proposed for *Hi*SAT (*35*). The mechanism is equilibrium ordered at pH 6.5, with AcCoA binding prior to serine, while at pH 7.5, a steady-state ordered mechanism is observed, showing a near parallel initial velocity patterns.

The change in mechanism of *Hi*SAT as a function of pH is thought to result from pH dependent change in reactant affinity. Such pH dependent mechanism changes are also found in creatine kinase. At low pH, the kinetic mechanism of creatine kinase is equilibrium ordered, with MgATP binding prior to creatine (*72*), while at neutral pH, a steady-state random mechanism is shown (*73*), and this mechanism changes again to rapid equilibrium random at high pH (*74*).

Though K_{serine} and K_{OAS} are 13 mM and 24 mM at pH 6.5, respectively, the *Hi*SAT is a good enzyme in both reaction directions, with k_{cat} values of 1080 ± 170 s^{-1} in the forward reaction direction and 300 ± 30 s^{-1} in the reverse reaction direction (*35*). The equilibrium constant for *Hi*SAT, as calculated by the Haldane relationship at pH 6.5 is in agreement with the pH independent equilibrium constant of 15 measured directly (*35, 75*).

1.2.3 Rate-limiting Steps

Detailed studies of rate-limiting steps were carried out for *Hi*SAT using solvent deuterium isotope effects (SKIEs) and proton inventory methods (76). The SKIEs are measured as 1.9 and 2.5 to V and V/K_{serine}, respectively, and a linear proton inventory suggests a single proton is in flight in the rate-limiting step of the reaction (*77*). This rate-limiting step is likely the nucleophilic attack by the serine hydroxyl group on the acetyl thioester, with a general base accepting a proton. However, this step is not the only rate limiting step for the overall reaction, since the SKIE on V is larger than that on V/K_{serine}. If SKIE of V is assumed as the intrinsic solvent kinetic isotope effect, the relative rate of 1.5 would be calculated for the release of CoA compared to the proton transfer.

1.2.4 Chemical Mechanism of SAT

pH-rate profile studies have been utilized to probe the chemical mechanism of *Hi*SAT (*76*). The pH dependence of *V/K* reflects the protonation state of group(s) on free enzyme and/or reactant responsible for binding and/or catalysis, while the pH dependence of *V* reflects groups required for catalysis. A group with a p*K* of 6 is shown in the V/K_{AcCoA} pH-rate profile. Since the *V/K* for the first substrate bound in the ordered mechanism, it is the on-rate constant for AcCoA, and this group is thought to reflect a binding group for AcCoA. However, no ionizable residues with a p*K* around 6 are found in the CoA binding site. The closest one is the 2′-phosphate group of CoA, which may be the binding group for AcCoA but still need to be further investigated.

The V_1/K_{serine} and V_2/K_{OAS} pH-rate profiles decreases at pH below a single pK value of ~7, which suggests a single residue may acts as a general base to accept a proton in both reaction directions and the identity of the p*K*s indicate that there is no perturbation of the p*K* from the environment. The p*K* value of 6.8 observed in V_1 profile is slightly lower than the p*K* of 7.2 observed in the V_1/K_{serine} profile, which reflects the slow release of CoA. The release of AcCoA from the *Hi*SAT:AcCoA complex may also be a rate limiting step due to the difference in p*K*s observed for the V_1 and V_2 pH-rate profiles, and the difference in p*K*s observed for the V_2 and V_2/K_{OAS} profiles.

Finally, a chemical mechanism for *Hi*SAT is proposed on the basis of the pH-rate profiles and the solvent deuterium isotope effect studies (*76*). A single enzyme residue is proposed as a general base to catalyze the reaction. Once both substrates are bound, a nucleophilic attack by the β-hydroxyl group of serine on the thioester carbonyl of AcCoA occurs, with the general base accepting a proton from the side chain hydroxyl group. The carbonyl group is proposed to be stabilized through the reaction by positive dipoles from peptide backbone or side chain hydrogen bonds (*78*). The resulting tetrahedral intermediate then collapses as the general base donates a proton to the sulfur of CoA, to give the final products, OAS and CoA.

Although the chemical mechanism has been proposed, the general base residue and other active site residues important for binding have not yet been identified. Fortunately, the crystal structures of *Hi*SAT, especially the one with cysteine bound, shows several potential active site residues, which could be responsible for substrate binding and catalysis (*36*). From the structure, two residues, H154(A) and H189(B), are likely to be the general base and H154(A) is of primary interest due to its dyad linkage with D139(B), which is mechanistically similar to other LβH enzymes (*60*). The structures also show four possible residues for serine binding, R188(B), E162(B), D88(A) and D153(A).

The general base mechanism of *Hi*SAT is similar to the general mechanism proposed for the other hexapeptide acyltransferases that catalyze a direct attack. This enzyme superfamily shares a number of mechanistic similarities (*60*), including a common active site location, separate subsites in the active site for substrates, and a histidine residue important for catalysis, which is also in a dyad linkage with a carboxylate side chain.

1.3 *O*-Acetylserine Sulfhydrylase

Pyridoxal 5′-phosphate (PLP) is one of the active forms of vitamin B6. It acts as a coenzyme to participate in a variety of reactions related to the metabolism of the amino acids. *O*-acetylserine sulfhydrylase (OASS) is a PLP-dependent enzyme, which catalyzes the last step of the *de novo* biosynthesis of L-cysteine in bacteria and higher plants (*27*). In this step, OASS converts *O*-acetylserine (OAS) and sulfide to L-cysteine and acetate via a ping-pong kinetic mechanism (*29*). The active site PLP in OASS forms a Shiff base linkage with a lysine residue, playing important roles in enzyme catalysis and other aspects, such as enzyme stability and dynamics (*79*-*81*). OASS has two isozymes, OASS-A and OASS-B, existing in enteric bacteria. These two isozymes are expressed differentially, with the A-isozyme found under aerobic and the B-isozyme found under anaerobic growth conditions (*82*). OASS-B is less substrate selective than OASS-A to both amino acid and nucleophilic substrates (*29*). The B-isozyme can especially use more reduced forms of sulfur, like thiosulfate, a physiologic substrate and thus provides an alternative way for cysteine biosynthesis without the need for sulfate reduction (*83*).

OASS is a prospective target for the design of herbicides and antibiotics due to its function in L-cysteine biosynthesis (*84*). Also, the broad substrate specificity of OASS, especially the B-isozyme, makes the enzyme suitable for the production of the novel β-substituted amino acids, which can then be used for the synthesis of pharmaceuticals and agrochemicals (*85-88*). As a result, mechanistic studies of OASS are drawing a lot of interest.

1.3.1 Structure of OASS

1.3.1.1 Structure of OASS-A

The crystal structure of *St*OASS-A without ligands bound has been solved to 2.2 Å (*89*). The enzyme is a homodimer with an active site for each monomer. There are 315 amino acids in a monomer and the homodimer has a M.W. of about 68900 Da. Two monomers interact with each other on the dimer interface and the dimer is arranged as the entries to the two active sites are on the same side.

There are two domains in each monomer, an N-terminal domain, containing residues 1-145 and a C-terminal domain with residues 146-315. A central twisted β-sheet is surrounded by α-helices for each monomer, showing a structure of α/β fold. The active site is deeply buried in the cleft between two domains with a PLP cofactor forming an internal Shiff base with the ε-amino group of K41. The pyridine ring of the PLP cofactor is supported on the back by V40 and fits into the shallow crevice of the active site. Eight hydrogen bonds are formed between the 5′-phosphate of PL P and the functional group of the main chains and side chains of the G176-T180 loop. Thus the 5′-phosphate is tightly anchored in the active site by the hydrogen-bonding network. ^{31}P NMR data suggest that the 5′-phosphate of PLP is dianionic (*90*) and its charge is neutralized by H152 and the dipole of helix 7. The phenolic O3′ of PLP forms hydrogen bond with the amide nitrogen of the side chain of N71 and the Schiff base nitrogen. N71 is also a part of the asparagine loop, which includes residues 68-72. This loop, along with Q142, is proposed to bind to the substrate carboxylate group of the external Shiff base and subsequent intermediates in the reaction pathway. The pyridine nitrogen of PLP is within hydrogen-bonding distance to S272 and the dipole of helix 10, which makes the N1′ of PLP most likely unprotonated. The 3-D structure also reveals that the *re* face of the PLP imine is accessible to the amino acid substrate.

A crystal structure of the K41A mutant enzyme of OASS-A shows an external Schiff base of PLP cofactor with methionine in the active site (*91*). The mutant enzyme was resistant to the reduction of $NaBH_4$, suggesting that the mutant enzyme is in a closed conformation (*79*). A large conformational change was shown by the structure overlay of the free OASS-A and the K41A mutant enzyme, where a subdomain of N-terminal domain closes the active site by the relaxation of its central β-sheet. The cleft of the active site turns into a narrow channel, only allowing the passage of the small molecules, such as the first product, acetate, and the second reactant, bisulfide. Thus the deeply buried external Shiff base is no longer accessible to the bulk solvent and molecules.

The PLP cofactor rotates 13^{o} along its longitudinal axis when forming external Schiff base with methionine in K41A mutant enzyme, which results in a movement of C4′ of PLP toward the entrance of the active site. The side chain of methionine also moves closer to the entrance in the structure of mutant enzyme. A strong hydrogen-bonding network is formed between the asparagine loop and the carboxylate group of the amino acid substrate. Therefore, the closure of the active site is important to properly position the functional groups for catalysis.

A crystal structure of *St*OASS-A with chloride bound at an allosteric site and sulfate bound at the active site has also been solved (*92*). A new inhibited conformation is shown for this structure, which is different with the open and closed conformation of OASS-A. The allosteric site locates at the dimmer interface, indicting that the dimeric structure of OASS-A is not solely responsible for the enzyme stability. The moveable domain, including residue 87-131, positions differently from that in the open and closed forms. The conformational change of the moveable domain prevents the interaction between the asparagine loop and carboxylate group of amino acid substrate, and hinder the formation of the external Schiff base and subsequent chemistry. This structure clearly indicates that OASS-A is regulated by small anions.

1.3.1.2 Structure of OASS-B

The crystal structure of *St*OASS-B without ligands bound has been solved to 2.3 Å and overall is very similar to the structure of the A-isozyme (*93*), Fig. C1-3. It is a homodimer with a M.W. of 64000 Da. For each monomer, there are 303 residues and a PLP, forming a internal Schiff base with the ε-amino group of K41. It has N-terminal and C-terminal domains, too. And it exhibits a α/β fold structure for each monomer, also very similar to that of OASS-A. The average temperature factors of the structure of OASS-B are higher than those of the structure of OASS-A, which indicates that B-isozyme has a higher protein flexibility.

The binding site of PLP cofactor for OASS-B locates in the cleft between two domains with the *re* face of the internal Schiff base facing the active site entrance. The phosphate group of PLP is proposed to be dianionic, neutralized by the dipole of helix 7 and H150. It interacts with the phosphate binding loop, residue 174-178. T176 is the only different residue in the binding loop of OASS-B compared with the loop of A-isozyme. It replaces a glycine residue in OASS-A, but the side chain of T176 doesn't contribute to the interaction of phosphate. The N1 nitrogen of the pyridine ring of PLP forms a hydrogen bond with the side chain of S255 as observed for OASS-A (S272). The amide nitrogen of the side chain of N71 is within hydrogen-bonding distance with O3′ of the PLP cofactor. In addition, V40 supports the *si* face of the pyridine ring of PLP, which is also found in OASS-A.

OASS-B has a less hydrophobic active site in comparison to OASS-A, due to the presence of two ionizable residues, D281 and C280. D281 is above the *re* face of the PLP cofactor and forms hydrogen bond with Y286. It replaces S300 of the A-isozyme. While C280 is a replacement of P299 in OASS-A, contributing a more acidic group to the active site of B-isozyme. Both isozymes have two arginine residues, R99 and R285 at or near the active site.

OASS-B does not show an apparent allosteric binding site at the dimer interface, although it can be inhibited by chloride ion (*29*). The lack of an allosteric site is due to the replacement of C42 in OASS-A by D42 in OASS-B, which results in a negative charge in the interior of the B-isozyme. The transduction of the allosteric signal is thus less possible in B-isozyme in comparision with A-.

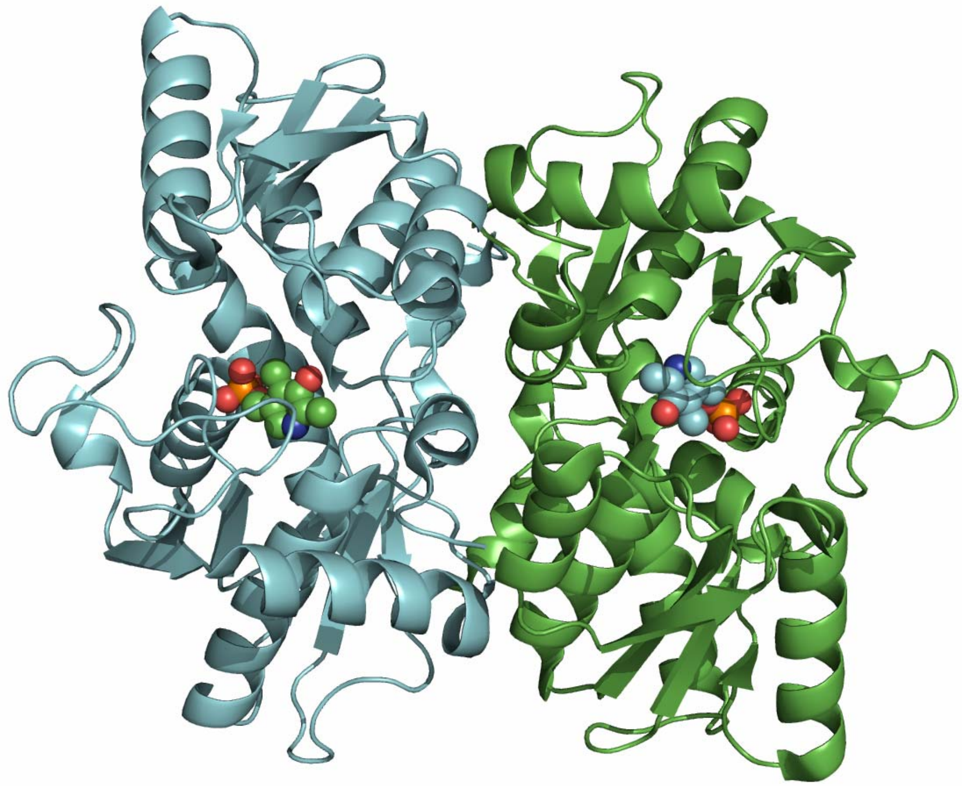

Figure C1-3. Homodimeric structure of *St*OASS-B. PLP cofactor is shown in spheres. This figure was created using Pymol from DeLano Scientific LLC. The structure used in this figure has access number of 2JC3 in the Protein Data Bank.

A subdomain of OASS-B with residue 86-130 is proposed to be the movable domain to close the active site upon binding of the carboxylate group of the amino acid substrate and the asparagines loop (substrate-binding loop) of OASS-B (residue 68-71), which is similar to OASS-A. The position of the substrate-binding loop suggests that the structure of *St*OASS-B without ligands bound is in open conformation. It is consistent with the open conformation reported for wild type OASS-B from *E. coli* (*94*). A mutant enzyme of *Ec*OASS-B (CysM-rke), interestingly, shows a closed conformation with the asparagines loop positioned as that of the closed conformation for A-isozyme. Therefore, S69 of *St*OASS-B is expected to be one of the main residues, responsible for the ligand binding based on the structure similarities of the asparagine loops in two isozymes.

1.3.2 Kinetic Mechanism of OASS

Both isozymes of OASS, OASS-A and OASS-B, have a ping pong Bi Bi kinetic mechanism based on initial velocity studies in the absence and presence of product and dead-end inhibitors (*29*). Both isozymes exhibit competitive inhibition by both substrates. The first substrate OAS binds to the enzyme in external Schiff base form to release acetate as the α-aminoacrylate intermediate form of the enzyme is formed. Bisulfide then adds as the second substrate to the α-aminoacrylate intermediate, and cysteine is released as the final product upon transimination by the active site lysine.

The k_{cat} of OASS-A is 130 s^{-1} using OAS and bisulfide as substrates, and it is limited by the first-half reaction. The second-half reaction of OASS-A is likely diffusion limited, with a first-order rate constant of >1000 s^{-1} obtained at 5 μM bisulfide at pH 6.5 (*95*). TNB is an alternative substrate for bisulfide. The turnover number of OASS-A is decreased to 0.56 s^{-1} when OAS and TNB is used for rate assay and in this case, the second half reaction would be rate-limiting. The k_{cat} of OASS-B is 115 s^{-1} and 8 s^{-1} for substrate pair of OAS/bisulfide and OAS/TNB, respectively. The first-half reaction is supposed to limit the overall reaction for OAS/bisulfide substrate pair and the second-half reaction is the rate-limiting step for OAS/TNB pair, which is qualitatively identical to A-isozyme.

An individual half-reaction is independent of the concentration of the substrate for the other half-reaction in a classical one-site ping pong mechanism. But it is not true for OASS, as OASS-A shows a 4000-fold higher value for V/K_{OAS} when sulfide is the nucleophile compared to that obtained with TNB (*29*). However, regardless of the amino acid substrates used, the *V/K* values for nucleophiles are in agreement. As for OASS-B, 3-fold higher value of V/K_{OAS} is obtained for bisulfide in comparision with that of TNB, and the $V/K_{sulfide}$ values is 6-fold higher when OAS is the amino acid substrate compared to that of BCA.

The AA form of OASS is not stable. It decomposes to free enzyme, pyruvate and ammonia in the absence of nucleophilic substrate. This reaction occurs by the transimination of K41 to displace the AA, which then decomposes into pyruvate and ammonia by a β-elimination reaction. The pH-independent rate of decomposition is 0.1 s^{-1} for OASS-A, about 40-times lower than that of OASS-B, consisting with its more than 10-fold lower k_{cat} value in comparision with B.

1.3.3 Chemical Mechanism of OASS

1.3.3.1 Chemcial Mechanism of OASS-A

OASS-A catalyzes its reaction in two steps, exhibiting an elimination-addition reaction based on its ping pong kinetic mechanism. The resting enzyme is an internal Schiff base form with λ_{max} at 412 nm in UV-visible absorbance spectrum (*90, 96-98*).

After elimination of the β-acetoxy group, the enzyme shows a α-aminoacrylate external Schiff base form, absorbing maximumly at 330 and 470 nm.

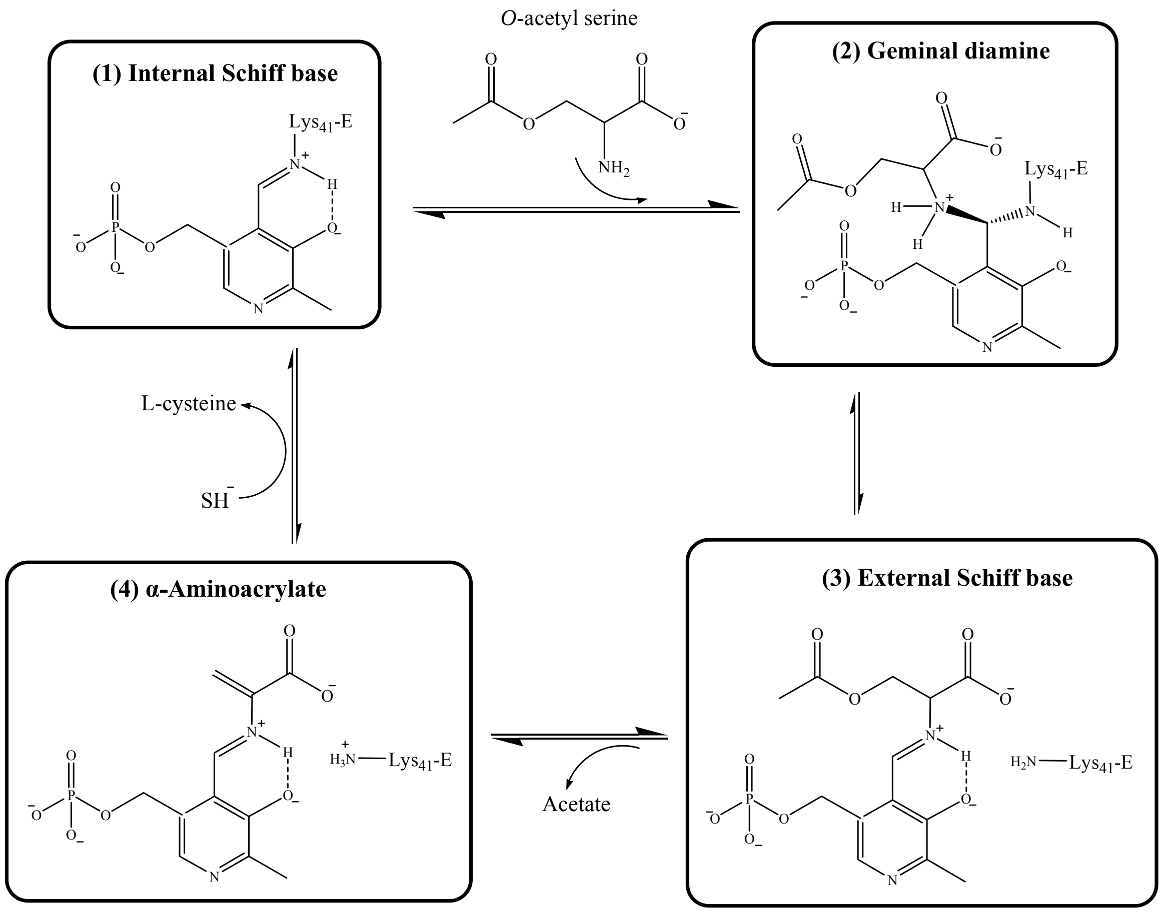

Scheme C1-5. Minimal chemical mechanism of *St*OASS-A.

The pH-rate profile of V/K_{OAS} exhibits a p*K* of 7 on the acidic side, different with the pH-rate profile for V/K_{BCA}, which has pK of 6.7 on the acidic side and 8.3 on the basic side (*99*). A p*K* of 6.9-7.1 on the acidic side is observed on the pH-rate profile of V/K_{TNB}, along with a p*K* of 8.3 on the basic side. Since no ionizable groups in the active site of

OASS-A have a p*K* of ~7 and the elimination of acetate or chloride does not need general base catalysis, the group with a p*K* of ~7 on the acidic side is proposed to be responsible for stabilizing the optimum catalytic conformation of the enzyme when it is unprotonated. The p*K* of ~7 is also observed in the following process. Excitation of OASS-A at 298 nm results in two emission peaks. A peak at 340 nm comes from Trp emission and the other peak at 500 nm is given by the triplet to singlet energy transfer between W51 and the PLP cofactor. The 500 nm peak thus reflects the relative orientation of the two fluorophores. A p*K* of 7 is shown in the pH profile of the enhancement of the 500 nm emission by acetate (*100*). The pH-dependence of interconversion of two conformers of OASS-A also gives a p*K* of 7 in both phosphorescence (*101*) and time-resolved fluorescence studies (*102-104*). The above data of the p*K* of ~7 suggests that the pH-dependent conformational change may be the closure of the active site prior to chemistry. The basic p*K* in V/K_{BCA} profile is assigned as the α-amine of BCA, which needs to be unprotonated for nucleophilic attack on C4′ of the PLP Schiff base. The basic p*K* in V/K_{TNB} profile is proposed to the ε-amino group of K41, acting as a general acid to donate a proton to Cα as the product external Schiff base is formed. The first-order rate constant for decomposition of AA is also pH-dependent, giving a p*K* of 8.2. This p*K* is attributed to the ε-amino group of K41 and is in agreement with the p*K* value shown in V/K_{TNB} profile (*90*).

A general chemical mechanism is proposed for OASS-A using the natural substrate OAS and bisulfide based on the above information, scheme C1-5. In resting enzyme, the active site lysine, K41, forms an internal Schiff base with the PLP cofactor. The enzyme is in open conformation and changes to a closed conformation when the pH is above 7. OAS, the amino acid substrate, binds as a monoanion with its α-amine unprotonated to attack the C4′ of the internal Schiff base. The external Shiff base is then formed via *geminal*-diamine intermediates and the active site is closed by the interaction between the substrate-binding loop and the α-carboxylate of the amino acid substrate. K41 serves as a general base to accept a proton from Cα, which generates acetate in the elimination reaction and ends the first half-reaction. The enzyme now is in α-aminoacrylate Schiff base form in a closed conformation. The active-site is only partially open, but allows diffusion of acetate and the entry of bisulfide. In the second half-reaction, K41 is protonated as bisulfide attacks Cβ of the α-aminoacrylate. The cysteine external Schiff base forms and is followed by a transimination reaction, which gives the cysteine as the final product.

The crystal structure of the K41A mutant of OASS-A indicates that the α-proton of the ESB is directed away from the *si* face of the PLP cofactor and the side chain of methionine is directed away from the *re* face toward the entrance of the active site, which suggests an *anti*-elimination mechanism for AA formation. Since there is no requirement for protonation of the leaving group for OASS-A, an *E2* reaction is suggested compared to an *E1* reaction (*105*). No quinonoid intermediate is observed along the reaction pathway, even using D_2O to slow down the protonation at Cα, which is consistent with the proposed *E2* mechanism since a quinonoid intermediate should be produced in an E1 reaction (*105, 106*). In addition, the presence of the dipole of helix 10 and S272 makes the pyridine nitrogen of the PLP cofactor unlikely to be protonated as mentioned above under structure.

At neutral pH, a primary deuterium isotope effect of 1.7 is obtained at steady-state using OAS-2D. This isotope effect is pH-dependent, increasing to a limiting value of 2.8 at low pH, which indicates stickiness of OAS (*107*). The stickiness factor is calculated to be 1.5, suggesting that the rate of OAS producing AA is 1.5 faster than the rate of OAS dissociating from the enzyme. An isotope effect on the appearance of AA at 470 nm in the pre-steady state is, within error, identical to the value of 2.8 measured at steady state. Thus the value of 2.8 is the intrinsic isotope effect on the abstraction of the α-proton, indicating an early or late transition state in comparison with the value of 6-8 for primary deuterium isotope effects in a symmetric transition state (*108*). A secondary kinetic deuterium isotope effect is measure to be 1.1 with deuterium labeled at C3 of OAS. The value is less than a value of 1.8 predicated for the secondary isotope effect on the equilibrium constant for formation of AA and thus suggests very little change on hybridization at Cβ in the transition state (*109*). An asynchronous transition state is proposed based on the above data, with little bond formation occurring between the ε-amino of K41 and the α-proton of the OAS external Schiff base, and even less bond cleavage taking place between Cβ and the acetoxy oxygen.

1.3.3.2 Chemical Mechanism of OASS-B

OASS-B catalyzes a two-steps β-substitution reaction, similar to the reaction of A isozyme. The internal Schiff base is the resting enzyme, and absorbs maximally at 414 nm in UV-visible absorbance spectra (*93*). Once OAS binds to the enzyme, the AA external Schiff base is given by elimination of the β-acetoxy group, exhibiting λ_{max} values at 327 and 472 nm.

The chemical mechanism of OASS-B is proposed to be qualitatively identical to that of OASS-A. The pH-rate profile of V/K_{OAS} exhibits p*K* values of 6 and 7 on the acidic side, while on V/K_{BCA} profile, two p*K*s with values of 7.6 and 9.0 are shown on the acidic side and the basic side, respectively (*99*). The basic p*K* on V/K_{BCA} profile is attributed to the α-amine of BCA, which needs to be unprotonated for nucleophilic attack on C4′ of the PLP cofactor. The pH-rate profile of V/K_{TNB} exhibits a p*K* of 7.6 on acidic side and another p*K* of 8.7-8.9 on basic side. The p*K* of ~7.6 is proposed to be an enzyme group that needs to be unprotonated to close the enzyme active site for optimum catalysis as a counterpart to the p*K* of ~7 for OASS-A. The p*K* of 8.7-8.9 on basic side of the V/K_{TNB} profile is attributed to the ε-amino group of K41, which needs to be protonated at the beginning of the second-half reaction to donate a proton to the Cα of the AA. The pH-rate profiles on *V* for OAS/TNB and BCA/TNB substrate pairs exhibit a p*K* of 6.5-6.7 on the acidic side and another p*K* of 8.2-9.0 on the basic side. K41 is responsible for both p*K*s since it acts as a general base in the first half-reaction to accept a proton from Cα of the OAS external Schiff base and acts as a general acid in the second half-reaction as mentioned above. The p*K* of 8.2-9.0 is also consistent with the basic p*K* of 8.7-8.9 observed on the V/K_{TNB} profile.

1.4 Research Carried Out in This Dissertation

In this dissertation, roles of H154, H189, and D139 in the active site of *Hi*SAT were investigated using initial velocity studies, pH-rate profiles and solvent deuterium kinetic isotope effects. H154 was proposed to be the general base, accepting a proton from the β-hydroxyl group of serine as the tetrahedral intermediate is formed. H189 was proposed to aid in binding and orienting of the substrate serine. As to D139, it was proposed to facilitate catalysis by hydrogen bonding the proposed general base, H154 to give a catalytic dyad. Data were interpreted in term of the mechanisms of *Hi*SAT.

^{31}P NMR studies were carried out to probe the conformational dynamics of *St*OASS-B. Binding of the PLP cofactor in *St*OASS-B was proposed to change as different intermediates are formed along the reaction pathway. Changes in the orientation of bound PLP are reflected in ^{31}P NMR spectra of those intermediates; NMR spectra are proposed to exhibit differences in chemical shift and line width. In addition, NMR data of *St*OASS-B were proposed to be similar to those obtained for *St*OASS-A, due to the structural similarity of the PLP binding sites of these two isozymes. Data were interpreted in term of the overall mechanism of *St*OASS-B, particularly with respect to binding of PLP in the ISB and ESB forms of the enzyme.

A method was developed to prepare apo *St*OASS-B, using hydroxylamine as the resolving reagent. The apoenzyme is important to furture studies on fluorescence spectroscopy of *St*OASS-B. The properties of the apoenzyme and its reconstitution with

PLP were also studied.

Other research carried out in this dissertation includes fluorescence studies of *St*OASS-B, subcloning and expression of *St*OASS-A, obtaining a p$K_{i(cysteine)}$ profile for *Hi*SAT, and UV-visible and fluorescence studies of K120Q and H152A mutants of *St*OASS-A.

The fluorescence properties of three tryptophans of *St*OASS-B were investigated using site-directed mutagenesis to change each to tyrosine or histidine alone or in pairs. Mutant enzymes were characterized using kinetic and spectroscopic methods, including intial velocity studies, rapid-scanning stopped-flow, UV-visible spectra, steady-state fluorescence spectra, and fluorescence lifetime mesurment. The three tryptophans of OASS-B were proposed to have different contributions to the total fluorescence emission and engery transfer to the PLP cofactor. It was hypothesized that each of the tryptophans has different fluorescence lifetimes and fractional intensities due to their different positions in enzyme and their specific environments and mobilities. The values of lifetime and fractional intensity of these three tryptophans were proposed to change as intermediates are formed along the reaction pathway, reflecting the dynamics of the enzyme during catalysis. Studies on tryptophans in OASS-B will provide detailed information of the conformational dynamic of the enzyme, and thus results in better understanding of the mechanism of the enzyme.

Subcloing and expression of *St*OASS-A were performed to prepare the enzyme for future studies of the A-isozyme. A p$K_{i(cysteine)}$ profile of HiSAT was investigated to explore the binding of cysteine in the enzyme as a competitive and dead-end inhibitor. Data were discussed in term of the different binding of the substrate serine and the inhibitor cysteine in term of the mechanisms of *Hi*SAT. In addition, two *St*OASS-A mutant enzymes, H152A and K120Q, were studied using UV-visible absorption spectra and steady-state fluorescence spectra to provide the roles of these two residues. Data were published in two papers and will not be discussed in this thesis.

Chapter 2

Roles of H154, H189, and D139 in the Active Site of Serine Acetyltransferase from *Haemophilus influenzae*

C2.1 Introduction

Serine acetyltransferase (SAT) catalyzes the conversion of acetyl CoA and L-serine to CoA and *O*-acetyl-L-serine (OAS), the first and rate-limiting step of the biosynthesis of L-cysteine in bacteria and higher plants (*27, 57*).

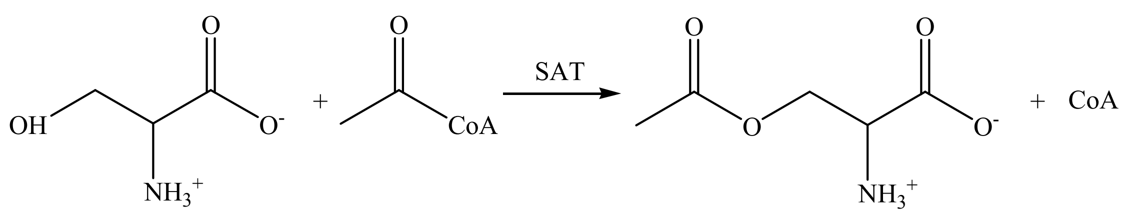

(L-serine) (AcCoA) (OAS) (CoA)

SAT is a member of the hexapeptide repeat acyltransferase superfamily, which have imperfect tandem repeats of a hexapeptide sequence described as [LIV]-[GAED]-X_2-[STAV]-X (*58, 59*). The repeat sequences generate an unusual left-handed parallel β–helix (LβH) domain (*61*), that generates an equilateral prism-like structure. All of the enzymes are trimeric (SAT is a dimer of trimers) with the LβH domains forming a triangular structure. The active site is found at the interface between two LβH domains.

A sequential kinetic mechanism was proposed for serine acetyltransferase from *Haemophilus influenzae* (*Hi*SAT) with AcCoA bound first followed by L-serine, and with release of OAS prior to CoA (*35*). On the basis of the pH dependence of kinetic parameters and solvent isotope effects, a chemical mechanism has been proposed, Fig. C2-1 (*76*). The reaction begins with nucleophilic attack of the β-hydroxyl of serine on the thioester carbonyl of acetyl CoA catalyzed by a general base to give a tetrahedral intermediate. The general base then functions as a general acid, donating a proton to the sulfur atom of CoA, once the tetrahedral intermediate has collapsed to give the products, OAS and CoA.

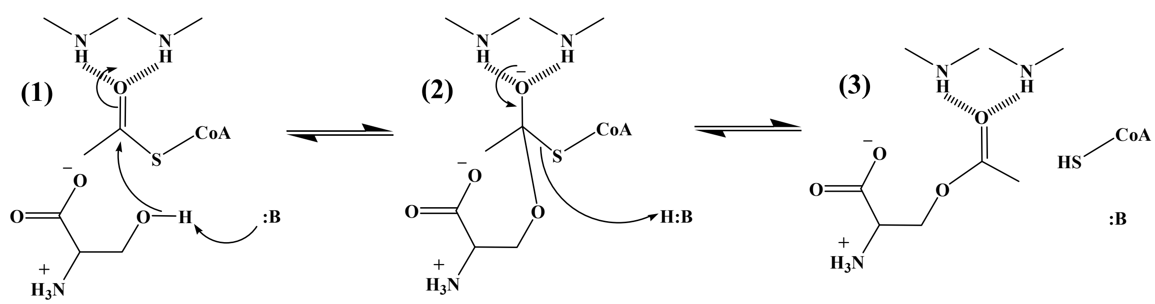

Figure C2-1. Proposed chemical mechanism of *Hi*SAT. (A) E-AcCoA-serine complex. (B) Tetrahedral intermediate. (C) E-CoA-OAS complex.

The crystal structure of *Hi*SAT with cysteine bound at the L-serine subsite of the active site shows H154 and H189 within hydrogen-bonding distance to the cysteine thiol; H154 is in dyad linkage to D139, Fig. C2-2 (*36*). The SAT exhibits mechanistic similarities to other LβH enzymes, which have a His-Asp (Glu) catalytic dyad (*60*). Amino acid sequence alignments of fifteen SATs (*62*) indicate complete conservation of H154 and H189, while D139 can be either Asp or Glu.

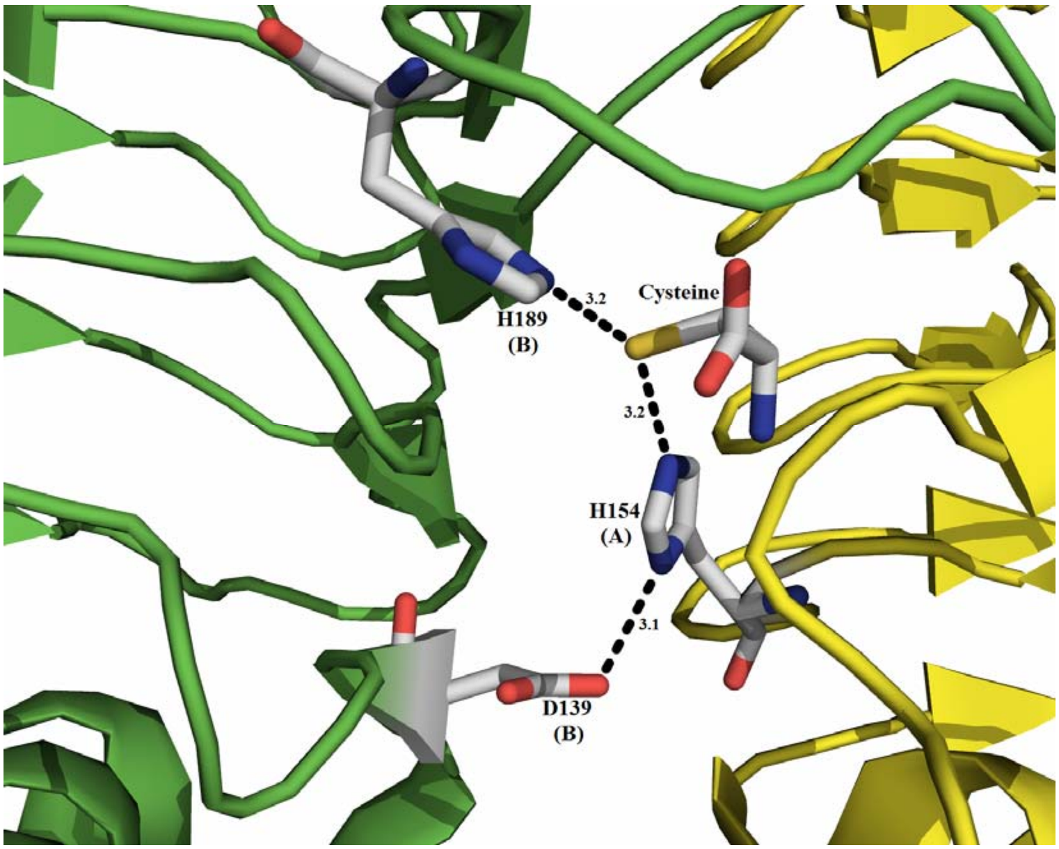

Figure C2-2. Close-up of the active site of *Hi*SAT with cysteine bound. Locations of two subunits of the trimer of *Hi*SAT are shown in yellow and green, respectively. The dashed lines represent potential hydrogen bonds and the numbers close to dashed lines are distances in Å. The (A) and (B) next to numbered residues indicate the subunit that contributes the residue. The figure was created using Pymol from DeLano Scientific LLC. The *Hi*SAT structure with cysteine bound has an access number of 1SSQ in the Protein Data Bank.

In this paper, the roles of H154, H189 and D139 were investigated. Site-directed mutagenesis was used to make three single mutant enzymes by changing these three residues to Asn, one at a time, and a double mutant enzyme, changing H154 and H189 to Asn at the same time. Initial velocity studies, pH-rate profiles and solvent deuterium kinetic isotope effects were carried out to characterize the mutant enzymes. Data are discussed in terms of the overall mechanism of SAT.

C2.2 Materials and Methods

C2.2.1 Chemicals

L-serine, DTNB, and AcCoA were from Sigma. The buffers Mes, Tris, Hepes, and Ches were from Research Organics, Inc. Deuterium oxide (99.9 atom % D) was from Cambridge Isotope Laboratories, Inc. All other chemicals and reagents were obtained from commercial sources, were reagent grade, and were used without purification.

C.2.2.2 Plasmid construction and site-directed mutagenesis

The *cysE* gene encoding *Hi*SAT (GenBank accession number P43886) was cloned into a pET28a vector via the *Nde*l/*BamH*1 sites (*36*). Site-directed mutagenesis was performed using the QuikChange® method to make three single mutant enzymes by changing H154, H189 and D139 to Asn, one at a time, and a double mutant, H154N/H189N, by mutating H189 to Asn in the H154N mutant enzyme. The templates for the single and double mutant enzymes were the recombinant *Hi*SAT plasmid and the mutated H154N plasmid, respectively. The oligonucleotide primers to generate the mutations were listed in Table C2-1. The resulting mutant genes were sequenced at the Laboratory for Genomics and Bioinformatics of the University of Oklahoma Health Science Center to be certain that no mutations other than the one desired were present; none were found. All constructs encoded an N-terminal 6-His-tagged enzyme. Plasmids were transformed into *E. coli* BL21-(DE3)-RIL cells for expression.

Table C2-1. Sequence of oligonucleotide primers

H154N $_f$	GGCCACGGAATTATGTTCGAC**AAT**GCAACAGGTATTGTTGTGG
H154N $_r$	CCACAACAATACCTGTTGC**ATT**GTCGAACATAATTCCGTGGCC
H189N $_f$ [a]	CGGGAAAAGAATCAGGCGATCGT**AAT**CCCAAAGTACGCGAGGGTG
H189N $_r$ [a]	CACCCTCGCGTACTTTGGG**ATT**ACGATCGCCTGATTCTTTTCCCG
D139N $_f$	CAGTAGCTTTCGATGTA**AAT**ATTCACCCAGCGGCG
D139N $_r$	CGCCGCTGGGTGAAT**ATT**TACATCGAAAGCTACTG

Codons for mutation are in bold. Subscripts f and r represent forward and reverse primers, respectively.

[a] These two primers were used to make H154N/H189N double mutant, and the plasmid of H154 is the template.

C2.2.3 Enzyme

The strain containing the mutated plasmid was grown overnight at 37 ^{o}C in 50 mL of LB medium with 30 μg/mL kanamycin. This culture was transferred into 1 liter of

LB/kanamycin medium on the morning of the next day and the cell growth was continued at 30 °C until the A_{600} reached 0.7. IPTG was added to a final concentration of 1 mM to initiate expression. After 4 hours of induction at 30 °C, the cells were harvested by centrifugation at 4,500 *g* for 30 min. The cell pellet was suspended in 50 mM phosphate, 300 mM NaCl and 10 mM imidazole, pH 8.0 and sonicated on ice for 3 min with a 30 s pulse followed by a 1 min rest, using a MISONIX Sonicator XL. The supernatant was obtained by centrifugation at 20,000 *g* for 30 min and then loaded onto a Ni-NTA column with a 6 mL bed volume. The column was washed with 6 volumes of 20 mM imidazole at pH 8.0 and enzyme was eluted with 3 volumes of 250 mM imidazole, pH 8.0. The purified enzyme was then dialyzed against 20 mM Tris, 50 mM NaCl and 10% glycerol at pH 7.5, and stored frozen at –80 °C. The wild type and mutant enzymes, with the exception of D139N, were purified in the same way. For D139N, 10% glycerol was added to sonication, wash and elution buffers and the dialysis buffer was 20 mM Tris, 600 mM NaCl and 50% glycerol at pH 7.5.

C2.2.4 Enzyme assays

In the forward reaction direction, the appearance of CoA was coupled to the production of TNB via a disulfide exchange reaction with DTNB (*110*). Initial rates were calculated using an extinction coefficient of 14,150 $M^{-1}cm^{-1}$ for TNB at 412 nm (*111*). Reactions were carried out at room temperature in 1 cm pathlength cuvettes in a final volume of 0.3 mL. Reaction mixtures contained 100 mM buffer, 0.45 mM DTNB, variable amounts of AcCoA and L-serine, and an appropriate amount of enzyme.

Reaction was initiated by addition of enzyme. A unit of enzyme is defined as the amount of enzyme required to produce 1 μmol of product in 1 min at 25 ^{o}C. The wild type *Hi*SAT was stabilized by adding 100 μg/mL BSA when diluted for use in assays (*35*). Rates were measured using a Beckman DU 640 spectrophotometer to monitor the change in absorbance at 412 nm.

C2.2.5 pH studies

The initial velocity was measured as a function of AcCoA concentration (0.5-5 K_m) at different fixed concentrations of serine (0.5-5 K_m). These experiments were carried out as a function of pH to determine the kinetic parameters, V_1, V_1/K_{ser} and V_1/K_{AcCoA}. The pH was maintained using the following buffers at a concentration of 100 mM in the forward reaction direction: Mes, pH 5.5-6.5; Hepes, pH 6.5-8.5; Ches, pH 8.5-10.0. The pH was measured before and after the reaction with observed changes smaller than 0.1 pH unit.

C2.2.6 Solvent deuterium kinetic isotope effects

Initial velocity studies were carried out as discussed above in H_2O and D_2O at the pH(D) independent region of the V_1, V_1/K_{ser} and V_1/K_{AcCoA} pH(D)-rate profiles. The solvent deuterium kinetic isotope effect (*SKIE*) was then estimated as the ratio of the pH and pD independent values of the parameters. The *SKIE*s were then more accurately obtained by direct comparison of initial rates at a single pH(D) in the pH independent region of the curve.

C2.2.7 Data processing

Data were fitted to appropriate rate equations, using the Marquardt-Levenberg algorithm (*112*) supplied with the EnzFitter program or the programs developed by Cleland (*113*). All of the initial rate data were fitted using equations C2-1 and C2-2, which conform to sequential and equilibrium ordered kinetic mechanisms, respectively. Data for pH-rate profiles that decrease with a limiting slope of 1 at low pH were fitted using equation C2-3, while those that decreased with limiting slopes of 1 and -1 were fitted using equation C2-4. The *SKIE*s data were fitted using equation C2-5, which allows the *SKIE*s on *V* and *V/K* to be equal to one another.

$$v = \frac{VAB}{K_{ia}K_b + K_aB + K_bA + AB} \qquad \text{(C2-1)}$$

$$v = \frac{VAB}{K_{ia}K_b + K_bA + AB} \qquad \text{(C2-2)}$$

$$\log y = \log\left(\frac{C}{1 + \frac{H}{K_1}}\right) \qquad \text{(C2-3)}$$

$$\log y = \log\left(\frac{C}{1 + \frac{H}{K_1} + \frac{K_2}{H}}\right) \qquad \text{(C2-4)}$$

$$v = \frac{VA}{(K_a + A)(1 + F_iE_v)} \qquad \text{(C2-5)}$$

In equations C2-1, C2-2 and C2-5, *v* and *V* represent initial and maximum velocities, respectively, **A** and **B** represent substrate concentrations, K_a and K_b are K_m values for substrates **A** and **B**, respectively, and K_{ia} is the dissociation constant for E-AcCoA. In equation C2-5, F_i is the fraction of D_2O in the solvent, and E_v is the isotope effect minus 1 when the isotope effects on V and V/K are the same. In equations C2-3 and C2-4, y is the value of V or V/K at any pH, while C is the pH-independent value of y, **H** is the hydrogen ion concentration, and K_1 and K_2 are the acid dissociation constants of functional groups on enzyme or substrate.

C2.3 Results

C2.3.1 Kinetic parameters of the mutant enzymes

Initial velocity patterns were obtained by measuring the initial rates at pH 7.3 using variable concentrations of AcCoA and L-serine; data are summarized in Table C2-2. V_1/E_t decreased by about 1240-fold, 19-fold, 11-fold and 23700-fold for H154N, H189N, D139N and H154N/H189N, respectively, compared to wild type. The value of K_{AcCoA} decreased for the H154N, D139N and the H154N/H189N mutant enzymes compared to wild type, while K_{ser} decreased about 8-fold for H154N, but increased by about 7-, 34- and 6-fold for the H189N, D139N and H154N/H189N mutant enzymes, respectively. The largest decrease in V_1/E_t among three single mutant enzymes is observed for H154N, suggesting it is important for catalysis, while H189 and D139, are likely important for both binding and catalysis.

Table C2-2. Kinetic parameters for *Hi*SAT wild type and mutant enzymes at pH 7.3

	V_1/E_t (s^{-1})	$V_1/K_{ser}E_t$ ($M^{-1}s^{-1}$)	$V_1/K_{AcCoA}E_t$ ($M^{-1}s^{-1}$)	K_{AcCoA} (mM)	K_{ser} (mM)
Wild type [a]	360 ± 10[b]	(7.53 ± 0.07) × 10^4	(5.1 ± 0.8) × 10^5	0.7 ± 0.1	4.7 ± 0.4
H154N	0.29 ± 0.02	470 ± 80	1300 ± 400	0.21 ± 0.08	0.6 ± 0.1
(fold change)	-(1240 ± 90)[c]	-(160 ± 30)	-(390 ± 140)	-(3 ± 1)	-(8 ± 1)
H189N	18.7 ± 0.9	590 ± 70	N/A [d]	N/A	32 ± 4
(fold change)	-(19 ± 1)	-(130 ± 20)			+(7 ± 1)
D139N	34 ± 1	200 ± 10	(2.7 ± 0.4) × 10^5	0.12 ± 0.02	160 ± 10
(fold change)	-(10.6 ± 0.4)	-(380 ± 20)	-(1.9 ± 0.4)	-(6 ± 1)	+(34 ± 4)
H154N/H189N	0.0152 ± 0.0004	0.57 ± 0.03	64 ± 3	0.24 ± 0.02	27 ± 2
(fold change)	-(23700 ± 900)	-(132000 ± 7000)	-(8000 ± 1000)	-(2.9 ± 0.5)	+(5.7 ± 0.6)

[a] From Johnson *et al.* (*35*)

[b] Values are ± S.E.

[c] The symbols, - and +, represent decrease and increase, respectively.

[d] N/A is not applicable; K_{AcCoA} is zero in an equilibrium kinetic mechanism.

C2.3.2 pH dependence of kinetic parameters

The pH dependence of the kinetic parameters of the mutant enzymes were obtained by measuring initial velocity patterns as a function of pH. All of the mutant enzymes are stable over the pH range studied; the H154N/H189N mutant enzyme is inactive below pH

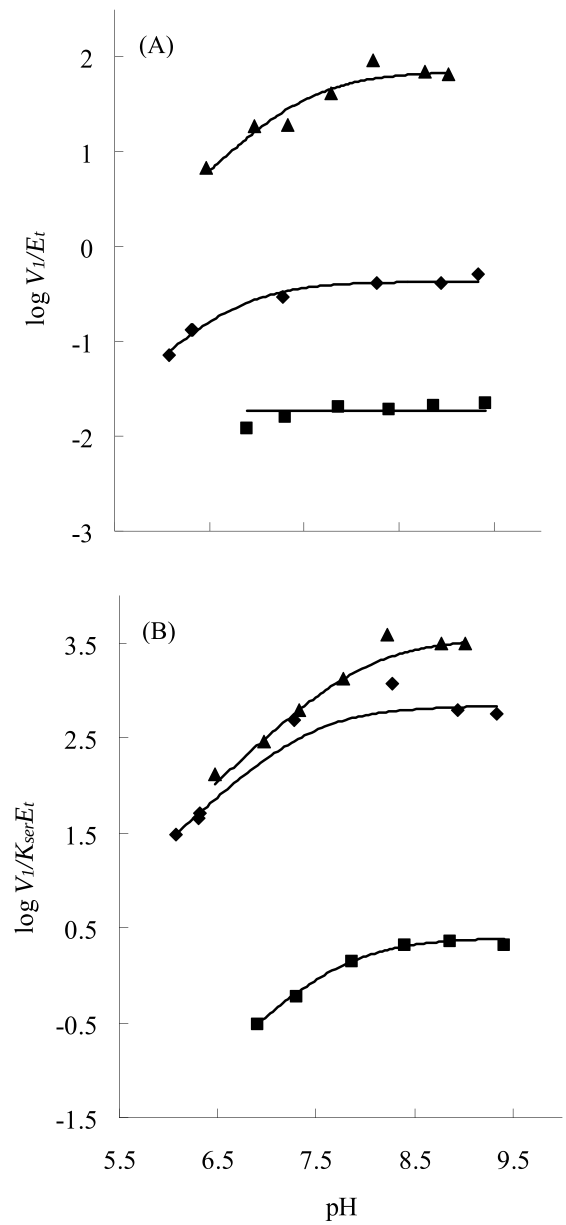

Figure C2-3. pH dependence of V_1/E_t (A) and $V_1/K_{ser}E_t$ (B) for the H154N, H189N and H154N/H189N mutant enzymes. Points for the H154N (◆), H189N (▲), and H154N/H189N (■) mutant enzymes are experimental values, while the curves are theoretical based on fits of the data using equation C2-3.

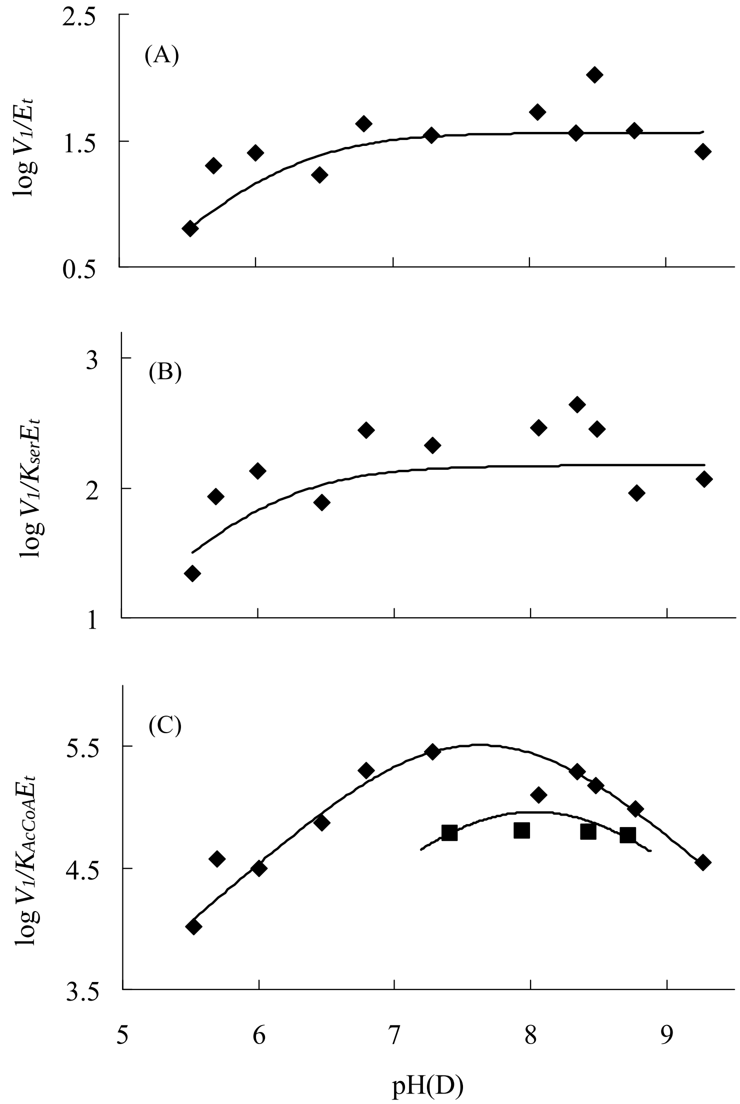

Figure C2-4. pH(D) dependence of V_1/E_t (A), $V_1/K_{ser}E_t$ (B) and $V_1/K_{AcCoA}E_t$ (C) for the D139N mutant of *Hi*SAT. The points shown are the experimentally determined values. pH and pD dependence are presented by (▲) and (■), respectively. The curves are theoretical based on fits of the data using equation C2-3 for the pH-rate profile of V_1/E_t and equation C2-4 for the pH-rate profile of $V_1/K_{AcCoA}E_t$. The curve for the pD dependence of $V_1/K_{AcCoA}E_t$ and the pH dependence of $V_1/K_{serine}E_t$ were drawn by hand.

6.9. In the forward reaction direction, initial velocity studies indicate the kinetic mechanism of the H154N, H189N and H154N/H189N mutant enzymes is ordered over the entire pH range studied, similar to wild type (*35*), but is equilibrium ordered for H154N below pH 6.3 and for H189N below pH 7.3. However, the kinetic mechanism of the D139N mutant enzyme is random with respect to binding AcCoA and serine, as suggested by the noncompetitive inhibition pattern for glycine vs AcCoA and ATP vs serine; glycine is uncompetitive versus AcCoA for the wild type enzyme.

Table C2-3. Summary of pK_a values for wild type and mutant *Hi*SAT

Enzyme	V_1 pK_a ± S.E.	V_1/K_{ser} pK_a ± S.E.	V_1/K_{AcCoA} pK_a ± S.E.
wild type [a]	6.8 ± 0.2	7.2 ± 0.2	N/A
H154N	6.7 ± 0.2	7.4 ± 0.4	N/A
H189N	7.5 ± 0.2	8.0 ± 0.3	N/A
D139N	6.2 ± 0.4	6.1 ± 0.5	7.2 ± 0.3 8.1 ± 0.2
H154N/H189N	N/A	7.8 ± 0.1	N/A

[a] **From Johnson *et al.* (*76*).**

V_1/E_t and $V_1/K_{ser}E_t$ decrease at low pH for all of the single mutant enzymes, giving a limiting slope of 1. A bell-shaped pH-rate profile with limiting slopes of 1 and -1 was obtained for $V_1/K_{AcCoA}E_t$ for D139. V_1/E_t and $V_1/K_{AcCoA}E_t$ are pH independent over the pH range studied for H154N/H189N double mutant enzyme, while $V_1/K_{ser}E_t$ decreases at low pH with a limiting slope of 1. In the case of the H154N and H189N mutant enzymes, data for the $V_1/K_{AcCoA}E_t$ pH-rate profile could not be collected at low pH, since K_{AcCoA} is zero. pK_a values are summarized in Table C2-3. pH-rate profiles are plotted in Fig. C2-3 for H154N, H189N and H154N/H189N mutant enzymes and Fig. C2-4 for D139N mutant enzyme.

C2.3.3 Solvent deuterium kinetic isotope effects

Table C2-4. Summary of *SKIE* values for wild type and mutant enzymes

Enzyme	$^{D_2O}V_1$	$^{D_2O}(V_1/K_{ser})$	$^{D_2O}(V_1/K_{AcCoA})$
Wild type [a]	1.9 ± 0.1	2.5 ± 0.4	N/A
H154N	1.64 ± 0.03	1.64 ± 0.03	N/A
H189N	3.4 ± 0.3	3.4 ± 0.3	N/A
D139N	2.3 ± 0.1	2.3 ± 0.1	3.5[b]
H154N/H189N	2.2 ± 0.1	2.2 ± 0.1	N/A

[a] **From Johnson *et al.* (*76*).**

[b] **Estimated graphically as the ratio of the pH(D) independent values in Fig. 4.**

Measurement of the V_1 and V_1/K_{ser} in H_2O and D_2O gave about equal values of $^{D_2O}V_1$

and $^{D_2O}(V_1/K_{ser})$. Values are about the same as those of wild type for D139N and H154N/H189N, slightly lower than wild type for the H154N mutant enzyme and significantly higher for the H189N mutant enzyme, Table C2-4. The pH(D) dependence of kinetic parameters was measured over the pH(D) range of 7.3-8.5 to determine the solvent deuterium kinetic isotope effects on V_1/K_{AcCoa} for D139N, Fig. C2-4. An average value about 3.5 was estimated for $^{D_2O}(V_1/K_{AcCoa})$ of D139N.

C2.4 Discussion

C2.4.1 H154N mutant enzyme

Site-directed mutagenesis was used to change H154 to Asn, which cannot act as a general base, but can still form a hydrogen bond with D139. The ~1240-fold decrease in V_1/E_t and ~160-fold decrease in $V_1/K_{ser}E_t$ indicate that H154 is important to catalysis, and suggests it acts as a general base that accepts a proton from the β-hydroxyl of serine. This result was anticipated given hydrogen-bond distance between H154 and D139, suggesting the two residues might act as a catalytic dyad.

The rate-limiting step for wild type *Hi*SAT is the formation of the tetrahedral intermediate once the E-AcCoA-serine complex is formed (*76*). In this step, a nucleophilic attack occurs on the carbonyl of the AcCoA thioester by the hydroxyl group of serine, with the general base accepting a proton from the hydroxyl group, Fig. 1. The difference in the values of $^{D_20}V_1$ (~1.9) and $^{D_20}(V_1/K_{ser})$ (~2.5) suggested that the chemical step is not the only rate-limiting step for the overall reaction, and that release of CoA also contributes to rate-limitation, with the rate of product release ~1.5 times faster than that of the chemical step (*76*).

In the case of the H154N mutant enzyme, ${}^{D_2O}V_1 \approx {}^{D_2O}(V_1/K_{ser}) \approx 1.6$. Since the release of CoA was only 1.5-fold greater than the chemical step(s), the 1240-fold decrease observed for the H154N mutant enzyme is a lower limit and is closer to 1860-fold when correcting for the small contribution made by product release. Therefore, the observed *SKIE*s are likely intrinsic values. However, the values are lower than those observed for wild type. Considering that the elimination of H154 gives an enzyme that still has H189 in position to potentially act as a base, accepting a proton from the serine hydroxyl, we believe the isotope of 1.6 reflects general base catalysis by H189.

The pH dependence of kinetic parameters provides information on functional groups required on enzyme and/or reactant in a given protonation state for optimum binding and/or catalysis (*114*). The V/K for a reactant is obtained at a limiting concentration of one reactant and saturating concentrations of all others, and reflects the free form of the enzyme the substrate binds to and the free reactant. V is obtained at saturating concentrations of all substrates, and reflects the enzyme form(s) that are present in the steady state.

The V_1/E_t and $V_1/K_{ser}E_t$ of the H154N mutant enzyme decrease at low pH, giving a limiting slope of 1, and exhibit pKs of about 6.7 and 7.4, respectively, which are, within error, equal to the pKs observed for the wild type enzyme. These data indicate that the group that acts as a base in the mutant enzyme has a pK very similar to that of wild type.

As suggested above, H189 may act as the general base in place of H154 in the mutant enzyme and the pK of 6.7-7.4 would thus reflect this group.

C2.4.2 H189N mutant enzyme

In the case of the H189N mutant enzyme, the mutation eliminates the possibility of H189 acting as a general base. However, the 19-fold decrease in V_1/E_t shows that H189 is important but not essential to catalysis. The 130-fold decrease in $V_1/K_{ser}E_t$ and 7-fold increase on K_{ser} indicate that H189 also contributes to the binding of serine. Thus the function of H189 may be that of orienting serine for efficient catalysis.

The observed values of ~3.4 for ${}^{D_2O}V_1$ and ${}^{D_2O}(V_1/K_{ser})$ indicate chemistry limits the overall reaction. The larger isotope effects suggest that when H154 acts as the base, it is not optimally positioned compared to H189 in the H154N mutant enzyme [**Recent evidence from the Klinman lab (personal communication) suggests hydrogen transfer reactions originate almost solely from quantum mechanical tunneling coupled to the breathing modes (thermal motions) of the protein. Thus, the more compressed the reaction coordinate, the smaller the isotope effect. Thus, H189N with a *SKIE* of ~3.4 suggests H154 is not optimally placed to act as the catalyst in the proton extraction reaction, while H154N, where H189 is the catalyst, with an *SKIE* of ~1.6 is better positioned.**]. The pH-rate profiles for H189N, also exhibit a limiting slope of 1 at low pH for V_1/E_t and $V_1/K_{ser}E_t$. However, the pK_a values have increased to ~7.5 for V_1/E_t and ~8.0 for $V_1/K_{ser}E_t$, compared to 6.8 and 7.2 obtained for wild type. The increases in the pK_a may result from removal of H189, which is likely protonated in the wild type enzyme.

C2.4.3 H154N/H189N mutant enzyme

The double mutant enzyme has eliminated H154 and H189 of *Hi*SAT, so that neither is able to act as general base. The activity of the double mutant enzyme is 23700-fold lower, while $V_1/K_{ser}E_t$ is 132000-fold lower than wild type values. The decrease in V_1/E_t is the product of the decreases observed for the H154N and H189N mutant enzymes. The $>10^4$-fold decrease is consistent with elimination of general base catalysis in *Hi*SAT. In addition, the $>10^5$-fold lower value of $V_1/K_{ser}E_t$ likely reflects the $\sim 10^4$-fold loss in catalytic function and a ~10-fold loss in affinity for serine. The V_1/E_t value of the H154N/H189N mutant enzyme is 19-fold lower than the value of H154N, which suggest H189 is responsible for most of the activity observed for the H154N mutant enzyme. The increase in K_{ser} observed for the double mutant enzyme is similar to the change observed for H189N, consistent with the proposed role of H189 in serine binding.

Also consistent with the proposed roles of H154 and H189 is the pH dependence of kinetic parameters. V_1/E_t is pH independent over the pH range 7.5-9.5 and only appears to decrease at low pH (<7.0), where the enzyme is no longer stable. Elimination of both imidazoles thus results in loss of the pK_a for the catalytic group. A pK_a of about 7.8 is observed in the $V_1/K_{ser}E_t$ profile, but this likely reflects the protonation state of a group that must be protonated for optimum binding of serine in the double mutant enzyme [**An alternative interpretation of the pH-rate profile would be selective-binding of the correctly protonated forms of enzyme and substrate, such that when the enzyme-substrate complex is formed, the protonation state of the enzyme and substrate functional groups are locked. Given**

the elimination of two active site residues, it is difficult to reconcile this as a reasonable possibility.]. This may be the same group observed in the $V_1/K_{AcCoA}E_t$ pH-rate profile of the D139N mutant enzyme.

A value of ~2.2 is observed for $^{D}V_1$ and $^{D}(V_1/K_{ser})$ for double mutant enzyme, and this is almost certainly an intrinsic effect. However, since it is not known whether catalysis is by water or some other base, it is not possible to further interpret this effect at this point.

C2.4.4 D139N mutant enzyme

Changing D139 to N changes the nature of the putative dyad linkage between D139 and H154 from a strong hydrogen bond between the negatively charged aspartate and N^{δ} of H154 to a weaker bond to the amide carbonyl oxygen of the asparagine. The mutation results in an 11-fold decrease in V_1/E_t, likely a result of decreasing the basicity of H154, a possible general base catalyst. The biggest effect of the mutation is seen as a 34-fold increase in K_{ser}, resulting in a 380-fold decrease in $V_1/K_{ser}E_t$. The majority of the increase in K_{ser} is likely associated with a decreased affinity. The decreased affinity may be a reflection of the weaker dyad linkage causing a repositioning of H154, but this will have to await additional studies.

Since H154 is available to act as the general base in the D139N mutant enzyme, and given the large decrease in $V_1/K_{ser}E_t$, one would expect $^{D_2O}(V_1/K_{ser})$ to approach a value of ~3.4, which is close to the observed value of $^{D_2O}(V_1/K_{AcCoA})$. However, $^{D_2O}V_1$ and $^{D_2O}(V_1/K_{ser})$ are smaller with values of ~2.3.

Finite *SKIE* values on all three kinetic parameters indicate the kinetic mechanism has become random for this mutant enzyme, but it exhibits a steady state mechanism with binding AcCoA before serine preferred. The relative off-rate of serine and AcCoA from E-AcCoA-serine can be estimated from the isotope effect data and mechanism C2-6.

On the basis of the mechanism C2-6, expressions for V_1, V_1/K_{AcCoA} and V_1/K_{ser} and the respective *SKIE*s are given in equations C2-7 to C2-9.

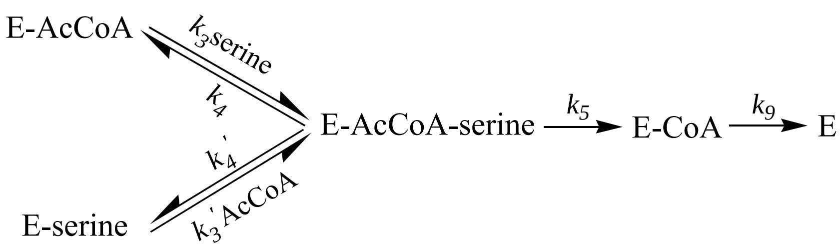

(C2-6)

$$V = \frac{k_5 k_9}{k_5 + k_9} \qquad {}^{D_2O}V = \frac{{}^{D_2O}k_5 + \frac{k_5}{k_9}}{1 + \frac{k_5}{k_9}} \tag{C2-7}$$

$$V/K_{AcCoA} = \frac{k_3 k_5}{k_4 + k_5} \qquad {}^{D_2O}(V/K_{AcCoA}) = \frac{{}^{D_2O}k_5 + \frac{k_5}{k_4}}{1 + \frac{k_5}{k_4}} \tag{C2-8}$$

$$V/K_{ser} = \frac{k_3' k_5}{k_4' + k_5} \qquad {}^{D_2O}(V/K_{ser}) = \frac{{}^{D_2O}k_5 + \frac{k_5}{k_4'}}{1 + \frac{k_5}{k_4'}} \tag{C2-9}$$

Using the value of ${}^{D_2O}(V_1/K_{AcCoA})$ (3.5) for ${}^{D_2O}k_5$ and the value of ${}^{D_2O}V_1 = {}^{D_2O}(V_1/K_{ser})$

≈ 2.3, values of k_5/k_9 and k_5/k_4' is approximate 0.9 and value of k_5/k_4 is very close to zero. The ratio of k_5/k_4 and k_5/k_4' gives a value of k_4/k_4' (the off-rate constant for AcCoA and serine) that would be a very large number. The change in mechanism is consistent with an increase in the off-rate constant for AcCoA from the E-serine-AcCoA complex. Since V_1/E_t was decreased by an order of magnitude, and the pathway with serine adding to E-AcCoA gives isotope effects that are very similar to those of the wild type enzyme, data suggest a decrease in the rate of all of the steps from addition of serine to release of OAS in mechanism C2-6. This could result from a decrease in the amount of catalytically active enzyme generated when serine binds, that is nonproductive binding of serine. The large isotope effect observed on V_1/K_{AcCoA} is consistent with an increase in the off-rate constant for AcCoA from the E-serine-AcCoA complex resulting in rate-limiting chemistry. The increased off-rate for AcCoA may result from an inability of AcCoA to generate the catalytically active enzyme as a result of its binding modes as D139 is changed. These two effects may be linked in that enzyme binding of AcCoA to give E-AcCoA may result in a decreased amount of productive enzyme as serine binds. In addition, when serine is bound to give E-AcCoA-serine, AcCoA is released rapidly to give E-serine. It thus appears that D139 in dyad linkage to H154 contributes to generating the catalytically competent E-AcCoA-serine complex.

V_1/E_t and $V_1/K_{ser}E_t$ pH-rate profiles give a limiting slope of 1 at low pH for the D139N mutant enzyme, similar to wild type. However, a bell-shaped pH-rate profile is observed for $V_1/K_{AcCoA}E_t$, with limiting slopes of 1 and -1. The predominant enzyme form for V_1/K_{ser} and V_1/K_{AcCoA} in this case are the E-AcCoA and E-serine complexes, respectively, while for V_1, the E-AcCoA-serine and E-CoA complexes are likely present. The pK_as observed in V_1 and V_1/K_{ser} are about 6.2 and 6.1, respectively, about a pH unit lower than that observed for wild type, consistent with a decreased basicity of H154 when D139 is changed to N. The pK_a on the acid side of the $V_1/K_{AcCoA}E_t$ pH-rate profile is ~7.2, a pH unit higher than that observed in $V_1/K_{ser}E_t$, consistent with formation of a hydrogen bond between H154 and the serine β-hydroxyl, as expected with H154 acting as a base to accept the proton. The group with a pK_a of ~8.1 shown on the basic side of the $V_1/K_{AcCoA}E_t$ profile was not observed for the wild type enzyme, and is likely important for binding AcCoA since it is not observed in the V_1/E_t pH-rate profile. This group may reflect the protonation state of H189, or some other active site residue.

C2.4.5 Proposed roles of H154, H189 and D139 in *Hi*SAT

The kinetic parameters, pH-rate profiles, and *SKIE*s discussed above provide a picture of how the three catalytic residues might function in the active site of the *Hi*SAT. Optimum binding of reactants requires the dyad composed of H154 and D139. Since these residues are donated to the active site by different subunits at the interface, Fig. C2-2, it is not surprising in retrospect, that the catalytic conformation depends on a functional H154-D139 dyad.

Once AcCoA and serine are bound, we propose that N^{ε} of H154, is hydrogen-bonded to the β-hydroxyl of serine in preparation for accepting a proton as the tetrahedral intermediate between serine and AcCoA is formed. In the ternary complex H189 is likely protonated and donates a hydrogen bond to the serine hydroxyl to properly orient it in the site.

It should be stated at this point that it is possible neither H154 nor H189 serves as a base, and some other enzyme side chain serves in this capacity. However, on the basis of all of the data obtained, we believe this is only a remote possibility.

Interestingly, when H154 is mutated, H189 can serve as an alternative catalyst. The lower activity of H154N compared to wild type suggests there is likely no biological significance to this back-up behavior. A similar back-up system was reported for fructose 2, 6-bisphosphatase (*115*). H256 acts as the nucleophilic catalyst for this enzyme and becomes phosphorylated by fructose 2, 6-bisphosphate. A second imidazole side chain (H390) facilitates phosphoryl transfer, and acts as a general base catalyst to activate water as the phospho-imidazole is hydrolyzed. Mutation of H256 to Ala gives an enzyme that retains 17% activity. In the H256A mutant enzyme, H390, acts as a general base to directly catalyze the hydrolysis of the 2-phosphate of the fructose 2, 6-P_2.

Chapter 3

^{31}P NMR Studies of *O*-Acetylserine Sulfhydrylase-B from *Salmonella typhimurium*

C3.1 Introduction

O-Acetylserine sulfhydrylase (OASS) is a pyridoxal 5′-phosphate (PLP)-dependent enzyme that catalyzes the final reaction of the cysteine biosynthetic pathway in bacteria and plants, the conversion of *O*-acetylserine (OAS) and bisulfide to L-cysteine and acetate (*27*). In enteric bacteria, there are two isoenzymes of OASS, A and B. The B-isozyme of *O*-acetylserine sulfhydrylase (OASS-B) is expressed in *Salmonella typhimurium* under anaerobic growth conditions (*116*), and it appears to be less substrate selective than the A-isozyme for both the amino acid and nucleophilic substrates (*29*). OASS-B adheres to a Bi Bi ping-pong kinetic mechanism on the basis of initial velocity studies (*29*). The proposed chemical mechanism of OASS-B is similar to that observed for the A-isozyme (*99*). The substrate, OAS, binds with its α-amine unprotonated to facilitate a nucleophilic attack on C4′ of the internal Schiff base (ISB) to generate the OAS external Schiff base (ESB). The lysine (K41) that participates in internal Schiff base linkage, acts as a general base to deprotonate C_α in the β-elimination reaction, giving the α-aminoacrylate ESB and acetate. The B-isozyme has a turn-over number 12.5-fold higher than the A-isozyme and an approximately 10-fold lower value of K_{OAS} (*29, 93*).

The three-dimensional structures of OASS-A and -B from *S. typhimurium* have been solved to 2.2 and 2.3 Å, respectively, in the absence of ligands as an open form (*89*). As expected, these two homodimeric structures exhibit an overall fold very similar to each other, given the 40% identity in amino acid sequences of A- and B-isozyme (*93, 117*). The main difference between the two isozymes is the more hydrophilic active site of the B-isozyme with two ionizable residues, C280 and D281, replacing residues S300 and P299, respectively, in the A-isozyme (*93*). Aspartate-281 is above the *re* face of the cofactor and is within hydrogen-bonding distance of Y286, which is within hydrogen-bonding distance to O3′ of PLP, while C280 is located 3.4 Å from the pyridine nitrogen of the internal Schiff base. Structural data also suggest that OASS-B has a higher degree of conformational flexibility along the reaction pathway in comparison with -A.

The cofactor PLP provides a valuable probe of protein dynamics and catalysis for PLP-dependent enzymes, due to its localization at the enzyme active site and the sensitivity to changes in enzyme structure along the reaction pathway. Considering the tight link between electronic and conformational states, it is not surprising that ^{31}P NMR methods have been exploited for PLP-dependent enzyme to reveal the conformational landscape of catalytic actions by focusing on the binding modes of the phosphate group on PLP (*90, 98, 118-121*).

Resolution of the PLP cofactor and its reconstitution with the apoenzyme has been used to study the binding site of PLP for several PLP-dependent enzymes, including the A-isozyme of OASS (*81, 122-125*). Preparation of apo OASS-A by resolution of PLP was shown to be crucial for the studies of enzyme stability and dynamics (*80, 101, 104,* *126*). A method for resolving PLP from the active site of OASS-B would thus be useful.

In this paper, ^{31}P NMR studies of OASS-B were carried out to probe the conformational dynamics of OASS-B. The binding of the PLP cofactor in *St*OASS-B was proposed to change as different intermediates are formed along the reaction pathway and this is reflected in the ^{31}P NMR spectra of those intermediates, giving different values of chemical shift and line width. Values of chemical shift and line width of *St*OASS-B were proposed to be similar to those obtained for *St*OASS-A, due to structural similarity of the PLP binding sites of two isozymes. Data are discussed in term of cofacotr dynamics of OASS-B during catalysis as different enzyme intermediate are formed. In addition, we report a method for resolution of PLP from OASS-B, using hydroxylamine as the resolving reagent. The properties of the apo OASS-B and its reconstitution with the PLP cofactor have also been studied.

C3.2 Materials and Methods

C3.2.1 Chemicals

L-Serine, L-cysteine and hydroxylamine were from Sigma. Deuterium oxide (99.9 atom % D) was from Cambridge Isotope Laboratories, Inc. Hepes and Mes were from Research Organics, Inc. All other chemicals and reagents were obtained from commercial sources, were reagent grade, and were used without purification.

C3.2.2 Enzyme

Recombinant OASS-B from *Salmonella typhimurium* was expressed and purified following the protocol of Chattopadhyay et al (*93*). The OASS-B used for NMR experiments was purified with a slightly modified protocol. In this modified protocol, PLP was not added to the crude enzyme (supernatant) before it was loaded onto the Ni-NTA column, to avoid PLP other than that in the active site bound to enzyme. The purified OASS-B was stored in 5 mM Hepes, pH 8.0, at –80 ^{o}C.

C3.2.3 ^{31}P NMR Spectroscopy

The Fourier transform ^{31}P NMR spectrum of OASS-B without ligand bound was collected at 121.5 MHz (Varian 300 MHz) and 160.9 MHz (Varian 400 MHz), respectively, using a 5 mm multinuclear probe head with broadband ^{1}H decoupling. ^{31}P NMR spectra of OASS-B in presence of L-cysteine and L-serine were collected using the Varian 400 MHz instrument, also using a 5 mm probe head. All NMR samples were maintained at 21.0 °C in a 5 mm NMR tube, with 10% D_2O in the solution as a field/frequency lock. A spectral width of 3004.8 Hz was acquired in 12288 data points with pulse angles of 30^{o} and 45^{o} for the 300 MHz and 400 MHz instruments, respectively. The acquisition time was 1.6 sec and a relaxation delay of 3.0 sec was applied. The exponential line broadening used prior to Fourier transformation was 10.0 Hz. Positive chemical shifts in ppm are downfield changes with respect to 85% H_3PO_4.

The application of higher frequency instruments leads to higher line width, because the chemical shift anisotropy becomes the dominant relaxation mechanism (*127*). The line width of ^{31}P NMR spectra obtained with the 400 MHz spectrometer can be adjusted to those obtained with a 300 MHz instrument, using the following equation derived from the frequency-dependent model in reference (*127*).

$$\frac{(LW_{300} - LW_{d-d})}{(LW_{400} - LW_{d-d})} = \frac{9}{16} \qquad \text{(C3-1)}$$

In equation 1, LW_{300} and LW_{400} represent line widths (Hz) measured with the 300 MHz and 400 MHz instruments, respectively, $LW_{d\text{-}d}$ (Hz) is the value of the field independent contribution given by dipole-dipole mechanisms. In this study, $LW_{d\text{-}d}$ is calculated to be 9.5 Hz using the line width data (LW_{300} and LW_{400}) of OASS-B with out ligand bound. The line widths of the ^{31}P NMR spectra of OASS-B in presence of L-cysteine and L-serine were corrected to those at 300 MHz for comparison to the data obtained with OASS-A.

C3.2.4 Enzyme assays

OASS-B activity was monitored as described by Tai *et al.* (*29*) using OAS and TNB as substrates. The disappearance of TNB was measured at 412 nm using a Beckman DU 640 spectrophotometer; the ε_{412} for TNB is 14,150 $M^{-1}cm^{-1}$ (*111*). All assays were performed in 100 mM Hepes, pH 7.0, with 0.2 mM OAS and 0.05 mM TNB at room temperature.

C3.2.5 Resolution of PLP from OASS-B

OASS-B in 5 mM Hepes, pH 8.0 was dialyzed overnight against resolving buffer containing 500 mM phosphate, pH 7.6, 1 mM hydroxylamine and 0.2 mM DTT. The resolved OASS-B was dialyzed against 100 mM phosphate, pH 7.0 with 0.1 mM DTT. The apoenzyme obtained was stored frozen at –80 ^{o}C.

C3.2.6 Reconstitution of PLP with Apo OASS-B

Reconstitution of apo OASS-B with PLP (1:3 molar ratio) was carried out at 4 ^{o}C in 100 mM phosphate, pH 7.0 with 0.1 mM DTT. A background rate (1.3%) observed for apo OASS-B was subtracted from all activity measurements. The reconstituted OASS-B used in the UV-visible and fluorescence spectra was prepared by combining apo OASS-B with PLP (1:1 molar ratio) at 4 ^{o}C in 100 mM phosphate, pH 7.0 with 0.1 mM DTT.

C3.2.7 Ultraviolet-visible Spectral Studies

Absorbance spectra of apo OASS-B and reconstituted OASS-B were obtained as described by Schnackerz et al. (*98*) for OASS-A. Spectra were collected at pH 7.0, using a Hewlett Packard 8452A photodiode array spectrophotometer. The blank consisted of all components minus enzyme.

C3.2.8 Steady-state Fluorescence Measurement

Fluorescence spectra of apo OASS-B and reconstituted OASS-B were recorded using a Shimadzu RF-5301 PC spectrofluorometer. Experiments were carried out at pH 7.0, 25 ^{o}C. The excitation and emission slit widths were set to 3 nm and 5 nm, respectively. The excitation wavelength was set to 298 nm, and the emission monochromator was scanned from 310 to 550 nm. The blank consisted of all components except enzyme.

C3.3 Results

C3.3.1 ^{31}P NMR Spectroscopy

^{31}P NMR spectra obtained for the ISB of native OASS-B from *Salmonella typhimurium* exhibits a ^{31}P chemical shift of 6.2 ppm, Fig C3-1. This can be compared to a chemical shift of 5.2 ppm for OASS-A (*90*). The line width of the ^{31}P resonance of the ISB of the B-isozyme was 19 Hz, similar to the value of 20.5 Hz measured for the A-isozyme. The chemical shift is independent of pH over the range 7.0 to 8.9 (data not shown), as observed for the A-isozyme (*98*).

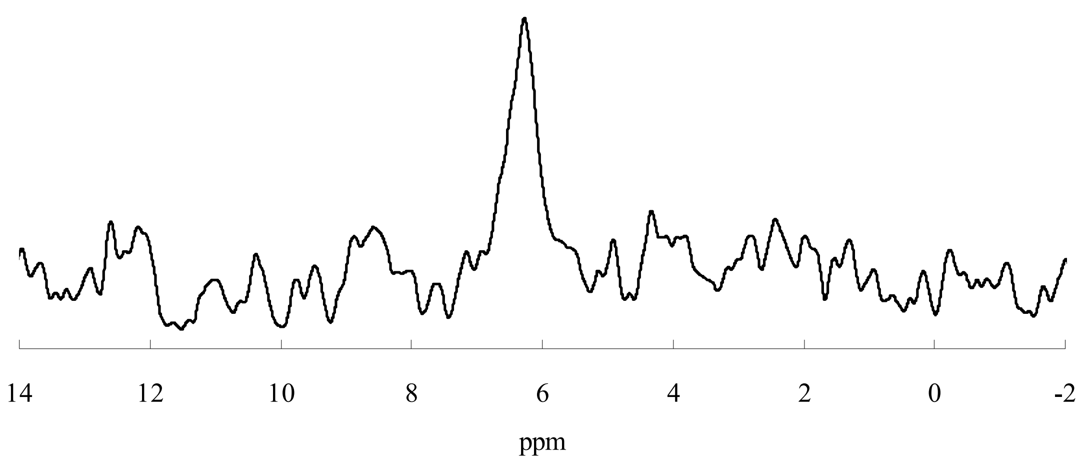

Figure C3-1. ^{31}P NMR spectrum for OASS-B without ligand bound. A chemical shift of 6.2 ppm with 19 Hz line width is comparable to those of OASS-A (5.2 ppm, 20.5 Hz).

^{31}P NMR spectra were also obtained for the B-isozyme in the presence of 30 mM L-cysteine or 300 mM L-serine at pH 8.0, the pH independent region of the dissociation constant for release of amino acid from the ESB (*93*). In the presence of lanthionine [**Cysteine is rapidly converted to the α-aminoacrylate intermediate, which is attacked by the thiol of a second cysteine molecule to generate the external Schiff base of lanthionine (*95*).**], the ^{31}P chemical shift moves upfield to 6.0 ppm, with a line width of 21 Hz. In the presence of 300 mM L-serine, the chemical shift moves downfield to 6.3 ppm, with a line width of 23 Hz. In comparison, the chemical shift of OASS-A for the ESBs with lanthionine and L-serine are 5.3 and 4.4 ppm, with line widths of 32.5 and 50.5 Hz, respectively, indicating significant differences depending on which amino acid forms the external Schiff base (*98*). Values of chemical shift (δ) and line width are summarized in Table C3-1, together with values obtained previously for OASS-A (*98*).

Table C3-1. ^{31}P NMR-Chemical Shifts and Line Widths of OASS-B

Ligand	OASS-A		OASS-B	
	δ, ppm	Line width, Hz	δ, ppm	Line width, Hz
None	5.2[a]	20.5[a]	6.2	19
L-cysteine[c]	5.3[b]	32.5[b]	6.0	21[d]
L-serine[c]	5.2, 4.4[b]	50.5[b]	6.3	23[d]

[a] from Cook *et al.* (*90*).

[b] from Schnackerz *et al.* (*98*).

[c] L-cysteine was 10 mM for OASS-A and 30 mM for OASS-B, while L-serine was 36.4 mM for OASS-A and 300 mM for OASS-B.

[d] Numbers are line widths corrected to a 300 MHz spectrometer.

C3.3.2 Resolution of PLP from OASS-B

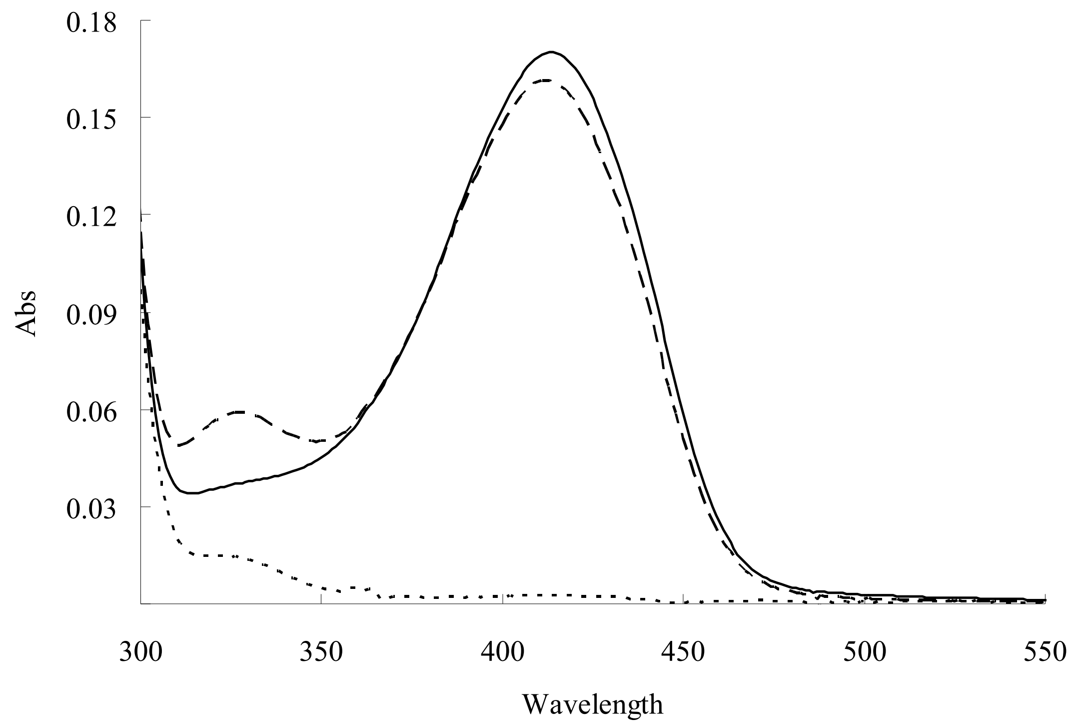

Figure C3-2. UV-visible absorption spectra of OASS-B. Spectra are for native enzyme prior to preparation of apoenzyme (—), apoenzyme (·····), and reconstituted holoenzyme (----). The spectra of holoenzyme and reconstituted enzyme were collected in 100 mM Hepes, at pH 6.5 and 7.0, respectively. The spectrum of apoenzyme was collected in 100 mM phosphate, pH 7.0.

Several procedures were tested for the preparation of apo OASS-B, including guanidine hydrochloride with OAS, which was effective with the closely related OASS-A (*81*), L-cysteine with imidazole citrate buffer (*128*), OAS with a high concentration of inorganic phosphate, and high concentrations of inorganic phosphate at low pH. None of these reagents were able to successfully resolve PLP from OASS-B. Treatment of OASS-B with 1 mM hydroxylamine in 500 mM phosphate, pH 7.6, with 0.2 mM DTT,

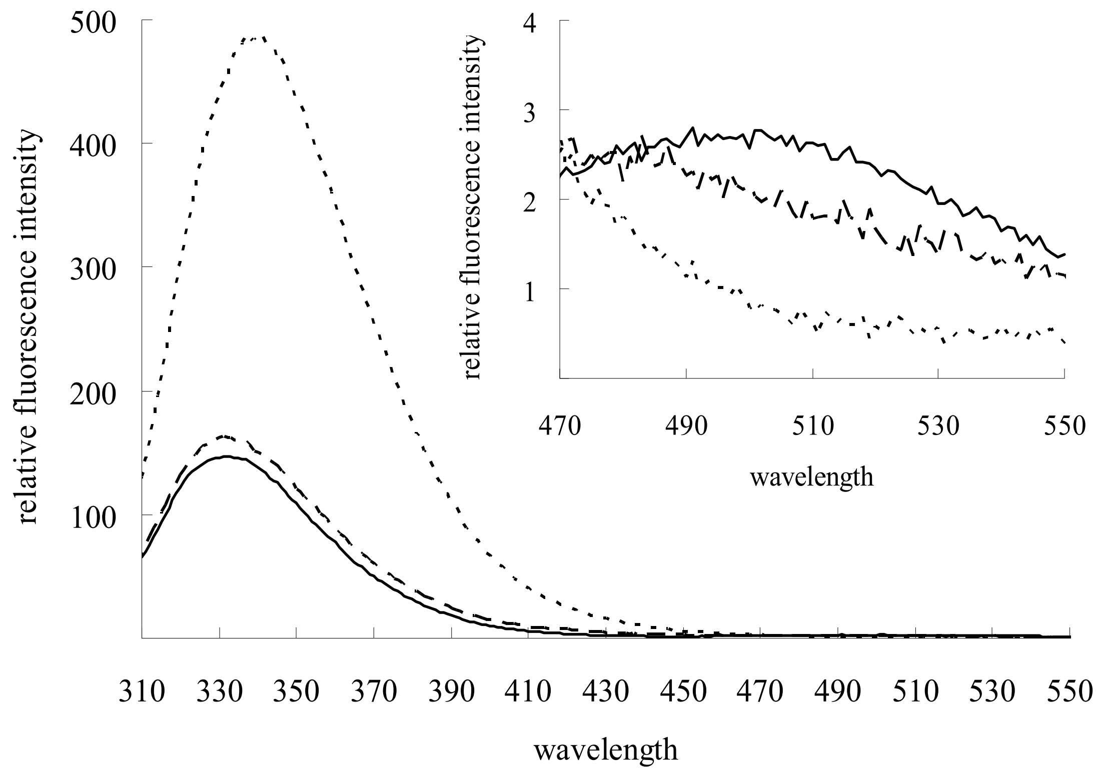

Figure C3-3. Steady-state fluorescence spectra of OASS-B. Spectra are for native enzyme prior to preparation of apoenzyme (—), apoenzyme (·····), and reconstituted holoenzyme (----). The spectra of holoenzyme and reconstituted enzyme were collected in 100 mM Hepes, at pH 7.0, while that of apoenzyme was collected at pH 7.0, 100 mM phosphate. The long wavelength fluorescence emissions are shown more detailed in inset.

followed by dialysis against 100 mM phosphate, pH 7.0 with 0.2 mM DTT generated apo OASS-B (*129*).

The internal Schiff base of OASS-B absorbs maximally at 414 nm with a small shoulder at 330 nm, suggesting the ketoenamine tautomer is favored, Fig. C3-2 (*93*). The absorbance spectrum of apo OASS-B, Fig. C3-2, exhibits no absorbance at 414 nm and only slight absorbance at 330 nm, consistent with removal of most of the PLP cofactor. Fluorescence emission spectra were obtained by excitation at 298 nm. The holoenzyme emits predominantly at 336 nm, Fig. C3-3, consistent with previously measured spectra (*93*). A very low-intensity emission band is also observed for holoenzyme and is centered at 500 nm. The long wavelength band results from resonance energy transfer from tryptophan to PLP. Apoenzyme exhibits an emission band at 336 nm with an intensity that is about 3.3 times greater than holoenzyme, while the 500 nm band is absent.

C3.3.3 Reconstitution of PLP with Apo OASS-B

The holoenzyme form of OASS-B was reconstituted by adding PLP at a 3:1 molar ratio to apoenzyme, as shown by regain of activity as a function of time. Reconstitution of OASS-B was pseudo-first ordered, as shown in Fig. C3-4, and gave a rate constant of about 0.035 min^{-1}, a $t_{1/2}$ of 20 min. Reconstituted OASS-B had 81.4% activity of the native enzyme. The absorption spectrum of the reconstituted OASS-B (Fig. C3-2) is nearly identical to that of the wild type, with the exception of a small broad-peak centered at about 330 nm. The extinction coefficient at 414 nm is 6400 $M^{-1}cm^{-1}$, slightly lower than the wild type value of 6800 $M^{-1}cm^{-1}$. The fluorescence emission spectrum of reconstituted OASS-B was also very similar to that of the native enzyme with excitation at 298 nm, Fig. C3-3.

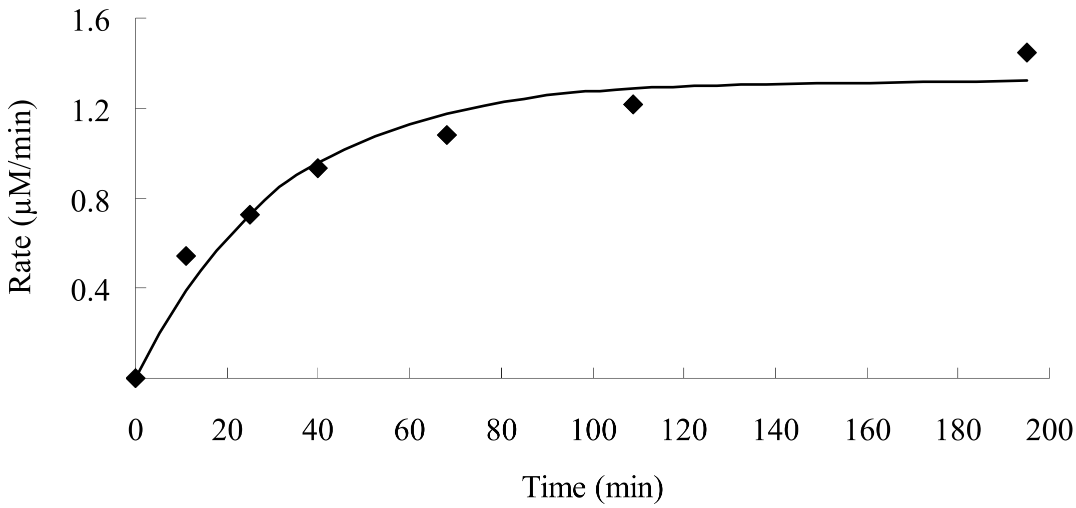

Figure C3-4. Kinetics of reconstitution of apo OASS-B upon addition of PLP. The points shown are the experimentally determined values. The curve is theoretical based on a fit of the data using the equation for a first order reaction.

C3.4 Discussion

C.3.4.1 Pyridoxal 5-phosphate binding site of OASS

The overall topology and the PLP binding site of OASS-A and -B are very similar, which is not surprising given the 40% sequence identity of the two isozymes (*93, 117*). The PLP cofactor is buried deeply between the large and small domains in both isozymes. The 5′-phosphate group of PLP in OASS-B interacts with the positive end of the dipole of helix 7 and the glycine-threonine (or phosphate-binding) loop (174-GTTGT-178) (*93*).

The loop forms an extended hydrogen-bonding network, anchoring the phosphate moiety of PLP to the protein matrix. The phosphate-binding loop in OASS-A is comprised of 176-GTGGT-180 (*89*); in OASS-B, threonine-176 replaces gylcine-178 in OASS-A. However, the hydroxyl group of T176 points away from the 5′-phosphate and does not participate in the hydrogen bonding network. For both isozymes, 6 hydrogen bonds are donated to the 5′-phosphate by the phosphate-binding loop and 2 by active site water molecules, Fig C3-5. The pattern and position of the 8 hydrogen bonds is nearly identical for the two isozymes.

C3.4.2 ^{31}P NMR Spectra

The ^{31}P chemical shift of the ISB of native OASS-B is 6.2 ppm. The chemical shift is about 1 ppm higher than that of OASS-A (*90*) and the highest reported for any PLP-dependent enzyme. The 5′-phosphate is dianionic given data measured for the pH dependence of the chemical shift of free PLP (*119*). The line width of 19 Hz is similar to data obtained for OASS-A, indicating a tightly bound phosphate group, the motion of which is determined by that of the protein (*90, 98*).

In OASS-B, PLP is in Schiff base linkage to K41 and deeply buried between two domains (*93*). At first glance, the phosphate-binding sites of PLP in OASS-A and OASS-B, especially around the 5′-phosphate group, are nearly identical, Fig. C3-5. The higher chemical shift for B-isozyme must thus result from a tighter binding of the 5′-phosphate. The distance between the Schifff base nitrogen of K41 and O4′ (the bridge oxygen of the phosphate ester) is 4.37 and 4.17 Å, respectively, in OASS-A and OASS-B,

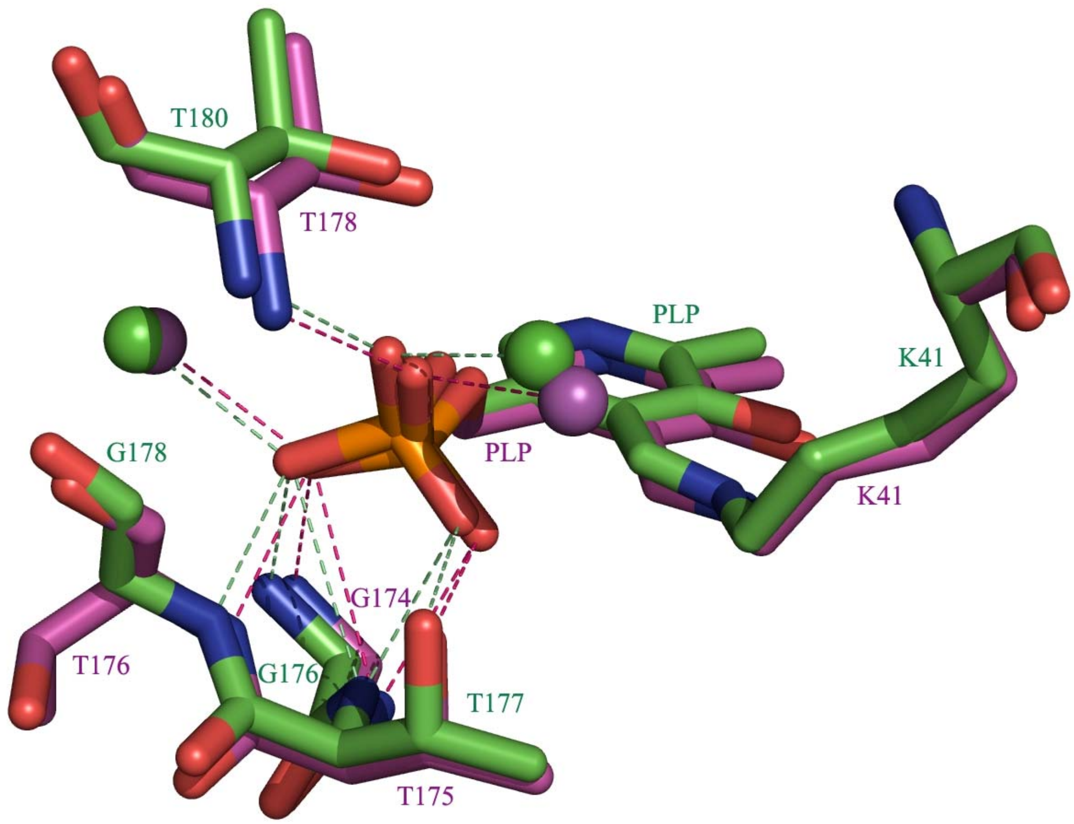

Figure C3-5. Superposition of the PLP cofactor in the phosphate binding site of OASS-A (green) and OASS-B (purple) and their respective hydrogen bonding networks. The dashed lines represent hydrogen bonds and the spheres represent water molecules. This figure was created using Pymol from DeLano Scientific LLC. The structures used in this figure have access number of 1OAS for OASS-A and 2JC3 for OASS-B in the Protein Data Bank.

Fig C3-6. In addition, the torsion angle Φ (O4′-C5′-C5-C4), responsible for the rotation around the C5-C5′ bond, is reduced from 67.8 degrees in OASS-A to 55.6 degrees in OASS-B, Fig C3-6. A similar phenomenon was observed in ^{31}P NMR spectra of aspartate aminotransferase where the chemical shift of the cofactor is higher at high pH than at low pH (*130*). The reduction in torsion angle results *a priori* in a decrease in the distance between C4′ and O4′ (*130*). The torsional stain of OASS-B in PLP must be relieved by small changes in bond angle, including those around the phosphorus atom. The ^{31}P chemical shift of phosphate esters correlates with even small changes in O-P-O bond angle (*131*) and can thus result in higher chemical shift values for the 5′-phosphate.

The 6.0 ppm chemical shift of the lanthionine ESB of OASS-B is upfield from the unliganded B-isozyme. This can be compared to OASS-A, where the chemical shift is found further downfield (5.2 ppm for the ISB and 5.3 ppm for the lanthionine ESB) (*98*). The slight upfield shift observed for the lanthionine ESB of OASS-B suggests a slight relaxation of the torsional strain, while the opposite is true for OASS-A. The increased strain in OASS-A was attributed to tight binding of the long lanthionine side chain, while the relaxation observed in OASS-B may reflect the higher degree of flexibility of the active site compared to OASS-A (*93*).

On the other hand, the further downfield shift of the 5′-phosphate of the serine ESB, 6.3 ppm compared to 6.2 ppm for the ISB, suggests an increase in torsional strain. This would appear to disagree with the explanation provided for the lanthionine ESB, but the serine side chain is much smaller and the orientation of PLP in serine ESB may be somewhat different with that of lanthionine ESB. These factors could contribute to the slight downfield chemical shift of serine ESB. Data for the serine ESB of OASS-A exhibit two conformations in intermediate exchange, one with a chemical shift of 5.3

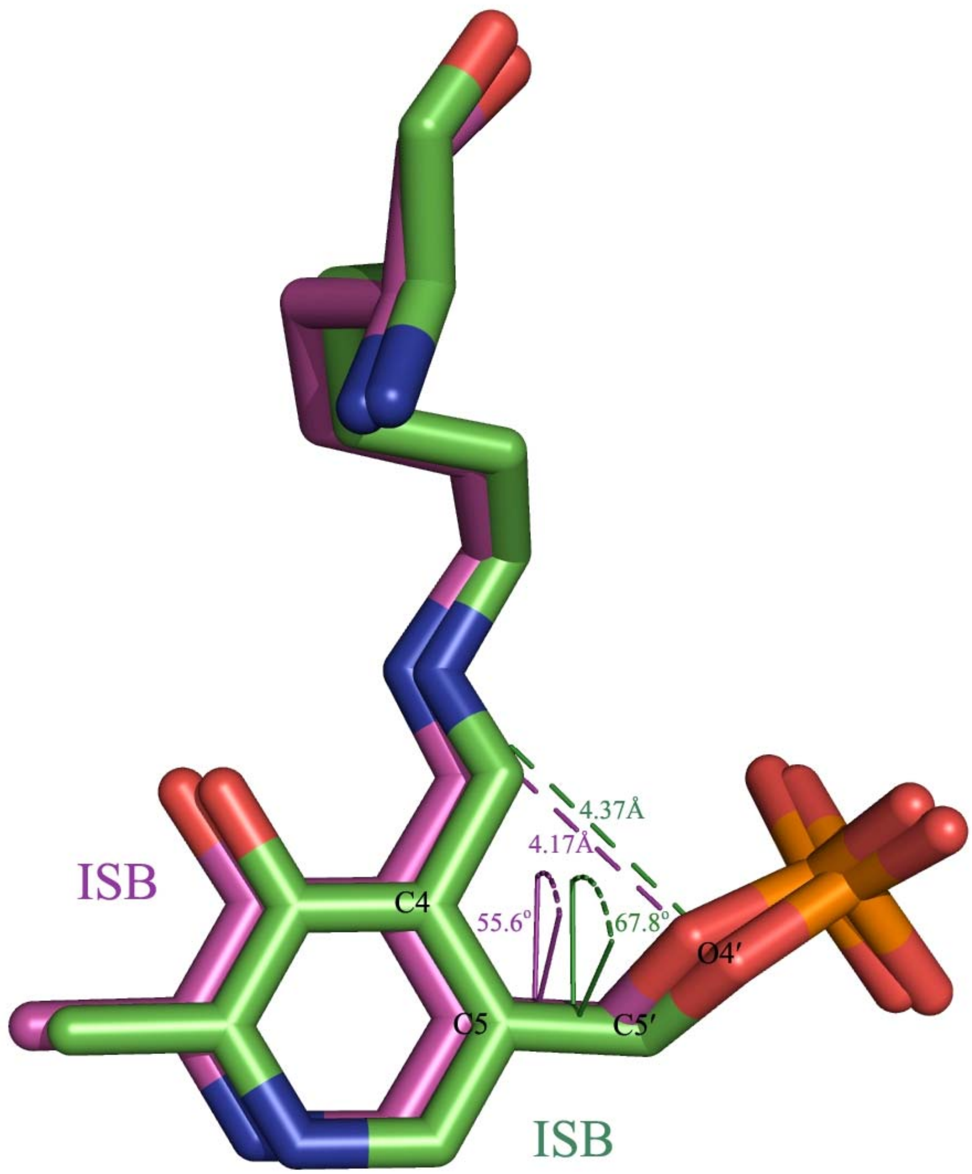

Figure C3-6. Superposition of the internal Schiff base of OASS-A (green) and OASS-B (purple). The torsion angle Φ (O4′-C5′-C5-C4) and the distance between K41Nz and O4′ of the phosphate group of PLP are labeled for each isozyme. The dashed lines represent the distance between K41Nz and O4′. Dihedral angles are also labeled. The figure was created using Pymol from DeLano Scientific LLC. The ISB of OASS-A comes from structure 1OAS in the Protein Data Bank, while 2JC3 is for the ISB of OASS-B.

ppm (slightly downfield to the 5.2 ppm chemical shift of the ISB) and another with an upfield chemical shift of about 3.5 ppm. The ^{31}P chemical shift of the serine ESB of the A-isozyme has a line width of 50.5 Hz, suggesting relatively slow inter-conversion between two tautomers of the serine ESB of OASS-A, the ketoenamine (δ, 5.3 ppm) and the enolimine (δ, 3.5 ppm) (*98*). Given values of line width that are very similar for the ISB and ESB of OASS-B, there is no evidence of multiple conformers of the serine ESB in the B-isozyme. In agreement, the UV-visible spectrum of the serine ESB of OASS-B is dominated by the ketoenamine tautomer (*93*). This appears to be true for the lanthionine ESB as well.

C3.4.3 Characterization of apo and reconstituted OASS-B

Similarities in the PLP binding site and the overall structure of the A- and B-isozyme suggested that the method used to resolve PLP from OASS-A might also be applicable to OASS–B. However, OASS-B is not as stable as OASS-A in denaturing reagents and was rapidly and irreversibly denatured in the presence of guanidine hydrochloride. Hydroxylamine was an effective resolving reagent, although it does not work with the A-isozyme (*81*). The difference may reside in the higher degree of conformational flexibility of the active site of OASS-B compared to OASS–A, consistent with the broader substrate specificity of the B-isozyme (*93*). The reconstitution of the PLP cofactor with apo OASS-B was pseudo-first order as was observed for reconstitution of OASS-A (*81*).

The UV-visible spectra of the apo and reconstituted OASS-B clearly indicate that both the resolution and the reconstitution of OASS-B were successful. Absorbance at the 414 nm λ_{max} for the ketoenamine tautomer is only observed for the reconstituted enzyme, while it is absent in the apoenzyme. The extinction coefficient at 414 nm for reconstituted OASS-B is very similar to native enzyme as well. In addition, the activity of apo OASS-B is very low and 81.4% of the activity is recovered upon reconstitution. The low-intensity 330 nm band is attributed to the absorbance of a small amount of unreconstituted PLP, which is about 18.6% of the total PLP used in reconstitution.

The quantum yield at 336 nm (excitation at 298 nm) of apo OASS-B is 3.3 times higher than that of native enzyme. The difference in quantum yield indicates that the PLP cofactor is a potent quencher of the tryptophan emission in OASS-B, consistent with the presence of the 500 nm band of native enzyme that results from energy transfer (*93*). The same phenomenon was observed for the A-isozyme (*104*). A ratio of about 2.5 was observed for fluorescence of native enzyme to apoenzyme, similar to the ratio of 3.3 obtained for the B-isozyme (*104*). Fluorescence emission spectra of reconstituted holoenzyme and native OASS-B are nearly identical. The 500 nm emission band is observed in the spectrum of native and reconstituted holoenzyme, but not in that of apoenzyme, indicating that there is no energy transfer from tryptophan to PLP in the apoenzyme, consistent with resolution of the PLP cofactor. A reproducible method for producing stable apoenzyme is important to future lifetime fluorescence studies of OASS-B that will provide information in protein dynamics along the reaction pathway.

Appendix I

Fluorescence Spectroscopy of *O*-Acetylserine Sulfhydrylase-B from *Salmonella typhimurium*

AI.1 Introduction

O-Acetylserine Sulfhydrylase (OASS) catalyzes the second step of the L-cysteine biosynthetic pathway in bacterial and higher plants, converting OAS and bisulfide to acetate and L-cysteine via a ping pong kinetic mechanism (*27, 29*). Two isozymes of OASS, OASS-A and OASS-B, exist in enteric bacteria and are expressed under aerobic and anaerobic growth condition, respectively (*82, 116*). The B-isozyme has broader substrate specificity than A- and can utilize more reduced forms of sulfur as psychological substrate (*29, 83*). A structure of OASS-B from *salmonella typhimurium* has been solved recently and overall is very similar to that of OASS-A, while with a more hydrophobic active site and higher degree of conformational flexibility during catalysis (*93*). OASS-B exists as homodimer and an internal Schiff base is formed by a PLP cofactor and the active site lysine (K41) for each monomer. There are three tryptophans in one subunit of OASS-B in comparison with two tryptophans in that of -A, Fig. AI-1. The fluorescence emission properties and the roles of tryptophans have been extensively studied for *St*OASS-A (*93, 102-104*), but not for the B-isozyme. To complement studies of OASS-A, three single and three double Trp mutants of OASS-B were prepared and investigated in this study. Kinetic and spectroscopic methods were used to characterize

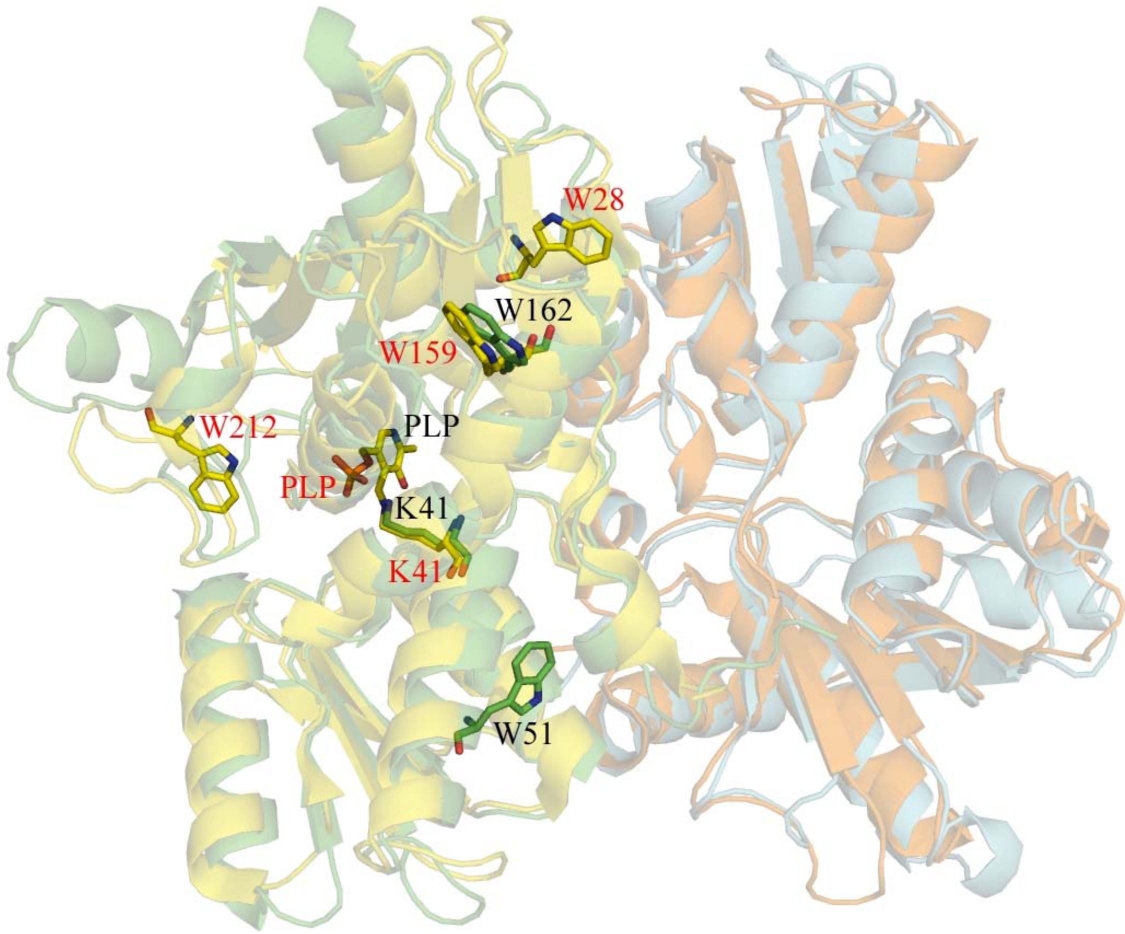

Figure AI-1. Overlay of *St*OASS-A and -B with their tryptophans of one subunit shown in sticks. *St*OASS-A is green and cyan for each subunit, respectively, labeled with black script. *St*OASS-B is yellow and orange for each subunit, respectively, labeled with red script. This figure was created using Pymol from DeLano Scientific LLC. The structures used in this figure have access number of 1OAS for OASS-A and 2JC3 for OASS-B in the Protein Data Bank.

the mutant enzymes, including intial velocity studies, rapid-scanning stopped-flow, UV-visible spectra, steady-state fluorescence spectra, and fluorescence lifetime experiments. Contribution to the total fluorescence emission and energy transfer to the PLP cofactor were proposed to differ for each tryptophan. Values of fluorescence lifetime and their fractional intensitiy were hypothesized to be different due to the specific positions, mobilities and environments of the three tryptophans. Lifetimes and fractional intensities were proposed to change as intermediates (ISB, ESB and AA) are formed along the reaction pathway, reflecting the dynamics of the enzyme during catalysis. These studies will give detailed information on the comformational dynamics of *St*OASS-B along the reaction pathway and provide further understanding of the mechanism of the enzyme.

AI.2 Materials and Methods

AI.2.1 Chemicals

All chemicals and reagents were obtained from commercial sources, were reagent grade, and were used without purification.

AI.2.2 Site-directed mutagenesis

The *cysM* gene encoding *St*OASS-B was subcloned into a pET16b vector via the *Nde*I/*Xho*I sites, using a pRSM17 vector (*93*). Site-directed mutagenesis was performed using the QuikChange® method to make three single Trp-mutant enzymes, W28Y, W159H and W212Y, and three double Trp-mutant enzymes, W28Y/W159H, W28Y/W212F, and W159H/W212F. The template for the single mutant enzymes was the recombinant *St*OASS-B plasmid. The templates for the double mutant enzymes were

W159H mutant plasmid for W28Y/W159H and W159H/W212F, and W212F mutant plasmid for W28Y/W212F. The oligonucleotide primers to generate the mutations were listed in table AI-1. The resulting mutant genes were sequenced at the Laboratory for Genomics and Bioinformatics of the University of Oklahoma Health Science Center to be certain that no mutations other than the one desired were present; none were found. All constructs encoded an N-terminal 10-His-tagged enzyme. Plasmids were transformed into *E. coli* BL21-(DE3)-RIL cells for expression.

Table AI-1. Sequence of oligonucleotide primers

$W28Y_f$	CGGCAGTGAAATC**TAT**GTCAAGCTGGAAGGC
$W28Y_r$	GCCTTCCAGCTTGAC**ATA**GATTTCACTGCCG
$W159H_f$	CCGGCCCGGAAATC**CAC**CGGCAAACGTCAGG
$W159H_r$	CCTGACGTTTGCCG**GTG**GATTTCCGGGCCGG
$W212F_f$	GGCATTCGACGC**TTC**CCTGCGGAATATATGCC
$W212F_r$	GGCATATATTCCGCAGG**GAA**GCGTCGAATGCC

Codons for mutation are in bold. Subscripts f and r represent forward and reverse primers, respectively.

AI.2.3 Enzyme Preparation

The strain containing the mutated plasmid was grown overnight at 37 ^{o}C in 50 mL of LB medium with 100 μg/mL ampicillin. This culture was transferred into 1 liter of

LB/ampicillin medium on the morning of the next day and the cell growth was continued at 30 ^{o}C until the A_{600} reached 0.7. IPTG was added to a final concentration of 1 mM to initiate expression. After 4 hours of induction at 30 ^{o}C, the cells were harvested by centrifugation at 4,500 *g* for 30 min. The cell pellet was suspended in 50 mM phosphate, 300 mM NaCl and 10 mM imidazole, pH 8.0 and sonicated on ice for 3 min with a 30 s pulse followed by a 1 min rest, using a MISONIX Sonicator XL. The supernatant was obtained by centrifugation at 20,000 *g* for 30 min and 0.05 g PLP was added into it, stirring at 4 ^{o}C for an hour. The supernatant was then loaded onto a Ni-NTA column with a 6 mL bed volume. The column was washed with 10 volumes of 50 mM imidazole at pH 8.0 and enzyme was eluted with 3 volumes of 250 mM imidazole, pH 8.0. The purified enzyme was then dialyzed against 5 mM Hepes at pH 8.0, and stored frozen at –80 ^{o}C. All of the mutant enzymes were purified in the same way as described above.

AI.2.4 Enzyme assay

Enzyme assays were performed exactly as described in reference (*93*).

AI.2.5 Initial Velocity Studies

Initial velocity data were obtained by fixing TNB concentration at 0.05 mM and varying OAS concentration around its K_m value. Data were fitted to Michaelis-Menten equation using the Marquardt-Levenberg algorithm (*112*) supplied with the programs developed by Cleland (*113*).

AI.2.6 Rapid-Scanning Stopped-Flow Studies

Experiments were performed as described in reference (*93*), but only using OAS and at pH 6.3. Global fitting of the RSSF spectra data were carried out using the fitting program provided by OLIS to generate k_{obs}s. The values of k_{obs}s were then processed according to reference (*132*) to give k_{max}/K_{ESB}, where k_{max} is the k_{obs} value at saturating OAS concentration and K_{ESB} is the dissociation constant for the external Schiff base. The EnzFitter program was used for RSSF data-fitting.

AI.2.7 UV-Visible Spectral Studies

Absorbance spectra of OASS-B and its Trp mutant enzymes were obtained using a Hewlett Packard 8452A photodiode array spectrophotometer, as described by Schnackerz et al. (*98*) for OASS-A. Spectra of enzymes alone were collected in 100 mM Hepes, at pH 6.5 and 8.0, respectively. Spectra of enzymes in presence of 30 mM L-cysteine or 300 mM L-serine were collected in 100 mM Hepes, at pH 8.0. Spectra of enzymes in presence of 2 mM OAS were collected in 100 mM Hepes, at pH 6.5. The blank consisted of all components minus enzyme for all spectra.

AI.2.8 Fluorescence Lifetime Studies

Fluorescence lifetime data were collected using an ISS Chronos time-resolved and steady-state spectrofluorometer, which is a frequency-domain instrument using laser diodes (LD) or light emitting diodes (LED) as light source. The Trp residues of OASSB and its Trp mutant enzymes were excited using a 300 nm LD and the emissions were collected for wavelenghts higher than 335 nm in 10 mM phosphate, at pH 6.3, 8.0, 9.5. The emission data were processed by Vinci program provided by ISS and gave values of fractional intensity (fi) and lifetime (τ) for each fluorophoer.

AI.3 Results and Disccussion

AI.3.1 Kinetic data

Table AI-2. Initial velocity and stopped-flow data of tryptophan mutants of *St*OASS-B

Enzyme	Initial velocity data	Stopped-flow data
	$V/K_{OAS}E_t$ ($M^{-1}s^{-1}$)	k_{max}/K_{ESB} ($M^{-1}s^{-1}$)
wild type *St*OASS-B[a]	$(3.5 \pm 1.3)\times10^4$	4.45×10^3
W28Y	$(8.1 \pm 0.4)\times10^4$	$(1.67 \pm 0.02)\times10^4$
W159H	$(5.1 \pm 0.2)\times10^4$	$(1.02 \pm 0.01)\times10^4$
W212F	$(3.08 \pm 0.08)\times10^3$	1700 ± 200
W28Y/W159H	$(8 \pm 1)\times10^4$	$(1.59 \pm 0.04)\times10^4$
W28Y/W212F	$(4.6 \pm 0.1)\times10^3$	1200 ± 200
W159H/W212F	$(3.1 \pm 0.1)\times10^3$	820 ± 80

[a] **Wild type *St*OASS-B data are from Rabeh (*133*).**

The initial velocity and RSSF data were collected for the first-half reaction of Trp mutant enzymes of OASS-B. Data are summarized in table AI-2. These kinetic data suggest that the mutation of Trp residues in OASS-B somewhat affects the enzyme activity. Mutation of W212 to F, whether in single or double mutant enzymes, results in a ~10-fold decrease in both $V/K_{OAS}E_t$ and k_{max}/K_{ESB} compared with those of wild type, which suggests that this residue is slightly relate to the enzyme catalysis. Since W212 is not close to the active site, it may be involved in a conformational change along the reaction pathway.

AI.3.2 UV-Visible Spectra

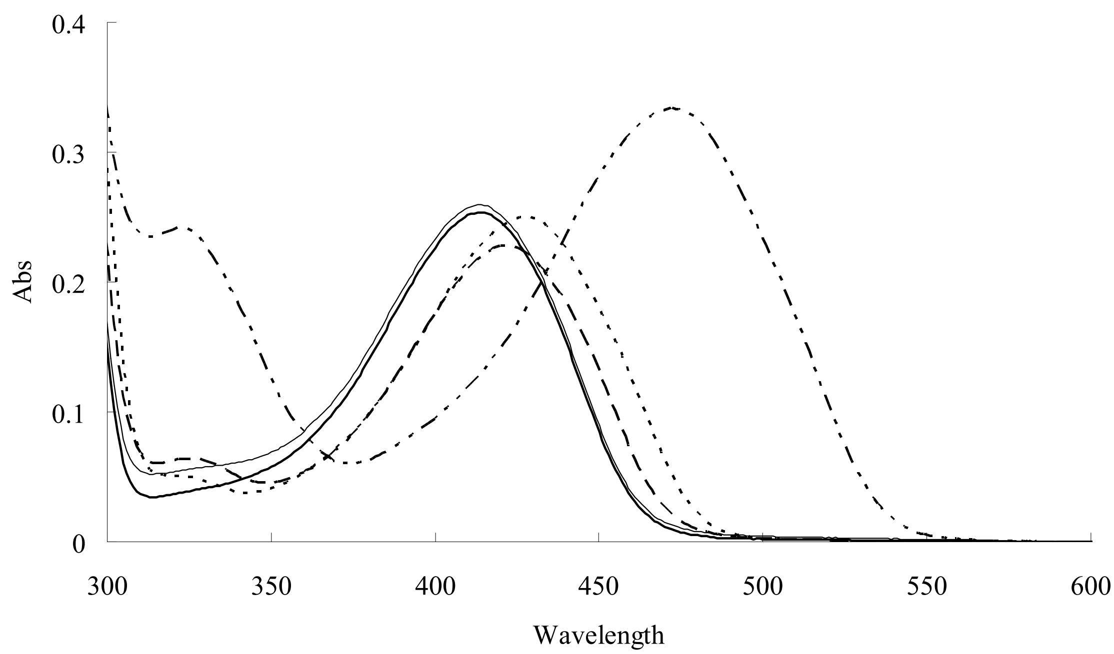

Figure AI-2. UV-visible absorption spectra of *St*OASS-B. Spectra are for StOASS-B at pH 6.5 (—), at pH 8.0 (—), with 30 mM cysteine at pH 8.0 (----), with 300 mM serine at pH 8.0 (·····) and with 2 mM OAS at pH 6.5 (-··-··). All spectra were collected in 100 mM Hepes.

The UV-Visible spectra of ISB of OASSB at pH 6.5 and 8.0 are nearly identical, exhibiting a peak centered at 414 nm, Fig. AI-1. This peak results from the predominant ketoenamine tautomer of PLP. In the spectra of the serine and lanthionine ESBs of OASS–B, the peak at 414 nm shifts to 427 and 422 nm, respectively, with a slightly increase in absorbance at 325 nm, attributed to the enolimine tautomer of PLP. Addition of OAS causes disappearance of the 414 nm peak and appearance of peaks at 472 and 327 nm, representing the ketoenamine and enolimine tautomers of AA. The absorption

Table AI-3. Extinction coefficient at 414 nm of tryptophan mutant enzymes

Enzyme	ε_{414} ($M^{-1}cm^{-1}$)
wild type *St*OASS-B	6800
W28Y	6576
W159H	5771
W212F	5851
W28Y/W159H	5461
W28Y/W212F	6034
W159H/W212F	6772

spectra of the ISB of wild type OASS-B and all the Trp mutant enzymes were very similar, and the spectroscopic changes of wild type OASS-B were observed for all the Trp mutant enzymes. These spectral data suggest that similar intermediates were formed along the reaction pathway for all the Trp mutant enzymes compared to wild type. The extinction coefficient at 414 nm for the wild type OASS-B and the mutants are slightly different and are summarized in Table AI-3.

AI.3.3 Fluorescence Lifetime Studies

Steady-state fluorescence spectra of wild type OASS-B and its Trp mutants were collected by Prof. Andrea Mozzarelli's group at University of Parma (unpublished data). Data suggest that W28, W159 and W212 are responsible for about 90%, 10%, and 2% of the total emission at 333 nm, respectively, when excited at 298 nm. W212 is predominantly responsible for the emission-energy transfer to the PLP cofactor. These conclusions were then used to analyze the lifetime properties of three Trps in OASS-B in this study.

Fluorescence lifetime data at pH 8.0 are summarized in table AI-4. W28 in W159H/W212F mutant exhibits two life times of 0.7 and 3.0 ns with intensity fractions of ~0.4 and ~0.6, respectively. W212 in W28Y/W159H mutant also exhibits two lifetimes; one is 0.6 ns with ~80% intensity, the other is 3.3 ns with ~20%. However, W159 in W28Y/W212F mutant enzyme only has one lifetime of 0.8 ns. The two life times observed for W28 and W212 may suggest two different conformations of the enzyme. The results of single Trp mutant enzymes are consistent with the life times and fractional intensities obtained for the double mutants. In wild type OASS-B, only W28 was observed as a fluorophore, exhibiting two lifetimes similar to that obtained from W159H/W212F mutant enzyme. Since W28 contributes about 90% of the total emission, it is not surprising to see above result. In apo OASS-B, three lifetimes are observed and

Table AI-4. Fluorescnece lifetime data of tryptophan mutant enzymes of *St*OASS-B

Enzyme	τ_1 (ns)	f_1	τ_2 (ns)	f_2	τ_3 (ns)	f_3	χ^2
wild type *St*OASS-B (W28, W159, W212)	0.59 (W28)	42%	2.86 (W28)	58%			1.80
apo *St*OASS-B (W28, W159, W212)	0.43	32%	2.96	22%	8.41	46%	0.99
W28Y (W159, W212)	0.79 (W159)	77%	1.33 (W212)	23%			1.94
W159H (W28, W212)	0.62 (W28)	50%	3.40 (W28)	50%			2.73
W212F (W28, W159)	0.69 (W28, W159)	38%	2.77 (W28)	62%			1.21
W28Y159H (W212)	0.60 (W212)	79%	3.29 (W212)	21%			1.81
W28Y212F (W159)	0.82 (W159)	100%					3.73
W159H212F (W28)	0.69 (W28)	39%	3.01 (W28)	61%			1.09

In the first column (enzyme), the tryptophan in parenthesis is the tryptophan available in the enzyme. In column 2 (τ_1) and 4 (τ_2), the tryptophans in parenthesis are those that contribute to lifetime studies. W28, W159 and W212 are in blue, green, and red, respectively. The identities of the tryptophans for the lifetime of apo *St*OASS-B are unknown. τ_1 of W212F may be attributed to a combination of the lifetimes of W28 and W159, on the basis of their emission intensities and their lifetime values obtained from the double mutants.

their identity can not yet be identified. The longer life time with a value of 8.4 ns could be attributed to a fluorophore that is quenched by PLP in holoenzyme.

Fluorescence lifetime data were also measured at pH 6.3 and pH 9.5 for three double Trp-mutant enzymes. These three tryptophans (W28, W159, and W212) show pH-independent values of lifetime and intensity faction, indicating that their emission properties are not affected by pH.

Appendix II

Subcloning and Expression of *O*-Acetylserine Sulfhydrylase-A from *Salmonella typhimurium*

The *cysK* gene encoding *St*OASS-A was subcloned into a pET16b vector via *Nde*I/*Xho*I sites, using a pCKM3 vector (*134*). This vector is the template for PCR of the *cysK* gene and the primers used in PCR are listed in table AII-1. PCR conditions were as follows: (1) 95 ^{o}C for 1 min, (2) 95 ^{o}C for 30 s, (3) 50 ^{o}C for 1 min, (4) 68 ^{o}C for 2 min and 30 s, (5) cycling 30 times from (2)-(4), (6) 68 ^{o}C for 10 min. pET16b vector and the amplified DNA fragment were digested with *Nde*I and *Xho*I, respectively, and then ligated to obtain the new construct. This new construct encoded an N-terminal 10-His-tagged enzyme and was transformed into *E. coli* BL21-(DE3)-RIL cells for expression.

Table AII-1. Sequence of oligonucleotide primers

*St*OASS-A_f	GGAATTC**CATATG**AGTAAGATTTATGAAGATAACTCGC
*St*OASS-A_r	CCG**CTCGAG**TCACTGTTGCAGTTCTTTCTC

Subscripts f and r represent forward and reverse primers, respectively. *Nde*I site in forward primer and *Xho*I site in reverse primer are in bold.

Enzyme expression and purification are identical to those described for *St*OASS-B in appendix I, except the purified enzyme was dialyzed against 10 mM Hepes at pH 8.0, not 5 mM Hepes as for the B-isozyme. The molecular weight of a monomer of the recombinant enzyme was measured to be 35.4 kDa using ESI mass spectrometry.

Appendix III

p$K_{i(Cysteine)}$ Profile of Serine Acetyltransferase from *Haemophilus influenzae*

AIII.1 Introduction

In bacteria and higher plants, *de novo* biosynthesis of L-cysteine proceeds via a two-step pathway (*27*). Serine acetyltransferase (SAT) catalyzes the first step, converting AcCoA and serine to CoA and OAS. In the second step, OAS and bisulfide are catalyzed by *O*-acetylserine sulfhydrylase (OASS) to give acetate and L-cysteine (*28*). The end product, L-cysteine, regulates its own synthetic pathway by competitive inhibition of SAT, suggested by inhibition studies and crystal structure of SAT:cysteine complex (*30, 35, 36*). Since L-cysteine and L-serine occupy the same active site and are nearly identical in structure, serine is expected to be able to bind to the free SAT as the cysteine does (*60*). However, the kinetic mechanism of SAT is determined as sequential and AcCoA is the first substrate to bind, indicating that there is no SAT:serine complex existing (*35*). Above data suggests that there must be some difference in the binding of these two amino acids to SAT. In this study, the pH-dependence of the inhibition constant of L-cysteine was investigated. Data were discussed in terms of the binding of L-cysteine in comparison to that of L-serine in the active site of *Hi*SAT.

AIII.2 Materials and Methods

AIII.2.1 Chemicals

All chemicals and reagents were obtained from commercial sources, were reagent grade, and were used without purification.

AIII.2.2 Enzyme Preparation

Wild type *Hi*SAT was purified according to reference (*135*).

AIII.2.3 Enzyme Assay and p$K_{i(cysteine)}$ Profile

Enzyme assays were performed as described in reference (*35*) for initial velocity measurements in the presence of L-cysteine. In the direction of serine acetylation, disappearance of absorbance at 232 nm was measured in 100 mM phosphate using 1 cm-pathlength cuvettes with a ε of 4500 $M^{-1}cm^{-1}$ (*35*), representing the disappearance of the thiolester bond of AcCoA. Inhibition data for L-cysteine at different pH (6.5-9.0, in 100 mM phosphate) were obtained by measuring the initial velocity at variable concentration of AcCoA with the concentration of L-serine fixed at about 5K_m, and at several concentrations of L-cysteine (competitive inhibitor) including zero. Inhibition data were fitted to equation AIII-1 to obtain the inhibition constant of L-cysteine at different pH. These inhibition constants were then fitted to equation AIII-2 to give the p*K* value for the binding group shown in the p$K_{i(cysteine)}$ profile.

$$v = \frac{VA}{K_a(1+\frac{I}{K_{is}})+A} \qquad \text{(AIII-1)}$$

$$\log y = \log\left(\frac{C}{1+\frac{K_1}{H}}\right) \qquad \text{(AIII-2)}$$

In equations AIII-1, v and V represent initial and maximum velocities, respectively, **A** represents substrate concentrations, K_a is K_m value for substrates **A**, and K_{is} is the competitive-inhibition constant for L-cysteine. In equations AIII-2, y is the value of $1/K_{is}$ at any pH, while C is the pH-independent value of y, **H** is the hydrogen ion concentration, and K_1 is the acid dissociation constant of functional group on enzyme or inhibitor.

AIII.3 Results and Disccussion

The p$K_{i(cysteine)}$ profile of *Hi*SAT exhibits a limiting slope of 1 on the basic side, Fig. AIII-1, indicating a group that needs to be protonated for optimum binding of cysteine with a pK_a value of 8.4 ± 0.1. This group can either be from the inhibitor, L-cysteine, or the enzyme. Since this group is not observed in the pH-rate profile of V/K_{ser}, which only exhibits a general base group on the acid side (*76*), it is unlikely that this group is from the enzyme, given the structural similarity of serine and cysteine. This group thus could represent the thiol of L-cysteine, which has a pK_a value of 8.37 when it is free in solution, nearly identical to the value of 8.4 obtained in the p$K_{i(cysteine)}$ profile.

Above data suggest that the protonated thiol group of L-cysteine is essential for its binding to the free enzyme and the difference between the thiol group of cysteine and the hydroxyl group of serine may be responsible for the nonexistence of SAT:serine complex.

The hydroxyl group of serine is already protonated as the optimum binding form of cysteine, indicating that the protonation state of serine should not contribute to its inability of binding free enzyme. The length of the C-O bond in hydroxyl group is about 1.4 Å, while the length of C-S bond in thiol is about 1.8, 0.4 Å longer then the C-O bond. In addition, the orientation of the thiol group of cysteine and the hydroxyl group of serine could be slightly different when they bind. These two factors, bond length and orientation, may be the key to explain why serine can not bind to the free *Hi*SAT.

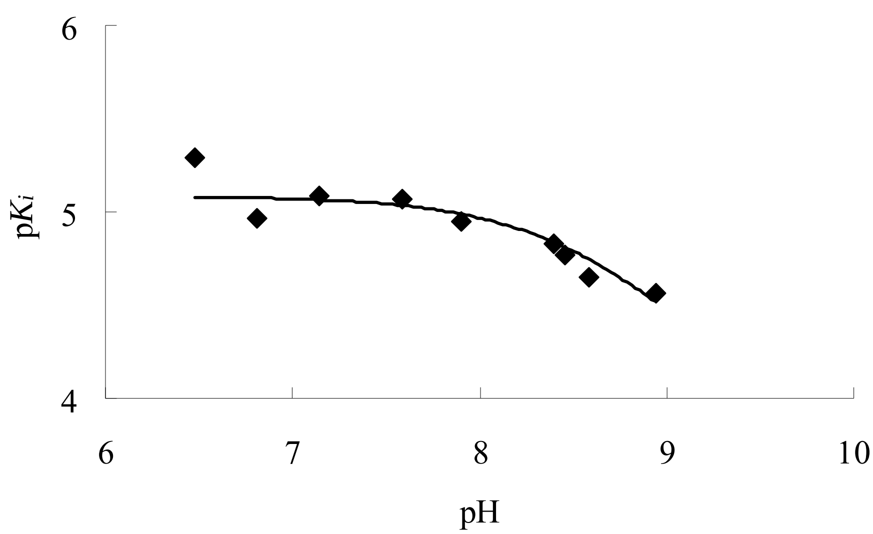

Figure AIII-1. pH dependence of p$K_{i(cysteine)}$ values of *Hi*SAT. Points (◆) are experimental values, while the curve is theoretical based on fits of the data using equation AIII-2.

Recently, roles of H154, H189 and D139 in the active site of *Hi*SAT were investigated and the mutation of D139 to N was reported to result in a change of kinetic mechanism from sequential to random (*135*), which suggests that serine can bind to the free *Hi*SAT by a single mutation of D139 although D139 has no direct interaction with serine, and thus indicates that even small change in the active site can lead to the change of serine binding. This confirms that the difference of bond length and orientation of thiol and hydroxyl group may cause the inability of serine binding to the free *Hi*SAT.

Although serine cannot bind to free enzyme, it can bind to the SAT:AcCoA complex, suggesting a structural difference between free enzyme and the complex. There must be a conformational change responsible for this structure difference when AcCoA binds to the enzyme.

Appendix IV

Other research

Two mutant enzymes of *St*OASS-A, H152A and K120Q, were constructed using site-directed mutagenesis (QuikChange® method) and purified as described for wild type OASS-A in appendix II. The template for mutagenesis is the OASS-A plasmid constructed in appendix II. The oligonucleotide primers to generate the mutations are listed in table AIV-1.

Table AIV-1. Sequence of oligonucleotide primers

$H152A_f$	CCTGCCAACCCGGAAATC**GCC**GAAAAAACCACC
$H152A_r$	GGTGGTTTTTTC**GGC**GATTTCCGGGTTGGCAGG
$K120Q_f$	CGAAGGGGCGAAAGGGATG**CAA**GGCGCTATTCAGAAAGC
$K120Q_r$	GCTTTCTGAATAGCGCC**TTG**CATCCCTTTCGCCCCTTCG

Codons for mutation are in bold. Subscripts f and r represent forward and reverse primers, respectively.

The UV-Visible and fluorescence emission properties of these two mutant enzymes were investigated and published in the following papers and will not be discussed further in this thesis.

Tai, C.-H., Rabeh, W. M., Guan, R., Schnackerz, K. D., and Cook, P. F. (2008) Role of Histidine-152 in cofactor orientation in the PLP-dependent O-acetylserine sulfhydrylase reaction, *Arch. Biochem. Biophys. 472*, 115-125. (*136*).

Tai, C.-H., Rabeh, W. M., Guan, R., Schnackerz, K. D., and Cook, P. F. (2008) Effect of mutation of lysine-120, located at the entry to the active site of *O*-acetylserine sulfhydrylase-A (OASS-A) from *Salmonella typhimurium*, *Biochim. Biophys. Acta, Proteins Proteomics 1784*, 629-637. (*137*).

References

1. Weinstein, C. L., and Griffith, O. W. (1987) Cysteinesulfinate decarboxylase, *Methods Enzymol. 143*, 404-410.
2. Giovanelli, J. (1987) Sulfur amino acids of plants: an overview, *Methods Enzymol. 143*, 419-426.
3. Kredich, N. M. (1996) Biosynthesis of cysteine, in *Escherichia coli and Salmonella: Cellular and Molecular Biology* (Neidhardt, F. C., Ed.) 2nd ed., pp 514-527, ASM Press, Washington, D.C.
4. Marzluf, G. A. (1997) Molecular genetics of sulfur assimilation in filamentous fungi and yeast, *Annu. Rev. Microbiol. 51*, 73-96.
5. Thomas, D., and Surdin-Kerjan, Y. (1997) Metabolism of sulfur amino acids in *Saccharomyces cerevisiae*, *Microbiol. Mol. Biol. Rev. 61*, 503-532.
6. Leustek, T., Martin, M. N., Bick, J.-A., and Davies, J. P. (2000) Pathways and regulation of sulfur metabolism revealed through molecular and genetic studies, *Annu. Rev. Plant Physiol. Plant Mol. Biol. 51*, 141-165.
7. Bykowski, T., van der Ploeg Jan, R., Iwanicka-Nowicka, R., and Hryniewicz Monika, M. (2002) The switch from inorganic to organic sulphur assimilation in *Escherichia coli*: adenosine 5'-phosphosulphate (APS) as a signalling molecule for sulphate excess, *Mol. Microbiol. 43*, 1347-1358.
8. Hryniewicz, M. M., and Kredich, N. M. (1991) The *cysP* promoter of *Salmonella typhimurium*: characterization of two binding sites for CysB protein, studies of in vivo transcription initiation, and demonstration of the anti-inducer effects of thiosulfate, *J. Bacteriol. 173*, 5876-5886.
9. Hellinga, H. W., and Evans, P. R. (1985) Nucleotide sequence and high-level expression of the major *Escherichia coli* phosphofructokinase, *Eur. J. Biochem. 149*, 363-373.

10. Hryniewicz, M., Sirko, A., Palucha, A., Bock, A., and Hulanicka, D. (1990) Sulfate and thiosulfate transport in *Escherichia coli K-12*: identification of a gene encoding a novel protein involved in thiosulfate binding, *J. Bacteriol. 172*, 3358-3366.

11. Sirko, A., Hryniewicz, M., Hulanicka, D., and Bock, A. (1990) Sulfate and thiosulfate transport in *Escherichia coli K-12*: nucleotide sequence and expression of the *cysTWAM* gene cluster, *J. Bacteriol. 172*, 3351-3357.

12. Tai, C. H., and Cook, P. F. (2000) *O*-acetylserine sulfhydrylase, *Adv. Enzymol. Relat. Areas Mol. Biol. 74*, 185-234.

13. Robbins, P. W., and Lipmann, F. (1958) Enzymatic synthesis of adenosine-5'-phosphosulfate, *J. Biol. Chem. 233*, 686-690.

14. Liu, C., Martin, E., and Leyh, T. S. (1994) GTPase activation of ATP sulfurylase: the mechanism, *Biochemistry 33*, 2042-2047.

15. Leyh, T. S., Taylor, J. C., and Markham, G. D. (1988) The sulfate activation locus of *Escherichia coli K12*: cloning, genetic, and enzymatic characterization, *J. Biol. Chem. 263*, 2409-2416.

16. Leyh, T. S., and Suo, Y. (1992) GTPase-mediated activation of ATP sulfurylase, *J. Biol. Chem. 267*, 542-545.

17. Leyh, T. S., Vogt, T. F., and Suo, Y. (1992) The DNA sequence of the sulfate activation locus from *Escherichia coli K-12*, *J. Biol. Chem. 267*, 10405-10410.

18. Leyh, T. S. (1993) The physical biochemistry and molecular genetics of sulfate activation, *Crit. Rev. Biochem. Mol. Biol. 28*, 515-542.

19. Satishchandran, C., and Markham, G. D. (1989) Adenosine-5'-phosphosulfate kinase from *Escherichia coli K12*. Purification, characterization, and identification of a phosphorylated enzyme intermediate, *J. Biol. Chem. 264*, 15012-15021.

20. Satishchandran, C., Hickman, Y. N., and Markham, G. D. (1992) Characterization

of the phosphorylated enzyme intermediate formed in the adenosine 5'-phosphosulfate kinase reaction, *Biochemistry 31*, 11684-11688.

21. Krone, F. A., Westphal, G., and Schwenn, J. D. (1991) Characterization of the gene *cysH* and of its product phospho-adenylylsulfate reductase from *Escherichia coli*, *Mol. Gen. Genet. 225*, 314-319.

22. Tsang, M. L., and Schiff, J. A. (1978) Assimilatory sulfate reduction in an *Escherichia coli* mutant lacking thioredoxin activity, *J. Bacteriol. 134*, 131-138.

23. Tsang, M. L. (1983) Function of thioredoxin of 3'-phosphoadenosine 5'-phosphosulfate in *E. Coli*, in *Thioredoxins-structure and function* (Gadal, P., Ed.), pp 103-110, Centre National de la Recherche Scientifique, Paris.

24. Siegel, L. M., and Davis, P. S. (1974) Reduced nicotinamide adenine dinucleotide phosphate-sulfite reductase of enterobacteria. IV. The *Escherichia coli* hemoflavoprotein: subunit structure and dissociation into hemoprotein and flavoprotein components, *J. Biol. Chem. 249*, 1587-1598.

25. Siegel, L. M., Murphy, M. J., and Kamin, H. (1973) Reduced nicotinamide adenine dinucleotide phosphate-sulfite reductase of enterobacteria. I. The *Escherichia coli* hemoflavoprotein: molecular parameters and prosthetic groups, *J. Biol. Chem. 248*, 251-264.

26. Siegel, L. M., Davis, P. S., and Kamin, H. (1974) Reduced nicotinamide adenine dinucleotide phosphate-sulfite reductase of enterobacteria. III. The *Escherichia coli* hemoflavoprotein: catalytic parameters and the sequence of electron flow, *J. Biol. Chem. 249*, 1572-1586.

27. Kredich, N. M., and Tomkins, G. M. (1966) The enzymic synthesis of L-cysteine in *Escherichia coli* and *Salmonella typhimurium*, *J. Biol. Chem. 241*, 4955-4965.

28. Becker, M. A., Kredich, N. M., and Tomkins, G. M. (1969) The purification and characterization of *O*-acetylserine sulfhydrylase-A from *Salmonella typhimurium*, *J. Biol. Chem. 244*, 2418-2427.

29. Tai, C. H., Nalabolu, S. R., Jacobson, T. M., Minter, D. E., and Cook, P. F. (1993) Kinetic mechanisms of the A and B isozymes of *O*-acetylserine sulfhydrylase from *Salmonella typhimurium LT-2* using the natural and alternative reactants, *Biochemistry 32*, 6433-6442.

30. Kredich, N. M., Becker, M. A., and Tomkins, G. M. (1969) Purification and characterization of cysteine synthetase, a bifunctional protein complex, from *Salmonella typhimurium*, *J. Biol. Chem. 244*, 2428-2439.

31. Wirtz, M., and Hell, R. (2003) Production of cysteine for bacterial and plant biotechnology: application of cysteine feedback-insensitive isoforms of serine acetyltransferase, *Amino Acids 24*, 195-203.

32. Sirko, A., Blaszczyk, A., and Liszewska, F. (2004) Overproduction of SAT and/or OASTL in transgenic plants: a survey of effects, *J. Exp. Bot. 55*, 1881-1888.

33. Noji, M., and Saito, K. (2002) Molecular and biochemical analysis of serine acetyltransferase and cysteine synthase towards sulfur metabolic engineering in plants, *Amino Acids 22*, 231-243.

34. Noji, M., Inoue, K., Kimura, N., Gouda, A., and Saito, K. (1998) Isoform-dependent differences in feedback regulation and subcellular localization of serine acetyltransferase involved in cysteine biosynthesis from *Arabidopsis thaliana*, *J. Biol. Chem. 273*, 32739-32745.

35. Johnson, C. M., Huang, B., Roderick, S. L., and Cook, P. F. (2004) Kinetic mechanism of the serine acetyltransferase from *Haemophilus influenzae*, *Arch. Biochem. Biophys. 429*, 115-122.

36. Olsen, L. R., Huang, B., Vetting, M. W., and Roderick, S. L. (2004) Structure of serine acetyltransferase in complexes with CoA and its cysteine feedback inhibitor, *Biochemistry 43*, 6013-6019.

37. Cook, P. F., and Wedding, R. T. (1976) A reaction mechanism from steady state kinetic studies for *O*-acetylserine sulfhydrylase from *Salmonella typhimurium*

LT-2, *J. Biol. Chem. 251*, 2023-2029.

38. Tai, C. H., Burkhard, P., Gani, D., Jenn, T., Johnson, C., and Cook, P. F. (2001) Characterization of the allosteric anion-binding site of *O*-acetylserine sulfhydrylase, *Biochemistry 40*, 7446-7452.

39. Beaman, T. W., Binder, D. A., Blanchard, J. S., and Roderick, S. L. (1997) Three-dimensional structure of tetrahydrodipicolinate *N*-succinyltransferase, *Biochemistry 36*, 489-494.

40. Hindson, V. J., Moody, P. C., Rowe, A. J., and Shaw, W. V. (2000) Serine acetyltransferase from *Escherichia coli* is a dimer of trimers, *J. Biol. Chem. 275*, 461-466.

41. Cook, P. F., and Wedding, R. T. (1977) Initial kinetic characterization of the multienzyme complex, cysteine synthase, *Arch. Biochem. Biophys. 178*, 293-302.

42. Denk, D., and Bock, A. (1987) L-cysteine biosynthesis in *Escherichia coli*: nucleotide sequence and expression of the serine acetyltransferase (*cysE*) gene from the wild-type and a cysteine-excreting mutant, *J. Gen. Microbiol. 133*, 515-525.

43. Mino, K., Yamanoue, T., Sakiyama, T., Eisaki, N., Matsuyama, A., and Nakanishi, K. (1999) Purification and characterization of serine acetyltransferase from *Escherichia coli* partially truncated at the C-terminal region, *Biosci. Biotechnol. Biochem. 63*, 168-179.

44. Bogdanova, N., and Hell, R. (1997) Cysteine synthesis in plants: protein-protein interactions of serine acetyltransferase from *Arabidopsis thaliana*, *Plant J. 11*, 251-262.

45. Wirtz, M., Berkowitz, O., Droux, M., and Hell, R. (2001) The cysteine synthase complex from plants. Mitochondrial serine acetyltransferase from *Arabidopsis thaliana* carries a bifunctional domain for catalysis and protein-protein interaction, *Eur. J. Biochem. 268*, 686-693.

46. Mino, K., Hiraoka, K., Imamura, K., Sakiyama, T., Eisaki, N., Matsuyama, A., and Nakanishi, K. (2000) Characteristics of serine acetyltransferase from *Escherichia coli* deleting different lengths of amino acid residues from the C-terminus, *Biosci. Biotechnol. Biochem. 64*, 1874-1880.

47. Takagi, H., Kobayashi, C., Kobayashi, S., and Nakamori, S. (1999) PCR random mutagenesis into *Escherichia coli* serine acetyltransferase: isolation of the mutant enzymes that cause overproduction of L-cysteine and L-cystine due to the desensitization to feedback inhibition, *FEBS Lett. 452*, 323-327.

48. Nakamura, K., and Tamura, G. (1990) Isolation of serine acetyltransferase complexed with cysteine synthase from *Allium tuberosum*, *Agric. Biol. Chem. 54*, 649-656.

49. Droux, M., Martin, J., Sajus, P., and Douce, R. (1992) Purification and characterization of *O*-acetylserine (thiol) lyase from spinach chloroplasts, *Arch. Biochem. Biophys. 295*, 379-390.

50. Droux, M., Ruffet, M. L., Douce, R., and Job, D. (1998) Interactions between serine acetyltransferase and *O*-acetylserine (thiol) lyase in higher plants--structural and kinetic properties of the free and bound enzymes, *Eur. J. Biochem. 255*, 235-245.

51. Huang, B., Vetting, M. W., and Roderick, S. L. (2005) The active site of *O*-acetylserine sulfhydrylase is the anchor point for bienzyme complex formation with serine acetyltransferase, *J. Bacteriol. 187*, 3201-3205.

52. Campanini, B., Speroni, F., Salsi, E., Cook, P. F., Roderick, S. L., Huang, B., Bettati, S., and Mozzarelli, A. (2005) Interaction of serine acetyltransferase with *O*-acetylserine sulfhydrylase active site: evidence from fluorescence spectroscopy, *Protein Sci. 14*, 2115-2124.

53. Zhao, C., Moriga, Y., Feng, B., Kumada, Y., Imanaka, H., Imamura, K., and Nakanishi, K. (2006) On the interaction site of serine acetyltransferase in the

cysteine synthase complex from *Escherichia coli*, *Biochem. Biophys. Res. Commun. 341*, 911-916.

54. Mino, K., Imamura, K., Sakiyama, T., Eisaki, N., Matsuyama, A., and Nakanishi, K. (2001) Increase in the stability of serine acetyltransferase from *Escherichia coli* against cold inactivation and proteolysis by forming a bienzyme complex, *Biosci. Biotechnol. Biochem. 65*, 865-874.

55. Mino, K., Yamanoue, T., Sakiyama, T., Eisaki, N., Matsuyama, A., and Nakanishi, K. (2000) Effects of bienzyme complex formation of cysteine synthetase from *Escherichia coli* on some properties and kinetics, *Biosci. Biotechnol. Biochem. 64*, 1628-1640.

56. Berkowitz, O., Wirtz, M., Wolf, A., Kuhlmann, J., and Hell, R. (2002) Use of biomolecular interaction analysis to elucidate the regulatory mechanism of the cysteine synthase complex from *Arabidopsis thaliana*, *J. Biol. Chem. 277*, 30629-30634.

57. Smith, I. K., and Thompson, J. F. (1971) Purification and characterization of L-serine transacetylase and *O*-acetyl-L-serine sulfhydrylase from kidney bean seedlings (*Phaseolus vulgaris*), *Biochim. Biophys. Acta. 227*, 288-295.

58. Vaara, M. (1992) Eight bacterial proteins, including UDP-*N*-acetylglucosamine acyltransferase (LpxA) and three other transferases of *Escherichia coli*, consist of a six-residue periodicity theme, *FEMS Microbiol. Lett. 76*, 249-254.

59. Bairoch, A. (1993) The PROSITE dictionary of sites and patterns in proteins, its current status, *Nuc. Acid Res. 21*, 3097-3103.

60. Johnson, C. M., Roderick, S. L., and Cook, P. F. (2005) The serine acetyltransferase reaction: acetyl transfer from an acylpantothenyl donor to an alcohol, *Arch. Biochem. Biophys. 433*, 85-95.

61. Raetz, C. R., and Roderick, S. L. (1995) A left-handed parallel beta helix in the structure of UDP-*N*-acetylglucosamine acyltransferase, *Science 270*, 997-1000.

62. Gorman, J., and Shapiro, L. (2004) Structure of serine acetyltransferase from *Haemophilus influenzae* Rd, *Acta. Cryst. D 60*, 1600-1605.

63. Beaman, T. W., Blanchard, J. S., and Roderick, S. L. (1998) The conformational change and active site structure of tetrahydrodipicolinate *N*-succinyltransferase, *Biochemistry 37*, 10363-10369.

64. Beaman, T. W., Sugantino, M., and Roderick, S. L. (1998) Structure of the hexapeptide xenobiotic acetyltransferase from *Pseudomonas aeruginosa*, *Biochemistry 37*, 6689-6696.

65. Wang, X., Olsen, L. R., and Roderick, S. L. (2002) Structure of the *lac* operon galactoside acetyltransferase, *Structure (Cambridge, MA, United States) 10*, 581-588.

66. Hindson, V. J. (2003) Serine acetyltransferase of *Escherichia coli*: substrate specificity and feedback control by cysteine, *Biochem. J. 375*, 745-752.

67. Sugantino, M., and Roderick, S. L. (2002) Crystal structure of Vat(D): an acetyltransferase that inactivates streptogramin group A antibiotics, *Biochemistry 41*, 2209-2216.

68. Nakamori, S., Kobayashi, S. I., Kobayashi, C., and Takagi, H. (1998) Overproduction of L-cysteine and L-cystine by *Escherichia coli* strains with a genetically altered serine acetyltransferase, *Appl. Environ. Microbiol. 64*, 1607-1611.

69. Pye, V. E., Tingey, A. P., Robson, R. L., and Moody, P. C. (2004) The structure and mechanism of serine acetyltransferase from *Escherichia coli*, *J. Biol. Chem. 279*, 40729-40736.

70. Hindson, V. J., and Shaw, W. V. (2003) Random-order ternary complex reaction mechanism of serine acetyltransferase from *Escherichia coli*, *Biochemistry 42*, 3113-3119.

71. Olsen, L. R., and Roderick, S. L. (2001) Structure of the *Escherichia coli* GlmU

pyrophosphorylase and acetyltransferase active sites, *Biochemistry 40*, 1913-1921.

72. Schimerlik, M. I., and Cleland, W. W. (1973) Inhibition of creatine kinase by chromium nucleotides, *J. Biol. Chem. 248*, 8418-8423.

73. Cook, P. F., Kenyon, G. L., and Cleland, W. W. (1981) Use of pH studies to elucidate the catalytic mechanism of rabbit muscle creatine kinase, *Biochemistry 20*, 1204-1210.

74. Morrison, J. F., and Cleland, W. W. (1966) Isotope-exchange studies of the mechanism of the reaction catalyzed by adenosine triphosphate: creatine phosphotransferase, *J. Biol. Chem. 241*, 673-683.

75. Leu, L. S., and Cook, P. F. (1994) Kinetic mechanism of serine transacetylase from *Salmonella typhimurium*, *Biochemistry 33*, 2667-2671.

76. Johnson, C. M., Huang, B., Roderick, S. L., and Cook, P. F. (2004) Chemical mechanism of the serine acetyltransferase from *Haemophilus influenzae*, *Biochemistry 43*, 15534-15539.

77. Quinn, D. M. a. S., L.D. (1991) Theoretical basis and mechanistic utility of solvent isotope effects, in *Enzyme Mechanism from Isotope Effects* (Cook, P. F., Ed.), pp 73-126, CRC Press, Boca Raton, FL.

78. Kisker, C., Schindelin, H., Alber, B. E., Ferry, J. G., and Rees, D. C. (1996) A left-hand beta-helix revealed by the crystal structure of a carbonic anhydrase from the archaeon *Methanosarcina thermophila*, *EMBO (Eur. Mol. Biol. Organ.) J. 15*, 2323-2330.

79. Rege, V. D., Kredich, N. M., Tai, C. H., Karsten, W. E., Schnackerz, K. D., and Cook, P. F. (1996) A change in the internal aldimine lysine (K42) in *O*-acetylserine sulfhydrylase to alanine indicates its importance in transimination and as a general base catalyst, *Biochemistry 35*, 13485-13493.

80. Bettati, S., Campanini, B., Vaccari, S., Mozzarelli, A., Schianchi, G., Hazlett, T. L.,

Gratton, E., and Benci, S. (2002) Unfolding of pyridoxal 5'-phosphate-dependent *O*-acetylserine sulfhydrylase probed by time-resolved tryptophan fluorescence, *Biochim. Biophys. Acta 1596*, 47-54.

81. Schnackerz, K. D., and Cook, P. F. (1995) Resolution of pyridoxal 5'-phosphate from *O*-acetylserine sulfhydrylase from *Salmonella typhimurium* and reconstitution of apoenzyme with cofactor and cofactor analogs as a probe of the cofactor binding site, *Arch. Biochem. Biophys. 324*, 71-77.

82. Mino, K., and Ishikawa, K. (2003) Characterization of a novel thermostable *O*-acetylserine sulfhydrylase from *Aeropyrum pernix K1*, *J. Bacteriol. 185*, 2277-2284.

83. Nakamura, T., Kon, Y., Iwahashi, H., and Eguchi, Y. (1983) Evidence that thiosulfate assimilation by *Salmonella typhimurium* is catalyzed by cysteine synthase B, *J. Bacteriol. 156*, 656-662.

84. Amadasi, A., Bertoldi, M., Contestabile, R., Bettati, S., Cellini, B., di Salvo, M. L., Borri-Voltattorni, C., Bossa, F., and Mozzarelli, A. (2007) Pyridoxal 5'-phosphate enzymes as targets for therapeutic agents, *Curr. Med. Chem. 14*, 1291-1324.

85. Lv, X., Fan, J., Ge, H., Gao, Y., Zhang, X., Teng, M., and Niu, L. (2006) Cloning, expression, purification, crystallization and preliminary X-ray diffraction analysis of the glutamate-1-semialdehyde aminotransferase from *Bacillus subtilis*, *Acta Crystallogr. Sect. F Struct. Biol. Cryst. Commun. 62*, 483-485.

86. Schulze, J. O., Schubert, W.-D., Moser, J., Jahn, D., and Heinz, D. W. (2006) Evolutionary Relationship between Initial Enzymes of Tetrapyrrole Biosynthesis, *J. Mol. Biol. 358*, 1212-1220.

87. Moser, J., Schubert, W. D., Beier, V., Bringemeier, I., Jahn, D., and Heinz, D. W. (2001) V-shaped structure of glutamyl-tRNA reductase, the first enzyme of tRNA-dependent tetrapyrrole biosynthesis, *EMBO (Eur. Mol. Biol. Organ.) J. 20*, 6583-6590.

88. Zhang, L., Cooper, A. J. L., Krasnikov, B. F., Xu, H., Bubber, P., Pinto, J. T., Gibson, G. E., and Hanigan, M. H. (2006) Cisplatin-Induced toxicity is associated with platinum deposition in mouse kidney mitochondria *in Vivo* and with selective inactivation of the a-ketoglutarate dehydrogenase complex in LLC-PK1 cells, *Biochemistry 45*, 8959-8971.

89. Burkhard, P., Rao, G. S., Hohenester, E., Schnackerz, K. D., Cook, P. F., and Jansonius, J. N. (1998) Three-dimensional structure of *O*-acetylserine sulfhydrylase from *Salmonella typhimurium*, *J. Mol. Biol. 283*, 121-133.

90. Cook, P. F., Hara, S., Nalabolu, S., and Schnackerz, K. D. (1992) pH dependence of the absorbance and ^{31}P NMR spectra of *O*-acetylserine sulfhydrylase in the absence and presence of *O*-acetyl-L-serine, *Biochemistry 31*, 2298-2303.

91. Burkhard, P., Tai, C. H., Ristroph, C. M., Cook, P. F., and Jansonius, J. N. (1999) Ligand binding induces a large conformational change in *O*-acetylserine sulfhydrylase from *Salmonella typhimurium*, *J. Mol. Biol. 291*, 941-953.

92. Burkhard, P., Tai, C. H., Jansonius, J. N., and Cook, P. F. (2000) Identification of an allosteric anion-binding site on *O*-acetylserine sulfhydrylase: structure of the enzyme with chloride bound, *J. Mol. Biol. 303*, 279-286.

93. Chattopadhyay, A., Meier, M., Ivaninskii, S., Burkhard, P., Speroni, F., Campanini, B., Bettati, S., Mozzarelli, A., Rabeh, W. M., Li, L., and Cook, P. F. (2007) Structure, mechanism, and conformational dynamics of *O*-acetylserine sulfhydrylase from *Salmonella typhimurium*: comparison of A and B isozymes, *Biochemistry 46*, 8315-8330.

94. Claus, M. T., Zocher, G. E., Maier, T. H., and Schulz, G. E. (2005) Structure of the *O*-acetylserine sulfhydrylase isoenzyme CysM from *Escherichia coli*, *Biochemistry 44*, 8620-8626.

95. Woehl, E. U., Tai, C. H., Dunn, M. F., and Cook, P. F. (1996) Formation of the alpha-aminoacrylate intermediate limits the overall reaction catalyzed by

O-acetylserine sulfhydrylase, *Biochemistry 35*, 4776-4783.

96. Cook, P. F. (1976) Kinetic studies on the cysteine biosynthetic enzymes from *Salmonella typhimurium LT-2*, p 153 pp.

97. Cook, P. F., Tai, C. H., Hwang, C. C., Woehl, E. U., Dunn, M. F., and Schnackerz, K. D. (1996) Substitution of pyridoxal 5'-phosphate in the *O*-acetylserine sulfhydrylase from *Salmonella typhimurium* by cofactor analogs provides a test of the mechanism proposed for formation of the alpha-aminoacrylate intermediate, *J. Biol. Chem. 271*, 25842-25849.

98. Schnackerz, K. D., Tai, C. H., Simmons, J. W., 3rd, Jacobson, T. M., Rao, G. S., and Cook, P. F. (1995) Identification and spectral characterization of the external aldimine of the *O*-acetylserine sulfhydrylase reaction, *Biochemistry 34*, 12152-12160.

99. Tai, C. H., Nalabolu, S. R., Simmons, J. W., 3rd, Jacobson, T. M., and Cook, P. F. (1995) Acid-base chemical mechanism of *O*-acetylserine sulfhydrylases-A and -B from pH studies, *Biochemistry 34*, 12311-12322.

100. McClure, G. D., Jr., and Cook, P. F. (1994) Product binding to the alpha-carboxyl subsite results in a conformational change at the active site of *O*-acetylserine sulfhydrylase-A: evidence from fluorescence spectroscopy, *Biochemistry 33*, 1674-1683.

101. Strambini, G. B., Cioni, P., and Cook, P. F. (1996) Tryptophan luminescence as a probe of enzyme conformation along the *O*-acetylserine sulfhydrylase reaction pathway, *Biochemistry 35*, 8392-8400.

102. Benci, S., Vaccari, S., Mozzarelli, A., and Cook, P. F. (1997) Time-resolved fluorescence of *O*-acetylserine sulfhydrylase catalytic intermediates, *Biochemistry 36*, 15419-15427.

103. Benci, S., Vaccari, S., Mozzarelli, A., and Cook, P. F. (1999) Time-resolved fluorescence of *O*-acetylserine sulfhydrylase, *Biochim. Biophys. Acta 1429*,

317-330.

104. Benci, S., Bettati, S., Vaccari, S., Schianchi, G., Mozzarelli, A., and Cook, P. F. (1999) Conformational probes of *O*-acetylserine sulfhydrylase: fluorescence of tryptophans 50 and 161, *J. Photochem. Photobiol. B: Biol. 48*, 17-26.

105. Tai, C. H., and Cook, P. F. (2001) Pyridoxal 5'-phosphate-dependent alpha, beta-elimination reactions: mechanism of *O*-acetylserine sulfhydrylase, *Acc. Chem. Res. 34*, 49-59.

106. Karsten, W. E., and Cook, P. F. (2002) Detection of intermediates in reactions catalyzed by PLP-dependent enzymes: *O*-acetylserine sulfhydrylase and serine-glyoxalate aminotransferase, *Methods Enzymol. 354*, 223-237.

107. Hwang, C. C., Woehl, E. U., Minter, D. E., Dunn, M. F., and Cook, P. F. (1996) Kinetic isotope effects as a probe of the beta-elimination reaction catalyzed by *O*-acetylserine sulfhydrylase, *Biochemistry 35*, 6358-6365.

108. Westheimer, F. H. (1961) The magnitude of the primary kinetic isotope effect for compounds of hydrogen and deuterium, *Chemical Reviews (Washington, DC, United States) 61*, 265-273.

109. Streitwieser, A., Jr., Jagow, R. H., Fahey, R. C., and Suzuki, S. (1958) Kinetic isotope effects in the acetolyses of deuteriated cyclopentyl tosylates, *J. Am. Chem. Soc. 80*, 2326-2332.

110. Cook, P. F., and Wedding, R. T. (1978) Cysteine synthetase from *Salmonella typhimurium LT-2*. Aggregation, kinetic behavior, and effect of modifiers, *J. Biol. Chem. 253*, 7874-7879.

111. Riddles, P. W., Blakeley, R. L., and Zerner, B. (1983) Reassessment of Ellman's reagent, *Methods Enzymol. 91*, 49-60.

112. Marquardt, D. W. (1963) An algorithm for least-squares estimation of nonlinear parameters, *J. Soc. Indust. Appl. Math. 11*, 431-441.

113. Cleland, W. W. (1979) Statistical analysis of enzyme kinetic data, *Methods*

Enzymol. 63, 103-138.

114. Cleland, W. W. (1977) Determining the chemical mechanisms of enzyme-catalyzed reactions by kinetic studies, *Adv. Enzymol. Relat. Areas Mol. Biol. 45*, 273-387.

115. Mizuguchi, H., Cook, P. F., Tai, C.-H., Hasemann, C. A., and Uyeda, K. (1999) Reaction mechanism of fructose-2, 6-bisphosphatase. A mutation of nucleophilic catalyst, histidine 256, induces an alteration in the reaction pathway, *J. Biol. Chem. 274*, 2166-2175.

116. Filutowicz, M., Wiater, A., and Hulanicka, D. (1982) Delayed inducibility of sulphite reductase in cysM mutants of *Salmonella typhimurium* under anaerobic conditions, *J. Gen. Microbiol. 128*, 1791-1794.

117. Rabeh, W. M., Mather, T., and Cook, P. F. (2006) A three-dimensional homology model of the *O*-acetylserine sulfhydrylase-B from *Salmonella typhimurium*, *Protein Pept. Lett. 13*, 7-13.

118. Mattingly, M. E., Mattingly, J. R., Jr., and Martinez-Carrion, M. (1982) Phosphorus-31 nuclear magnetic resonance of mitochondrial aspartate aminotransferase. The effects of solution pH and ligand binding, *J. Biol. Chem. 257*, 8872-8878.

119. Martinez-Carrion, M. (1975) Phosphorus-31 nuclear magnetic resonance studies of pyridoxal and pyridoxamine phosphates. Interaction with cytoplasmic aspartate transaminase, *Eur. J. Biochem. 54*, 39-43.

120. Schnackerz, K. D., and Mozzarelli, A. (1998) Plasticity of the tryptophan synthase active site probed by ^{31}P NMR spectroscopy, *J. Biol. Chem. 273*, 33247-33253.

121. Schnackerz, K. D., Feldmann, K., and Hull, W. E. (1979) Phosphorus-31 nuclear magnetic resonance study of D-serine dehydratase: pyridoxal phosphate binding site, *Biochemistry 18*, 1536-1539.

122. Groman, E., Huang, Y. Z., Watanabe, T., and Snell, E. E. (1972) Coenzymatic

activity of pyridoxal 5'-sulfate and related analogues of pyridoxal 5'-phosphate, *Proc. Natl. Acad. Sci., USA 69*, 3297-3300.

123. Schirch, L., and Schnackerz, K. D. (1978) Activation of aposerine transhydroxymethylase by pyridoxal-5'-phosphate monomethyl ester, *Biochem. Biophys. Res. Commun. 85*, 99-106.

124. Shimomura, S., and Fukui, T. (1978) Characterization of the pyridoxal phosphate site in glycogen phosphorylase b from rabbit muscle, *Biochemistry 17*, 5359-5367.

125. Merkl, I., Balk, H., Bartholmes, P., and Jaenicke, R. (1981) Interactions between tryptophan synthase from *Escherichia coli* and derivatives of the coenzyme pyridoxal 5'-phosphate, *Z. Naturforsch. [C] 36*, 778-783.

126. Bettati, S., Benci, S., Campanini, B., Raboni, S., Chirico, G., Beretta, S., Schnackerz, K. D., Hazlett, T. L., Gratton, E., and Mozzarelli, A. (2000) Role of pyridoxal 5'-phosphate in the structural stabilization of *O*-acetylserine sulfhydrylase, *J. Biol. Chem. 275*, 40244-40251.

127. Vogel, H. J., Bridger, W. A., and Sykes, B. D. (1982) Frequency-dependent phosphorus-31 nuclear magnetic resonance studies of the phosphohistidine residue to succinyl-CoA synthetase and the phosphoserine residue of glycogen phosphorylase a, *Biochemistry 21*, 1126-1132.

128. Dowhan, W., Jr., and Snell, E. E. (1970) D-serine dehydratase from *Escherichia coli*. 3. Resolution of pyridoxal 5'-phosphate and coenzyme specificity, *J. Biol. Chem. 245*, 4629-4635.

129. Demoss, J. A. (1962) Mechanism of the tryptophan synthetase reaction, *Biochim. Biophys. Acta 62*, 279-239.

130. Schnackerz, K. D., Wahler, G., Vincent, M. G., and Jansonius, J. N. (1989) Evidence that phosphorus-31 NMR is a sensitive indicator of small conformational changes in the coenzyme of aspartate aminotransferase, *Eur. J.*

Biochem. 185, 525-531.

131. Gorenstein, D. G. (1975) Dependence of phosphorus-31 chemical shifts on oxygen-phosphorus-oxygen bond angles in phosphate esters, *J. Am. Chem. Soc. 97*, 898-900.

132. Fierke, C. A., and Hammes, G. G. (1995) Transient kinetic approaches to enzyme mechanisms, *Methods Enzymol. 249*, 3-37.

133. Rabeh, W. M.-R. (2004) Characterization of the second-half reaction of *O*-acetylserine sulfhydrylase-A and the reaction of *O*-acetylserine sulfhydrylase-B from *Salmonella typhimurium*, in *Department of Chemistry and Biochemistry*, p 171 pp, Univ. of Oklahoma, Norman.

134. Campanini, B., Raboni, S., Vaccari, S., Zhang, L., Cook, P. F., Hazlett, T. L., Mozzarelli, A., and Bettati, S. (2003) Surface-exposed tryptophan residues are essential for *O*-acetylserine sulfhydrylase structure, function, and stability, *J. Biol. Chem. 278*, 37511-37519.

135. Guan, R., Roderick, S. L., Huang, B., and Cook, P. F. (2008) Roles of histidines 154 and 189 and aspartate 139 in the active site of serine acetyltransferase from *Haemophilus influenzae*, *Biochemistry 47*, 6322-6328.

136. Tai, C.-H., Rabeh, W. M., Guan, R., Schnackerz, K. D., and Cook, P. F. (2008) Role of Histidine-152 in cofactor orientation in the PLP-dependent *O*-acetylserine sulfhydrylase reaction, *Arch. Biochem. Biophys. 472*, 115-125.

137. Tai, C.-H., Rabeh, W. M., Guan, R., Schnackerz, K. D., and Cook, P. F. (2008) Effect of mutation of lysine-120, located at the entry to the active site of *O*-acetylserine sulfhydrylase-A (OASS-A) from *Salmonella typhimurium*, *Biochim. Biophys. Acta, Proteins Proteomics 1784*, 629-637.